Investigation of Neck Posture and Muscle Activity on Cervical Spine Impact Kinematics using a Finite Element Human Body Model

by

Matheus Augusto Correia

A thesis

presented to the University of Waterloo

in fulfilment of the

thesis requirement for the degree of

Doctor of Philosophy

in

Mechanical and Mechatronics Engineering

Waterloo, Ontario, Canada, 2025

©Matheus Augusto Correia 2025

Examining Committee Membership

The following served on the Examining Committee for this thesis. The decision of the Examining Committee is by majority vote.

External Examiner	F. Scott Gayzik Professor Wake Forest University
Supervisors	Duane S. Cronin Professor University of Waterloo
	Stewart D. McLachlin Associate Professor University of Waterloo
Internal Member	Arash Arami Associate Professor University of Waterloo
Internal Member	H. J. Kwon Associate Professor University of Waterloo
Internal-external Member	Andrew Laing Associate Professor University of Waterloo

Author's Declaration

This thesis consists of material all of which I authored or co-authored: see Statement of Contributions included in the thesis. This is a true copy of the thesis, including any required final revisions, as accepted by my examiners.

I understand that my thesis may be made electronically available to the public.

Statement of Contributions

The majority of the work presented in this thesis was previously published in peer-reviewed journals. The Correia et al. 2021[1] paper refers to the development of the closed-loop controller pertaining to Objective 1. The Correia et al. 2023[2] paper refers to the development of the muscle pre-tension and the neck reposturing pertaining to Objective 2. The Correia et al. 2025[3] paper refers to the tissue-level injury analysis using the model with closed-loop muscle activation and pre-tension pertaining to Objective 3.

For the three papers, Matheus Correia conducted the simulations, data post-processing, and drafting of the articles, while Duane Cronin and Stewart McLachlin supervised the research and edited the manuscript. Miguel Corrales developed and wrote the CBS section of the Correia et al. 2023[2] manuscript.

Additionally, two short communications related to this thesis were presented at the International Research Council on Biomechanics of Injury (IRCOBI) conferences in 2021 and 2023, as well as one poster was presented at the 2023 Ontario Biomechanics Conference.

For the IRCOBI 2023[4] and the OBC 2023 work, Matheus Correia conducted the simulations and data post-processing. Prasannaah Hadagali developed the simplified neck model. For the IRCOBI 2021[5], Miguel Corrales conducted the simulations, data post-processing, and article drafting while Duane Cronin and Stewart McLachlin supervised the research, and edited the manuscript. Matheus Correia worked on the muscle strain analysis and manuscript review.

Abstract

Whiplash-associated disorders (WAD) define a broad range of symptoms affecting the neck such as pain and stiffness, reported in up to half of motor vehicle collisions. WAD are typically associated with, but not limited to, low-severity rear impacts. The high incidence of WAD and high socioeconomic cost have led to significant, but still inconclusive, efforts to better understand the associated causal injury mechanisms. Neck posture and muscle behaviour are known factors that contribute to neck injuries during low-severity vehicle impacts. Quantifying the effects of such parameters at the tissue level is challenging in experimental studies but may be informed by computational human body models (HBMs). However, three limitations in neck models have been identified: (1) neck muscle controllers were often tuned to a narrow set of specific load cases, (2) neck models were unable to predict the S-shape (upper cervical spine flexion) magnitude observed in experiments during rear impacts, and (3) defining tissue-level injury thresholds remain elusive for the neck. To address these challenges, three studies were defined for this thesis using a contemporary head and neck finite element model from an average-stature male HBM (Global Human Body Models Consortium (GHBMC)) with the aim of enhancing and evaluating the tissue-level response associated with WAD injury risk following rear impact.

In the first study, a new closed-loop controller with a single set of parameters for neck muscle activation based on known reflex mechanisms was implemented in the GHBMC model. The updated model was assessed over a range of impact conditions. The closed-loop controller had an average cross-correlation to the experimental data of 0.699 for 14 load cases, including frontal, rear and lateral impacts, within 2% to 9% of previous calibrated open-loop approaches.

In the second study, a novel methodology was developed to integrate pre-tension in the neck muscles based on experimental cadaveric and volunteer data and assessed in rear impact scenarios. Only the model with pre-tension achieved flexion of the upper cervical spine at the same magnitude as reported in impact tests with volunteers. Pre-tension increased the muscle tissue strain relative to cases with no pre-tension, and, in some cases, led to potentially injurious-level strains, reinforcing that the initial muscle strain is essential for evaluating WAD injury risk.

In the third study, the methods from the first and second studies (closed-loop muscle activation controller and muscle pre-tension) were combined to assess possible WAD injury mechanisms based on tissue-level analysis of stresses and strains in 4g to 10g rear impacts. The existing injury metrics and tissue-level muscle strains identified that hyperextension was the main injurious phase in low-severity rear impacts. In addition, muscle pre-tension and activation changed the distribution of muscle strains, better representing the injury regions reported in the literature.

New model developments and knowledge obtained from the three studies completed in this research can be generalizable to other HBMs and can be applied to evaluate the efficacy of vehicle safety systems, ultimately reducing injury risk and diminishing societal costs related to low-severity neck injury in the future. Further, the enhanced neck model developed in this work has identified possible areas of experimental interest for future neck injury research.

Acknowledgements

First, I would like to express my gratitude to my supervisors, Duane Cronin and Stewart McLachlin, for all these years of wisdom and patience, guiding me through the maze of academia and industry. Our conversations were invaluable to my professional and personal growth during this extremely challenging time. I hope I can have a real positive impact on people's lives like you had on mine.

I would like to thank all my colleagues at the Impact Mechanics and Material Characterization Group for always being available to help and for making the environment safe and friendly. Special thanks to Prasannaah Hadagali, Matheus Reis, Miguel Corrales and Renan Portela for saving me whenever I needed it. Also, I would like to thank Brock Watson, Mike Bustamante and Devon Hartlen for sharing their kindness and expertise during the Biocore project.

In addition, I would like to thank the members of the Orthopaedic Mechatronics Lab for sharing a fresh view of my work and for always making the group outings a good time.

I would like to show appreciation to Honda Development and Manufacturing of America, Stellantis, GM Canada, the Digital Research Alliance of Canada, the Global Human Body Models Consortium, and the Department of Mechanical and Mechatronics Engineering at the University of Waterloo for providing the funding, technical support and computational resources that made the current work possible.

Most of all, I would like to thank my wife, my family and my friends for their love and support, keeping me sane during this journey.

Dedication

To my wife, Damaris

To my parents, Renato and Adriana

To my grandmothers, Aparecida and Robinete

To my grandfather, Manoel, my third grandmother, Divina and Odin, the cat.

Table of Contents

Examining Committee Membership ..... **ii**
Author's Declaration ..... **iii**
Statement of Contributions ..... **iv**
Abstract ..... **v**
Acknowledgements ..... **vii**
Dedication ..... **viii**
List of Figures ..... **xii**
List of Tables ..... **xv**
List of Abbreviations ..... **xvi**
List of Symbols ..... **xvii**
1 Introduction **1**
1.1 Whiplash-Associated Disorders 1
1.2 Neck Musculature and Posture 4
1.3 Modelling and Quantification of Tissue-Level Injury 7
1.4 HBM Limitations 8
1.5 Thesis Objectives 8
1.5.1 Objective 1: Development and Validation of a Novel Closed-Loop Muscle Controller Based on the Reflex Mechanisms of the Neck to Approximate the Response of Living Subjects 9
1.5.2 Objective 2: Implementation of Muscle Pre-Tension and Neck Posture to Replicate Local Kinematics of the Vertebrae and Muscles in Rear Impacts 10
1.5.3 Objective 3: Quantify Tissue-Level Injury Risk Associated with the Vertebral Kinematic Response Following Rear Impact Using the Enhanced Neck Model 11
2 Background **13**
2.1 Overview of the Neck 13
2.2 Whiplash Associated Disorders Epidemiology 14
2.3 Experimental Volunteer and PMHS Impact Studies 16
2.4 Head and Neck HBMs for Safety Research 19
2.5 Muscle Activation in HBMs 21
2.6 Muscle Activation Controllers in HBMs 24
2.7 Quantifying Muscle Strain in HBMs 28
2.8 Identification of Tissue-Level Injury in HBMs 29
3 Development and Validation of a Novel Closed-Loop Muscle Controller Based on the Reflex Mechanisms of the Neck to Approximate the Response of Live Humans. **34**
3.1 Introduction 34
3.2 Methods 35

3.2.1 Closed-Loop Muscle Activation Implementation 37
3.3 Results 43
3.4 Discussion 46
3.5 Conclusion 49
4 Implementation of Muscle Pre-Tension and Neck Posture to Replicate Local Kinematics of the Vertebrae and Muscles in Rear Impacts 51
4.1 Introduction 51
4.2 Methods 52
4.2.1 Muscle Pre-Tension 52
4.2.2 Enhanced Muscle Path Implementation in the M50 Model 55
4.2.3 Pre-impact Neck Model Reposturing 57
4.2.4 Low-Acceleration Rear Impact Simulations 59
4.3 Results 61
4.4 Discussion 66
4.5 Conclusion 69
5 Quantify Tissue-Level Injury Risk Associated with the Vertebral Kinematic Response Following Rear Impact Using the Enhanced Neck Model 70
5.1 Introduction 70
5.2 Methods 71
5.2.1 Neck Muscle Pre-Tension Implemented in the $M50_P$ and $M50_{PC}$ Head and Neck Model 72
5.2.2 Closed-Loop Neck Muscle Activation Implemented in the $M50_{PC}$ Head and Neck Model 72
5.2.3 Rear Impact Simulation 75
5.3 Results 77
5.3.1 Low-Severity 4 g Impact Simulations with the M50, $M50_P$ and $M50_{PC}$ Head and Neck Models 77
5.3.2 High-severity 7 g and 10 g Impact Simulations with the $M50_{PC}$ Head and Neck Model 83
5.4 Discussion 87
5.5 Conclusion 91
6 Thesis Conclusions, Limitations and Future Work 93
6.1 Thesis Conclusions 93
6.2 Limitations 95
6.3 Future Work 96

Letter of Copyright Permission **97**
References **101**
Appendices **119**

List of Figures

Figure 1: Rear impact dynamics 2

Figure 2: Transient stages of a rear impact 3

Figure 3: Structure of the sarcomere 6

Figure 4: Research studies and objectives 9

Figure 5: Main structures of the neck anatomy 13

Figure 6: Boundary conditions of the frontal impacts 17

Figure 7: Boundary conditions of the lateral impacts 17

Figure 8: Boundary conditions of the rear impacts 18

Figure 9: GHBMC average male model 20

Figure 10: Hierarchical structure of the muscle 22

Figure 11: Muscle force versus sarcomere length 23

Figure 12: Hill-type element 24

Figure 13: Curves of the open-loop activation schemes for the extensors 25

Figure 14: Summary of impact simulations 36

Figure 15: Schematics for the closed-loop controller 37

Figure 16: Block diagram of the closed-loop controller for the right flexors 38

Figure 17: Muscle elements used as input for the controller 39

Figure 18: Reflex response amplitude versus stimulus amplitude 40

Figure 19: Head kinematics from frontal impacts 44

Figure 20: Comparison of the activation schemes 45

Figure 21: Muscle scaling process 55

Figure 22: CBS implementation 57

Figure 23: Simulated neck postures 58

Figure 24: Rear impact simulation steps 60

Figure 25: Simulated head kinematics for the rear impacts 61

Figure 26: Intervertebral kinematics for the cadaveric specimen simulation 62

Figure 27: Intervertebral kinematics for the simulation of the volunteers 62

Figure 28: S-shape of the neck for the baseline and re-posture + pre-tension cases 63

Figure 29: S-shape behaviour during the simulations 64

Figure 30: Muscle strain analysis for the simulations 65

Figure 31: Maximum strain analysis for the simulations 66

Figure 32: Closed-loop controller schematic of the muscle activation 73

Figure 33: Muscles used as input for the CCR 74

Figure 34: Kinematics of the head CoG for the 4g rear impact simulations 78

Figure 35: Muscle activation level for the $M50_{PC}$ in the 4g impact simulation 78

Figure 36: S-shape of the neck for the M50 and $M50_{PC}$ cases 79

Figure 37: Intervertebral rotations from C0 (skull) to C7 for the three models 80

Figure 38: NIC values for the simulations 81

Figure 39: N_{km} values for the rear impact simulation for all three models 81

Figure 40: IV-NIC values for the rear impact simulation for all three models 82

Figure 41: Maximum muscle strain for the three models 83

Figure 42 : S-shape of the $M50_{PC}$ for the 4g and the 10g impacts 84

Figure 43: Intervertebral rotations for the simulations with different impact severities 84

Figure 44: $M50_{PC}$ N_{km} values for the 4 g, 7 g, and 10 g rear impact simulations 85

Figure 45: $M50_{PC}$ IV-NIC values for the 4 g, 7 g, and 10 g rear impact simulations..... 86

Figure 46: Maximum strain for the simulations with different severities..... 87

List of Tables

Table 1: Quebec Task Force Classification of WAD 4

Table 2: Strain failures for different strain rates for the neck ligaments presented by Mattucci et al. 2012..... 33

Table 3: Simulated impact cases with activation schemes, peak sled accelerations, and experimental data sets representing frontal, lateral and rear impact conditions. 42

Table 4: Flexor and Extensor muscles in the M50 neck model..... 53

Table 5: Intercept values for the calculation of the injury criteria. 76

List of Abbreviations

ATD	Anthropometric Testing Devices
CCR	Cervicocollic Reflex
CE	Contractile Element
CLA	Closed-Loop Activation
CMA	Cocontraction Muscle Activation
CoG	Center of Gravity
EMG	Electromyography
GHBMC	Global Human Body Models Consortium
HBM	Human Body Model
HNM	Head-and-Neck Model
IVD	Intervertebral disc
IV-NIC	Intervertebral Neck Injury Criterion
LNL	Lower-Neck Load Index
M50	50th percentile male model
$M50_P$	50th percentile male model with pre-tension
$M50_{PC}$	50th percentile male model with pre-tension and closed-loop activation
MMA	Maximum Muscle Activation
MPP	Massively Parallel Processing
MPS	Maximum principal strains
NBDL	Naval Biodynamics Laboratory
NDC	Neck Displacement Criterion
NIC	Neck Injury Criterion
OMA	Optimized Muscle Activation
PE	Parallel Element
PD	Proportional–Derivative controller
PID	Proportional–Integral–Derivative controller
PMHS	Post-Mortem Human Subjects
SE	Series element
SD	Standard Deviation
VCR	Vestibulocollic Reflex
WAD	Whiplash-Associated Disorders

List of Symbols

$a(t)$	Muscle activation level
F_{max}	Maximum muscle isometric force
$f(\lambda_f)$	Tension-length function
$f(\dot{\lambda}_f)$	Tension-velocity function
L_E	Experimental *in situ* length
L_M	Muscle *in situ* length in the model
L_O	Optimal muscle length
L_S	Slack muscle length
λ_E	Experimental muscle stretch
$\overline{\lambda_E}$	Average experimental muscle stretch
$\overline{\lambda_M}$	Average modelled muscle stretch
N_{km}	Neck injury criterion from Schmitt et al. 2002
N_{ij}	Neck injury criterion

1 Introduction

1.1 Whiplash-Associated Disorders

A study conducted from 2001 to 2021 indicated that from the more than 300,000 vehicle crashes investigated, 25% corresponded to rear impacts, of which 35% required medical treatment and 14% required hospitalization.[6] Whiplash-associated disorders (WAD) are of special interest in rear impacts due to the high economic cost involved, approximately $2.7 billion annually just in the United States.[7] WAD is a broad term that encompasses symptoms related to low-severity injuries of the neck, reported in 25-50% of motor vehicle collisions.[8] Typically, WAD are associated with low-speed rear impacts but have been reported to result from frontal and lateral impacts as well. The large incidence of this injury pattern has led to significant efforts to better understand the associated causal WAD injury mechanisms during impact; however, there remains no definitive answer.[9–13] Recently, the importance of the vertebral kinematics[10] and muscle behaviour[14] were highlighted, but past approaches have lacked detailed quantitative analysis of the effect of these parameters. Extensive work was conducted to understand the risk of such injuries in automotive impacts but a full explanation was still not found.[14–16] In addition, the soft tissues of the neck are frequently discussed as a probable region where such disorders originate[17–19]. However, the identification of soft tissue injuries using anthropometric testing devices (ATD) and post-mortem human subjects (PMHS) presented challenges as there are large differences from the in vivo tissue. One possible solution to this limitation is the use of computational human body models (HBMs).

A detailed look at rear impact mechanics shows that the acceleration of the vehicle is followed by the acceleration of the seat, which in turn is followed by the acceleration of the driver

(Figure 1). As the torso accelerates forward, the head stays in place due to inertia. The head usually moves backward in relation to the seat until contacting the headrest, which protects from hyperextension of the neck. However, many low-severity experiments with volunteers do not use the headrest, avoiding additional variables that can be difficult to replicate.

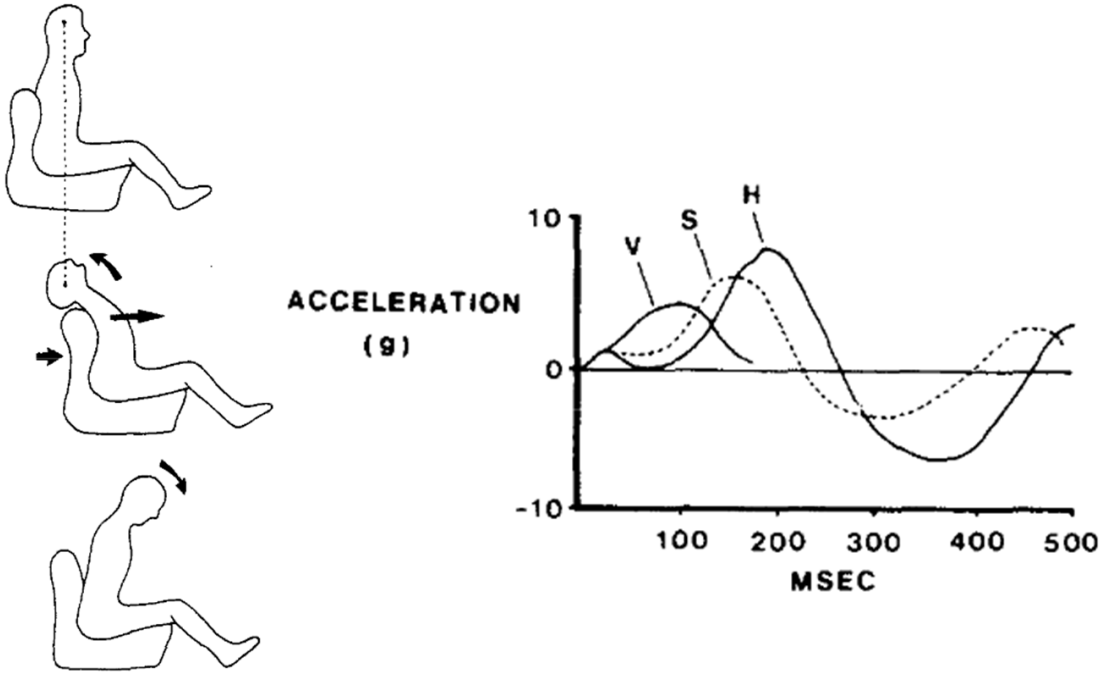


Figure 1: Rear impact dynamics

Head rotation sequence during a rear impact (on the left) and acceleration histories of the vehicle (V), the shoulder (S), and the head (H) during a rear impact. (Image adapted from Bogduk, 1986[20], used with permission.)

In rear impacts without a headrest, the neck initially forms an S-shaped curvature, due to upper cervical spine flexion and lower cervical spine extension (Figure 2). After that, the neck forms a C-shape with the extension of the entire cervical spine.[21]

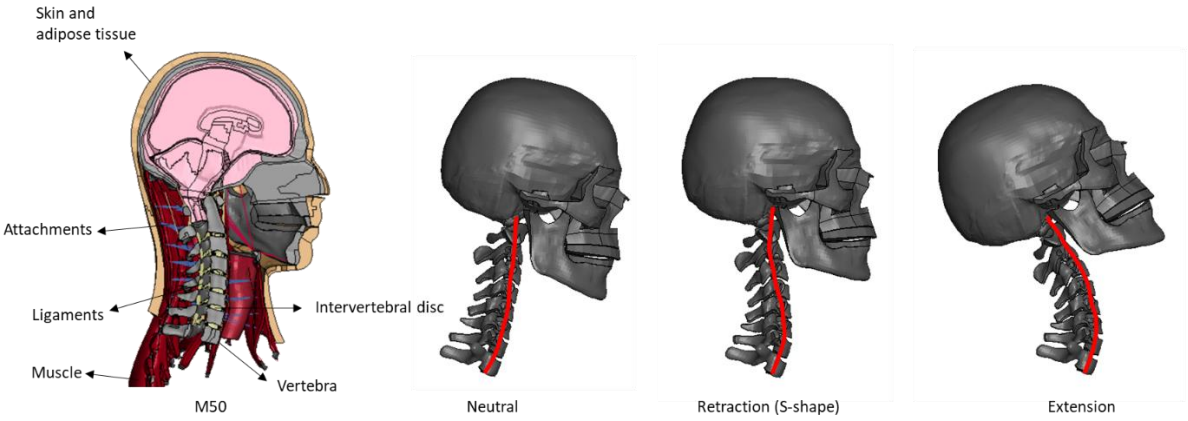


Figure 2: Transient stages of a rear impact
Initial S-shape (retraction) followed by the C-shape (extension) after the rear impact.

The onset of the S-shape has been identified as a probable injurious stage for the lower cervical levels.[22] The sudden motion of the torso resulting in the retraction of the head may cause injury due to strains in the ligaments, strains in the muscles, intervertebral disc (IVD) compression, transient pressure gradients, neural foramina shape changes, and vertebral bone fractures.[18,23,24] Yet, injuries associated with WAD are rarely identified on clinical imaging, instead being largely diagnosed by patient symptoms.[25] Therefore, WAD have been defined using the Quebec Task Force classification system (Table 1), which takes into consideration motor, sensory, and psychological symptoms.[26] Neck pain is always present for Grade I and above, but it can also be accompanied by other musculoskeletal and neurological symptoms.[26] These symptoms may or may not become chronic and typically start manifesting several hours after the impact.[17,25]

Table 1: Quebec Task Force Classification of WAD

Grade	Clinical presentation
0	No complaint about neck pain No physical signs
I	Neck complaint of pain, stiffness or tenderness only No physical signs
II	Neck complaint Musculoskeletal signs including: Decreased range of movement Point tenderness
III	Neck complaint Musculoskeletal signs Neurological signs including: Decreased or absent deep tendon reflexes Muscle weakness Sensory deficits
IV	Neck complaint and fracture or dislocation

As the Quebec Task Force Classification indicates, pain is the prevalent symptom of WAD.[26] However, the current expanded stress-diathesis model of chronic WAD development indicates that not only injury but also inflammation or psychological distress may trigger complex psychological and neurological responses that include chronic pain.[27] Therefore, HBM could be used to identify tissues affected by the impact, directly measuring stresses and strains, and, together with known injury criteria, infer, but not predict, possible regions of pain.

1.2 Neck Musculature and Posture

The natural reflex mechanisms of the cervical musculature play an important role in the stabilization of the head and neck,[28] increasing the stiffness of the spinal column and potentially influencing the risk of neck injury under impact conditions.[17] Muscle activation is of special importance for lower severity impacts as bracing impact studies show alterations in neck

kinematics and loads, and therefore, the potential for injury risk.[11,29] A collection of previous studies has worked on the hypothesis that WAD may occur during neck retraction before muscle reflex (e.g. strains in the capsular ligaments, facet joint injury, deformations of the nerve roots, and strains in the muscle),[18,24,30–33] while other research has indicated the potential for injury after the onset of the muscle reflex.[34] Therefore, a quantitative analysis to identify when the muscles are important for the injury outcome is still missing.

PMHS and ATD, commonly used to assess the risk of injury for vehicle safety tests, cannot represent physiologic muscle activation.[17,35] As occupants in real-life crash scenarios could have their response altered by muscle activation, vehicle safety tests may be limited when extrapolating post-mortem results.[36] Characterizing this phenomenon under a range of conditions, from low-severity accelerations in autonomous braking to high-severity frontal impacts, is not experimentally feasible, and an alternative approach like computational HBMs is required.

In general, active musculature implementations in HBMs use pre-defined muscle activation parameters for open-loop control of muscle onset time and activation level.[37] However, an open-loop approach limits the robustness of the model to effectively adapt to different impact scenarios or requires optimization to specific impact scenarios. Implementation of a closed-loop control approach could enable automation of the muscle activation allowing for adaptation of the parameters to suit different impact scenarios.[38]

The force magnitude produced by a muscle can be classified as a combination of an active force as well as a passive restorative force. Active contraction of a muscle is controlled by nerve impulses, originating in the central nervous system, and transmitted through motor neurons to the actuating cells. In response to this stimulus, the contraction is developed by the intracellular structure, called sarcomeres, which contain sliding filaments of actin and myosin parallel to the

longer dimension of the muscle fibres (Figure 3). The passive force is developed without the need for activation through the viscoelastic behaviour of the material and is directly related to the length of the tissue.

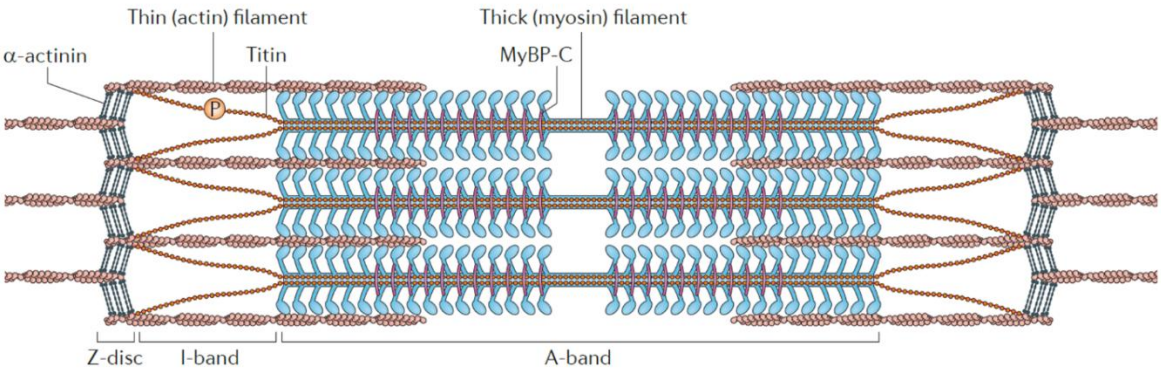


Figure 3: Structure of the sarcomere
The actin filaments slide on the Myosin filaments to contract the muscles. (Image from Hwang and Sykes, 2015[39], used with permission.)

The initial length of the muscles before being stretched has also been indicated to influence WAD.[40,41] This geometric effect is expected, as muscle damage is more likely due to higher strains than higher forces during muscle contractions.[42] Muscle geometric effects are of special interest to WAD[17] and large muscle strains have been directly correlated with this type of injury.[18,19] Yet, the challenge of understanding the role of muscle length arises due to the difficulty of obtaining precise measurements of muscle strain and strain rates in cadavers or human volunteers. As an alternative, computational HBMs can complement experimental studies to estimate local stress and strain values for any tissue. However, no studies to date have examined the effect of the initial stretch of the neck muscles before rear impact. Studies comparing tensed and not tensed subjects in sled impacts indicated that the initial muscle stretch values have a significant contribution to the neck response.[11,43]

Besides muscles, an important boundary condition is the neck posture prior to impact. Neck posture can be defined by the relative position of the head and spinal column. Previously, the head center of mass location has been shown to affect the magnitude of flexion and time to maximum S-shape during impact.[24] The S-shape is also more noticeable in females, and neck posture is postulated as a possible explanation for the differences in WAD between the two sexes.[24] Yet, quantifying the posture effect on the tissue-level injury risk remains an unsolved challenge.[17]

1.3 Modelling and Quantification of Tissue-Level Injury

The aim of detailed finite element HBMs is to predict where and when injury occurs through the tissue-level response. Complex loading scenarios can be addressed using HBMs,[44] but geometry and material properties must be appropriately defined, as the local tissue response can be sensitive to these parameters.[45] Experimental values for the failure criteria of muscles (failure strain from 0.227 to 0.629),[46,47] ligaments (failure strains from 0.40 to 1.15),[48] and the annulus fibrosus of the IVDs (average circumferential failure strain of 0.3)[49] have all been previously reported. This data raises the possibility for computational models to quantify tissue-level injury if the model input parameters are appropriate.

A few studies have tried to observe neck muscle strains prior to and during impact using simplified computational models and extrapolations from measurements at the surface of the skin.[18,50] However, the majority of these investigations have only focused on broad aspects of the role of spine curvature, gender differences, and vertebral kinematics; neglecting the region of the injury and the role of the physiologic muscle tissue mechanics, such as pre-tension. This has limited important quantitative aspects that could help to elucidate WAD injury mechanisms.

1.4 HBM Limitations

The Global Human Body Models Consortium (GHBMC) model is a detailed commercial HBM widely used in the automotive industry for safety testing. Notable limitations of the current GHBMC neck model include: (1) the need for a general controller for the muscle activation level and timing that applies to different impact directions and severities, (2) the lack of muscle pre-tension, and (3) the absence of the characteristic S-shape response of the neck identified during rear impact experiments. Addressing these model limitations would ultimately allow for improved assessment of neck injury risk during simulated impact conditions and, more specifically, quantify the importance of the S-shape on injury risk and WAD in low-severity rear impacts, which to date has not been achieved.

1.5 Thesis Objectives

The overall objective of this thesis was to develop a quantitative understanding of the role of neck posture and muscle behaviour in WAD through the improvement of HBMs for impact simulations. This development focused on improving the response and injury prediction capabilities with impact simulations of a contemporary HBM by enhancing the active and passive muscle implementation, as well as investigating the role of neck posture. These enhancements to the neck musculature behaviour would enable, for the first time, a detailed assessment of the importance of the S-shape on WAD injury risk, a major unsolved challenge in current HBMs. To achieve this goal, multidirectional impact studies in different accelerations with volunteers were identified to develop and validate the proposed closed-loop muscle controller. Further, additional impact studies with volunteers and PMHS displaying the vertebral displacements were obtained to observe the effect of muscle pre-tension implemented in the model due to the expected

sensitivity of the tissue deformation to the local kinematics.[10] These datasets were discussed in Chapter 2.

To achieve the overall goal of this thesis, the active and passive muscle implementation, as well as the role of neck posture, was investigated using the GHBMC neck model to improve response and injury prediction for rear impact simulations (Figure 4).

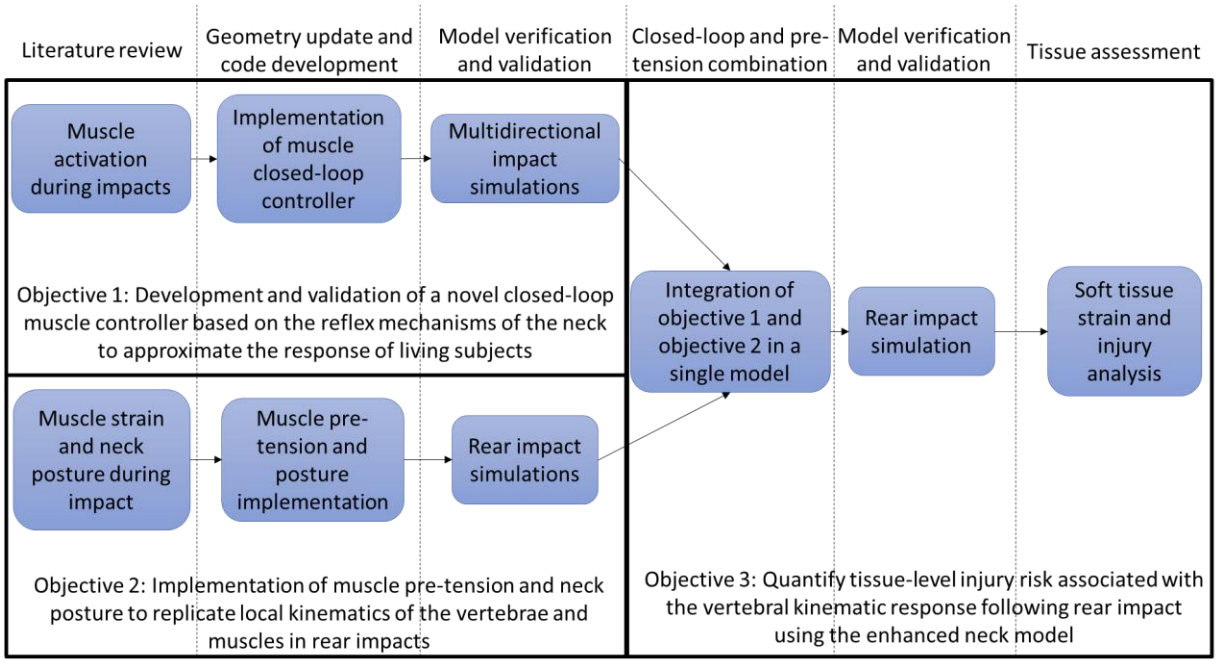


Figure 4: Research studies and objectives
Flow chart summarizing the three studies and objectives of the developed research.

1.5.1 Objective 1: Development and Validation of a Novel Closed-Loop Muscle Controller Based on the Reflex Mechanisms of the Neck to Approximate the Response of Living Subjects

The current computational neck models utilize open-loop (predetermined) muscle activation or simple closed-loop controllers that have been calibrated to a set of load cases. In addition to the optimization process for the controllers being time-consuming, the resulting control

parameters are often the best fit for specific data sets, such that the model may not be generalizable to different impact directions and severities.

The first objective of this thesis was to develop a novel closed-loop controller for neck muscle activation based on the Vestibulocollic reflex (VCR) and Cervicocollic reflex (CCR) mechanisms. The novel controller aimed to achieve a muscle activation similar to human volunteers using a physically based model. The closed-loop model required some parameter calibration where physical quantities were not available in the literature. Such calibration was limited to a small subset of human volunteer impact tests to maintain the general applicability of the muscle activation strategy. The predictive capability of the closed-loop controller was assessed using global kinematics of the head for volunteers in nine frontal sled impact cases, with impact severities ranging from 2 g to 15 g; four lateral impact cases (4 g to 7 g); and two rear impacts (3 g to 4 g). The correspondence of the model to the human volunteer data was assessed objectively using the cross-correlation method.

1.5.2 Objective 2: Implementation of Muscle Pre-Tension and Neck Posture to Replicate Local Kinematics of the Vertebrae and Muscles in Rear Impacts

The in vivo muscle includes some amount of passive pre-tension stress; however, current HBMs do not include pre-tension due to the paucity of data on muscle pre-tension and the complexity of achieving a stable implementation in numerical models.

The second objective of this work aimed to be the first computational study to integrate and observe the effect of muscle pre-tension on vertebral and head kinematics for impact scenarios. The muscle pre-tensions were estimated using muscle measurements from both cadavers and living subjects. Methods to achieve muscle pre-tension in the neck model were investigated,

including the use of dynamic relaxation to generate the initial stresses from the non-deformed and pre-tensioned geometries for the muscles. Two rear impact scenarios using boundary conditions and postures from the literature were used to assess the effect of muscle pre-tension. The first case was a cadaveric tissue testing, which does not include pre-tension, and the second case was a human volunteer data, which does include muscle pre-tension. The effect of the muscle pre-tension in the model was quantified by comparing the global head kinematics, vertebral rotations, and muscle strains of the two simulations to experimental data.

1.5.3 Objective 3: Quantify Tissue-Level Injury Risk Associated with the Vertebral Kinematic Response Following Rear Impact Using the Enhanced Neck Model

The characteristic and transient S-shape response of the neck during rear impacts is frequently attributed as the origin of WAD. Yet, how this kinematic response may be related to neck injuries is still inconclusive in the literature. HBMs could be used to further inform the possible injury risk associated with vertebral kinematics, but current models lack the level of detail for such an investigation.

The third objective of this study used the GHBMC neck model enhanced in Objectives 1 and 2 to observe vertebral kinematics during a rear impact and quantify tissue-level injury risk arising from the response of the cervical spine. The improved muscle activation strategy (*i.e*. method of controlling the activation level and timing), muscle pre-tension and posture enhancements were anticipated to enable the prediction of the biofidelic vertebral responses. As a consequence, the improved GHBMC neck model was subsequently used to analyze injury risk with the representative initial posture, muscle pre-tension and closed-loop controller simulating a 4 g rear

impact. The possibility of injury was analyzed by comparing stresses and strains in the muscles to injury criteria from the literature.

2 Background

2.1 Overview of the Neck

The main anatomical structures of the human neck are the vertebrae, intervertebral discs, ligaments, musculature, and surrounding tissues such as skin and adipose tissue (Figure 5). Specifically, the cervical spine comprises seven vertebrae (C1 to C7), organized sequentially from superior to inferior and subdivided into two distinct regions: the upper cervical spine, which includes the atlas (C1) and axis (C2), and the lower cervical spine, from vertebrae C3 to C7.

The atlas (C1) and axis (C2) exhibit structural adaptations that distinguish them from other cervical vertebrae. The atlas lacks both a vertebral body and a spinous process. Conversely, the axis is defined by the presence of the odontoid process, or dens, a prominent projection extending vertically from the superior surface of the vertebral body. This feature acts as a pivot point, allowing the atlas to rotate and facilitating substantial rotational movement of the head and neck.

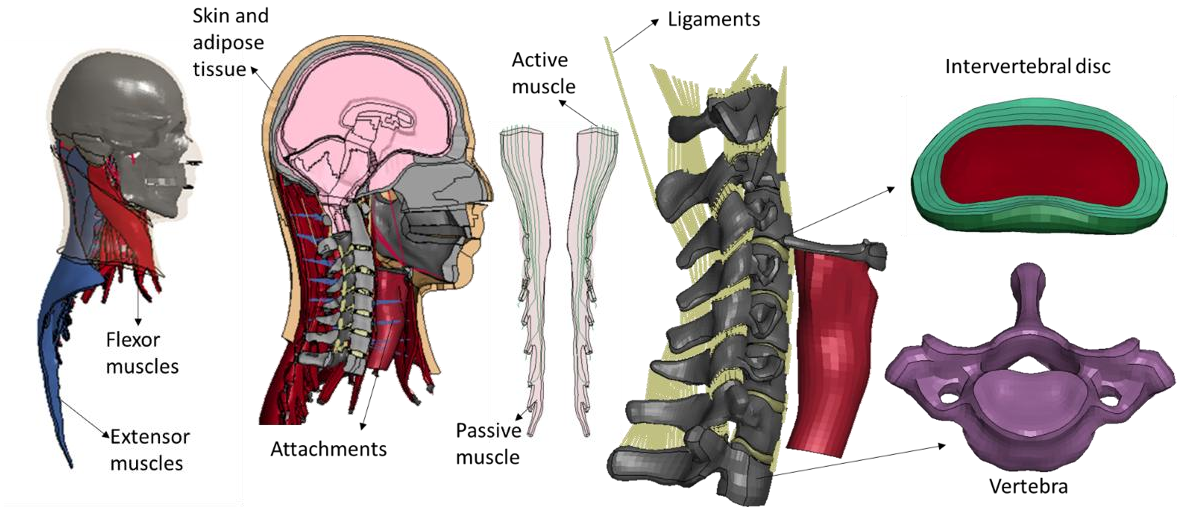


Figure 5: Main structures of the neck anatomy
The anatomical structures are displayed with an HBM. The attachments in blue are not present in real humans.

2.2 Whiplash Associated Disorders Epidemiology

WAD were described as a group of symptoms related to rapid acceleration and deceleration of the neck, usually seen in automotive crash scenarios. Although such symptoms include musculoskeletal and neurological signs (Table 1), WAD are mainly characterized by the presence of neck pain. Even though the cervical region is usually the focus of the WAD literature, the neck is rarely the single region affected and is usually accompanied by headache, back pain, upper extremity pain, and temporomandibular disorders.[51]

WAD are the most common type of injuries associated with motor vehicle crashes,[52] and the estimated annual cost of WAD in the U.S. is $2.7 billion.[7] In terms of the number of cases, a study using the National Automotive Sampling System - Crashworthiness Data System (NASS-CDS) database estimated that there were 841,000 whiplash injuries in the 869,000 cervical spine injuries seen in hospitals in the U.S. annually due to crash events.[53] Importantly, the total number of whiplash injuries is estimated to be much higher, as the total number of cervical spine injuries in the U.S. is underestimated by 84% in the NASS-CDS dataset.[53]

An important aspect related to WAD cost is chronicity, as the healthcare costs related to this type of injury are strongly correlated with multiple visits to doctors and alternative medicine.[7] This is especially costly as half of the people injured will continue to report persistent signs, ranging from mild symptoms to severe disability.[54]

Previous studies have shown that factors such as occupant body size, morphology, muscle size and muscle orientation affect the WAD probability, with a compound effect of these characteristics generating a higher risk for the female population.[17]

The difficulty in observing direct WAD signs in medical imaging[55] led to a series of hypotheses about the tissues injured. The literature raised the facet joint, ligaments, IVD, vertebral

artery, dorsal root ganglion, dorsal root and muscles as possible candidates for injury.[56] In addition, it was observed that anxiety, depression, and distress affect WAD outcome.[54] These psychological factors reinforce the idea of this condition being a multisystem physiological, psychological and socioenvironmental condition onset by an automotive crash scenario.[54]

Cervical muscle injuries in particular are a usually neglected aspect of WAD, even though they have been identified in injury in whiplash studies with animals and cadavers.[57] The muscles were generally overlooked in past studies because of the difficulty of measuring their forces and strains in impact experiments, and due to not known direct relation between chronic pain following muscle trauma. The usual assumption in the past was that the expected partial and complete muscle tears would recover in weeks, leaving the patient with scars but no residual pain.[58] However, considering the more recent multisystem view of WAD, chronic pain can be related to a psychological condition triggered by or correlated to a muscle injury, as well as a result of functionality changes due to scar formation in the muscles. For example, a study with 30 volunteers diagnosed with WAD found higher fat infiltration in the right trapezius, splenius capitis, semispinalis capitis, and semispinalis.[59] Although the only statistically significant increase was in the trapezius, probably due to a small sample size, the fat infiltration could be related to inadequate function recovery and possible damage to the muscles.[59] In addition, cadaveric testing of the rectus capitis posterior minor of female specimens revealed tearing of a few fibres to complete rupture for head distances to the headrest greater than 7.2 cm.[19] Other studies with chronic WAD patients identified reduced power, exaggerated fatigue, changed blood flow, and probable activation abnormalities in the trapezius as well as activation changes in the sternomastoid muscles.[57] Even though such muscle dysfunctions may be a secondary phenomenon due to pain generated by other

structures, they can also be due to direct muscle damage, as the injury mechanism is still not agreed upon.

Therefore, improving the understanding of WAD injury mechanisms may help the development of new protective measures as well as possible treatments, helping mitigate the high socioeconomic costs related to this condition.

2.3 Experimental Volunteer and PMHS Impact Studies

Many experimental impact studies have been conducted with volunteers and PMHS to better understand injury and improve vehicle safety. Previous experimental studies have investigated car and sled tests with volunteers in low-severity autonomous braking and impacts (1 g to 4 g) and reported the effect of muscle activation on the response.[60–67] However, many of these studies have not reported important experimental boundary conditions (*i.e.* seat inclination, presence of headrest, etc.), making it difficult to reproduce the experiments in a simulation environment or to quantify the effects of muscle activation.

An experimental dataset containing a wide range of volunteer impact severities[68] conducted by the Naval Biodynamics Laboratory (NBDL) includes head and neck kinematic data. Data were collected from 16 volunteers subjected to 119 frontal (Figure 6) and 72 lateral (Figure 7) impact sled tests.[69,70] The experimental peak sled accelerations ranged from 2 g to 15 g and demonstrated low variability within a specific impact condition, owing to the restraint system used in the experiments. A limitation of the experimental data was that no measurements of the volunteer's muscle activation were recorded during the impact tests.

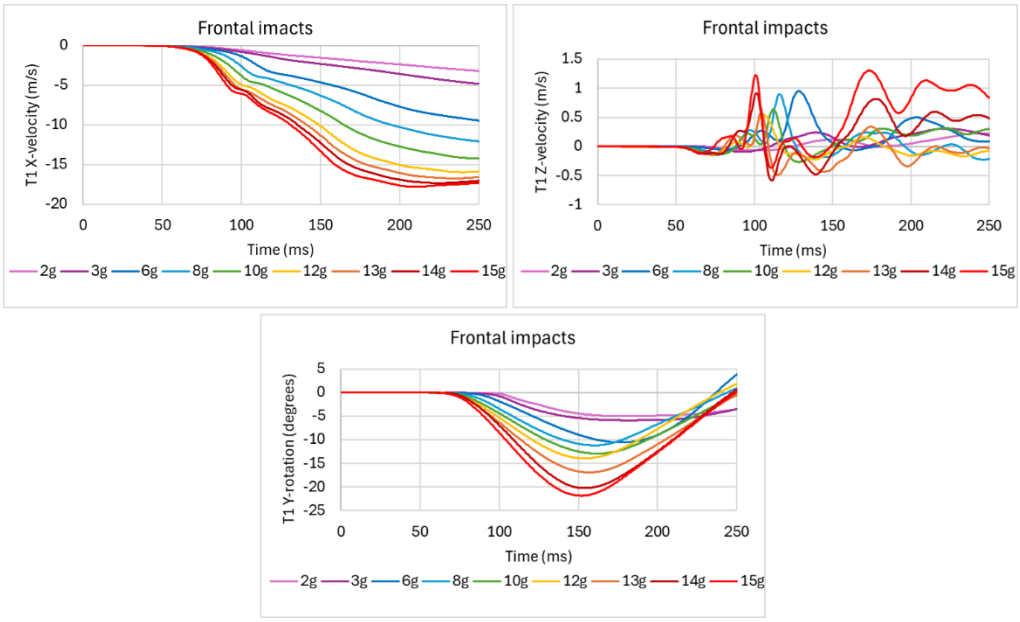


Figure 6: Boundary conditions of the frontal impacts

Average T1 kinematics in the Society of Automotive Engineers (SAE) coordinate system for the NBDL frontal impacts from 2 g to 15 g peak sled acceleration.

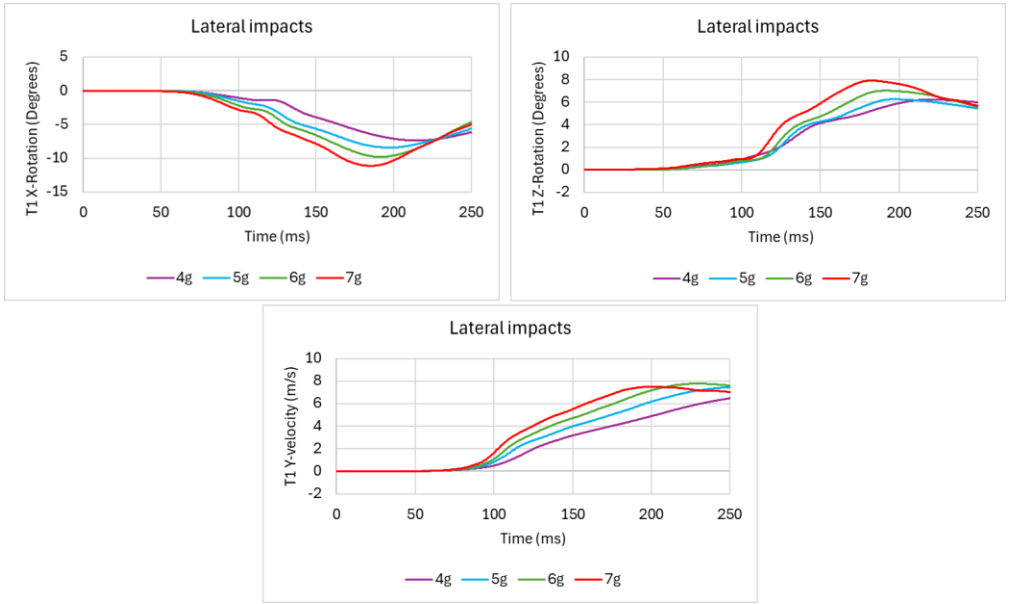


Figure 7: Boundary conditions of the lateral impacts

Average T1 kinematics in the SAE coordinate system for the NBDL lateral impacts from 4 g to 7 g peak sled acceleration.

There is a scarcity of higher severity rear impact volunteer studies owing to injury risk. A review in 2018 indicated that at least 1251 unique rear impact tests using volunteers are present in the literature.[71] However, only a few presented detailed vertebral kinematics, and only one study presented vertebral kinematics and related published work with detailed information on the pre-impact neck posture.[31,72,73] Due to the expected sensitivity of vertebral displacement to the pre-impact neck posture,[17] detailed information on the neck and head positions is essential to accurately describe the influence of the muscles during rear impacts in vertebral kinematics. A detailed rear impact study performed by Sato et al. 2014[73] over a series of 3 g and 4 g sled tests (Figure 8) with 12 human volunteers was used to assess the global head kinematics response. The rear impact tests in this study did not include a headrest so that the free motion of the head could be assessed; however, muscle activation levels were not measured during the tests. Additionally, Sato et al. 2014 used 4 male volunteers to record the kinematics of each vertebra using high-speed X-ray imaging during simulated rear impacts.[73]

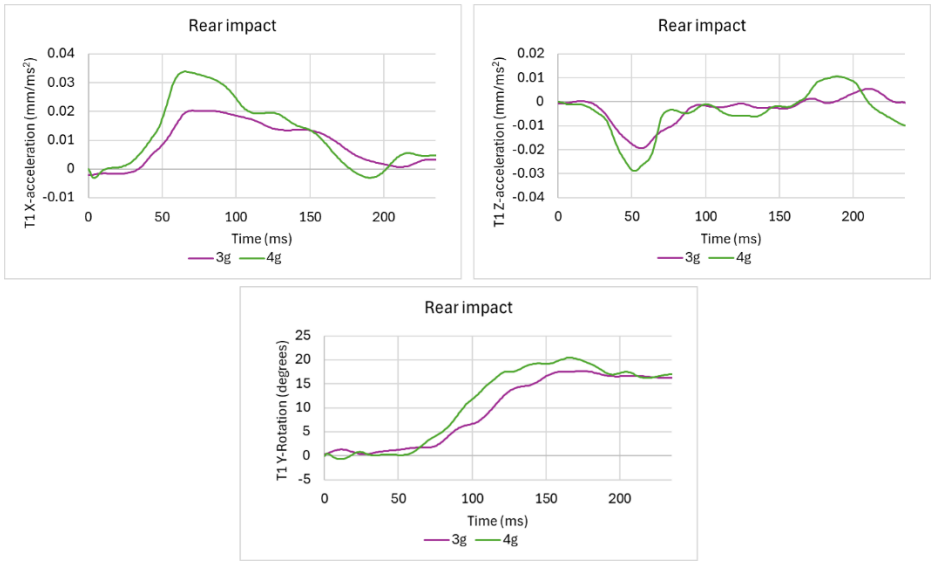


Figure 8: Boundary conditions of the rear impacts

Average T1 kinematics in SAE coordinate system for the Sato et al. 2014 rear impacts from 3 g and 4 g peak sled acceleration.

Similar to rear impact with volunteers, a vast literature exists about rear impact with PMHS. Again, only a few papers presented detailed vertebral kinematics, and the current study found only one paper presenting vertebral kinematics with information on the pre-impact neck posture at a similar acceleration to the detailed volunteer tests.[30,74,75] The paper was a PMHS sled study conducted by Stemper et al. 2004[30]. It used 5 male and 5 female cadavers with a peak sled acceleration of 4 g, with the excised head and neck with preserved skin and muscles potted at the T1 level to replicate a physiological pre-tension.[30]

2.4 Head and Neck HBMs for Safety Research

Due to the complexity of investigating the effects of the movement of the spine in WAD, HBMs were used in the past to simulate impacts to understand this type of injury. HBM with muscle activation includes the GHBMC, KTH, JAMA, THUMS, simTK and VIVA models.[13,76–79] Due to computational efficiency, models with only the head and neck, usually extracted from the HBM, were also frequently used to investigate muscle activation.[13,37,80] Considering contemporary neck and head models, only the GHBMC, THUMS and VIVA+ models incorporate a combination of skin, adipose tissue, 3D passive muscles, and active 1D muscles. The soft tissues are relevant for the head and neck kinematics because of the increase in stiffness of the system resulting from these tissues. Specifically, the GHBMC neck model has been assessed and validated in a hierarchical manner at the motion segment[81] and full neck levels,[82] and optimized open-loop muscle activation strategies have shown good correspondence to human volunteer data.[37] The model was developed from Magnetic Resonance Imaging (MRI) and Computed Tomography (CT) scans of a living 26-year-old adult with the anthropometrics of a mid-size male.[83]

The GHBMC 50th percentile male (M50-O v5.1) head and neck model used in the studies in this thesis was extracted from the full HBM (Figure 9) and includes 1D Hill-type elements representing the active portion of the muscles and 3D solid hexahedral elements with a hyper-viscoelastic material constitutive model representing the passive response of the muscle. The passive and active elements were connected through a series of one-dimensional attachments or support elements to maintain connectivity and the line of action of each muscle.[82]

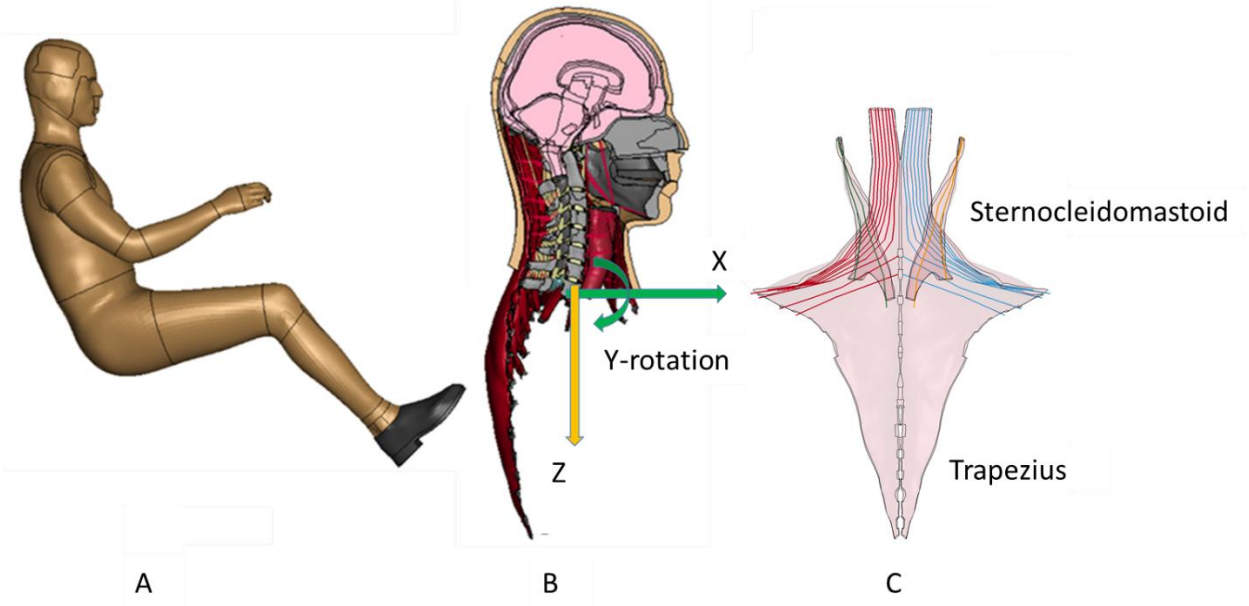


Figure 9: GHBMC average male model
A) GHBMC 50th percentile male full HBM. B) Sagittal view of the head and neck model with T1 coordinate system and muscle attachments. C) Frontal view of the 3D passive component (transparent geometry) of the trapezius and sternocleidomastoid with the embedded active Hill-type elements (coloured lines).

HBMs were previously used to analyze the possibility of injuries such as WAD in impacts. One study using a head and neck HBM model observed upper cervical ligament failures for high severity (>11.7g) frontal and rear impacts,[8] while another study obtained the S-shape using an osteo-ligamentous spine model with truss elements replicating passive muscle concluding that

peak flexion was influenced by disk height, vertebral depth, and head center of mass location.[84] In addition, recent studies have focused on the female VIVA model due to the increased risk of WAD in this population, proposing muscle activation strategies capable of reproducing the kinematics of lower-severity rear impacts.[13,85] However, no past studies used models with skin and adipose tissue as well as biofidelic muscle pathways and 3D muscles. Therefore, some improvement of the HBMs is still necessary to allow the observation of the localized response of the soft tissues during impacts.

2.5 Muscle Activation in HBMs

Muscle tissues are hierarchical structures (Figure 10) capable of producing both a passive restorative force and an active force.

The passive force is intrinsic to the muscle without activation, exhibiting viscoelastic and anisotropic characteristics, as expected for biological tissues with fibres.[86] Passive response behaviour has been modelled numerically using a linear-viscoelastic formulation, such as an Ogden formulation.[87] In contrast, active muscle force is controlled by nerve impulses originating in the central nervous system and transmitted through motor neurons to the actuating cells. Active muscle force is a function of the muscle length and rate of change in length. In response to this stimulus, contraction is developed by the intracellular structure (sarcomeres) through sliding filaments of actin and myosin parallel to the longer dimension of the muscle fibres (Figure 11).

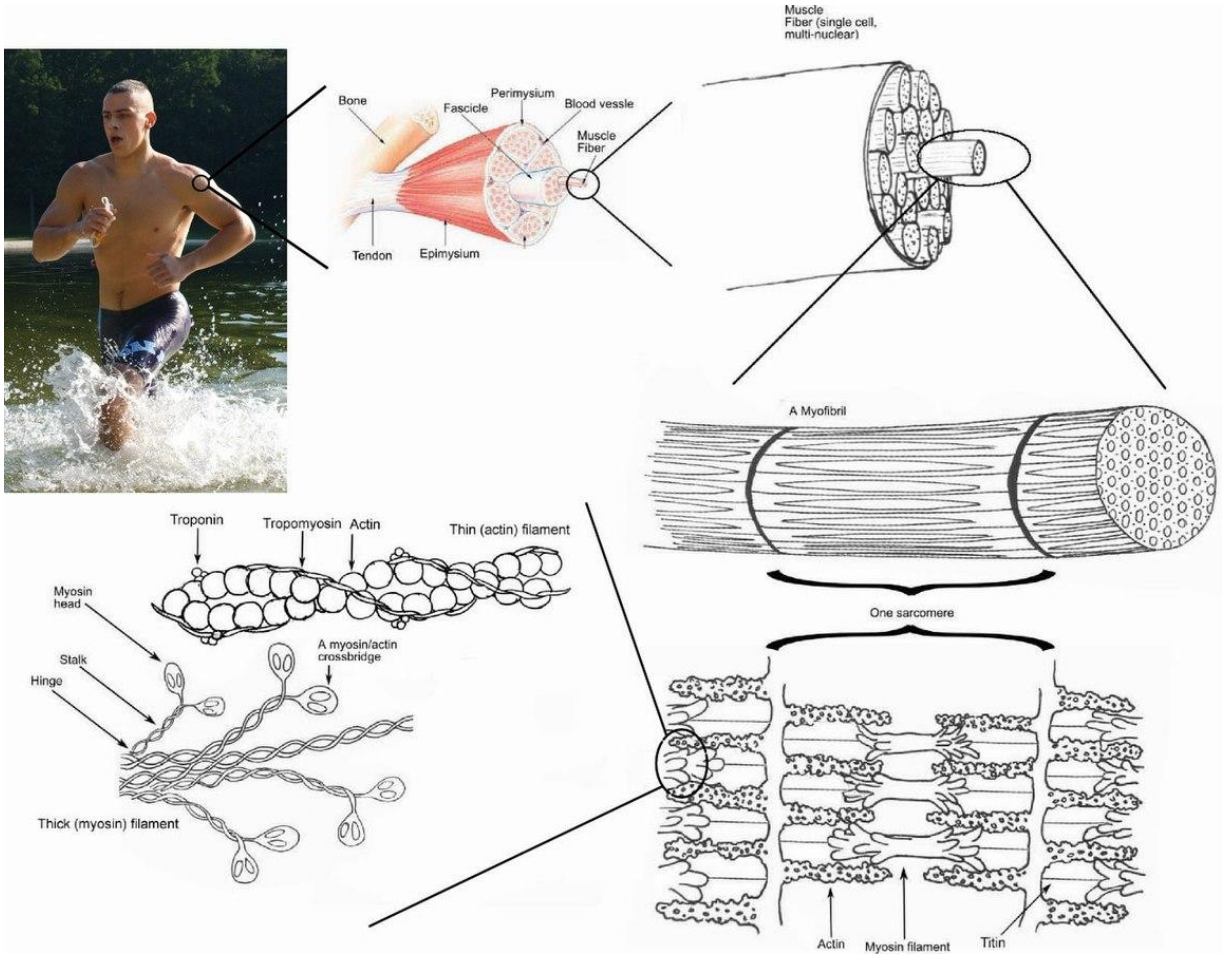


Figure 10: Hierarchical structure of the muscle

The muscle tissue is shown from the macroscopic level to the microscopic actin and myosin filaments of the sarcomere (Image: Skeletal muscle by Wikimedia Commons. Retrieved from https://commons.wikimedia.org/w/index.php?title=File:Skeletal_muscle.jpg&oldid=718022550. Creative Commons Attribution-Share Alike 3.0 Unported license).

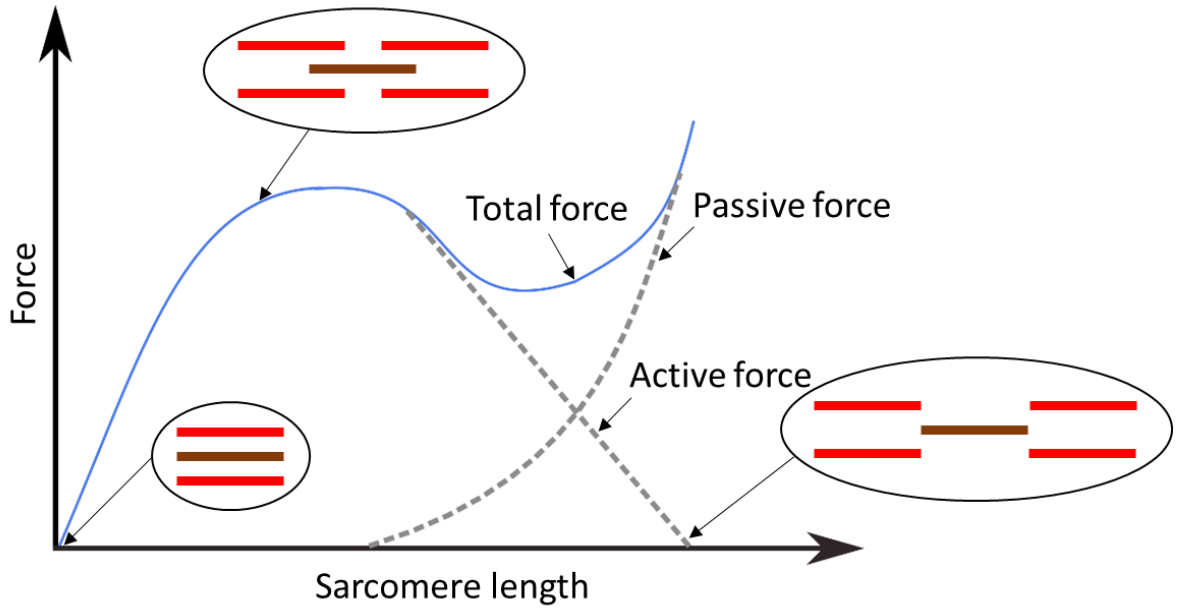
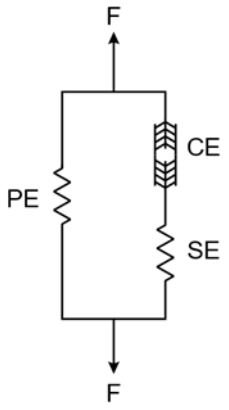


Figure 11: Muscle force versus sarcomere length

Active and passive forces generated by the muscle relative to the sarcomere length. The sarcomere filaments configuration is shown with myosin in brown and actin in red.

The Hill-type active muscle model is a widely used approach to model muscle activation and the resulting contractile force,[82,88] and is implemented in many commercial FE codes, often using one-dimensional elements joining two points to represent the muscle. The element is composed of a series element (SE) representing the elasticity of the actin-myosin connections, a parallel element (PE) representing the passive elastic properties of the muscle fibre and a contractile element (CE) representing the active force generated in the muscle (Figure 12). The CE activation in this formulation is represented by a curve describing the magnitude of activation with respect to time.



$$F_{CE} = F_{max}.a(t).f(\lambda_f).f(\dot{\lambda}_f)$$

Figure 12: Hill-type element

Hill-type active muscle model schematic (left) and CE force equation (right). In the equation, F_{max} is the maximum isometric force, a(t) is the muscle activation level, $f(\lambda_f)$ is the tension-length function and $f(\dot{\lambda}_f)$ is the tension-velocity function. (Image: Hill muscle model by Wikimedia Commons, adapted from https://commons.wikimedia.org/wiki/File:Hill_muscle_model.svg. Creative Commons Attribution-Share Alike 3.0 Unported license.)

As part of my previously published research, our group identified optimized activation onset times for the flexor and extensor muscles in the neck using experimental data from a series of rear impacts and frontal impacts sled tests conducted with volunteers.[37] The use of optimized muscle activation curves was found to improve the resulting head kinematics of detailed FE head and neck models over a wide range of impact severities in comparison to the best available data.[37] Such numerical optimizations prescribed a range of activation onset times (55-99 ms) and curve shapes that were bounded by experimental in vivo data.

2.6 Muscle Activation Controllers in HBMs

The GHBMC average stature male model incorporates open-loop controls for the muscles with predefined muscle activation curves that mimic the muscle reflexes in a prescribed manner. The previous versions of the model include an open-loop muscle activation scheme, defined as the

Maximum Muscle Activation (MMA),[37] corresponding to a neuronal impulse (step signal) of 100% for 100 ms, generating a maximum value of the activation function in the muscle of 0.871.[89] The onset time for this activation was 74 ms, an average of the values presented in the literature for a series of tests with volunteers.[89] In a previously developed work, two additional open-loop muscle activation strategies were proposed: Cocontraction Muscle Activation (CMA) and Optimized Muscle Activation (OMA).[37] The CMA had a generalized activation of 100% for flexors and 20% for the extensors (Figure 13) representing a muscle contraction that would minimize head rotation when no other load was applied, based on the simulation of a startle reflex. The OMA consisted of a specific activation curve for each simulated impact direction and severity, obtained from an optimization process of the muscle activation parameters to best achieve the average resultant head kinematics reported in the experimental data. However, closed-loop controllers present an opportunity to more effectively and efficiently address a wider range of impact severities and directions.

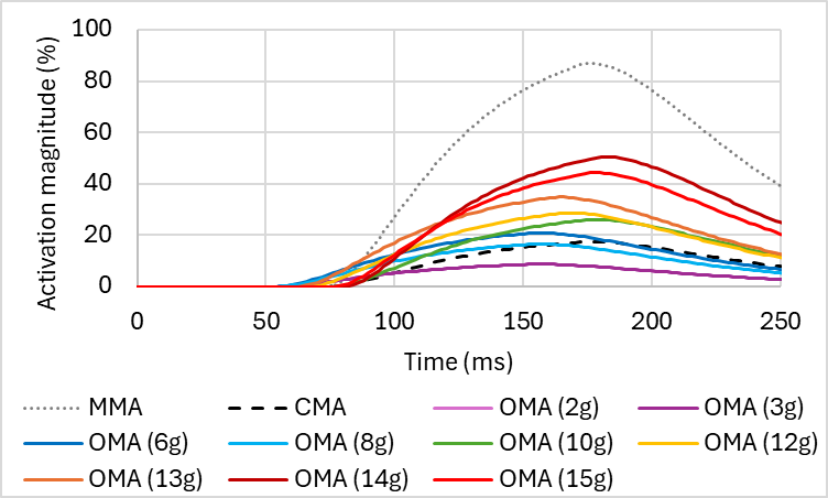


Figure 13: Curves of the open-loop activation schemes for the extensors

The OMA activation is different for each impact case as shown in the plot for the different frontal impact severities. For all the frontal impacts, the flexors presented the same activation curve as the MMA presented in the figure.

A number of closed-loop controllers have already demonstrated promising results in simulating natural muscle reflexes.[78,90–92] Current implementations based on the head rotation angle with respect to T1 and the muscle spindle response[13,93] have provided head kinematics with a good correlation to the experimental data for specific scenarios. A recent model incorporating a feedback controller based on physiological mechanisms was fitted to experimental data for studying neck stabilization,[94] but only assessed for accelerations lower than 1g without consideration for the higher accelerations resulting from impact scenarios.

Closed-loop control for muscle activation has typically been implemented using a proportional–integral–derivative (PID) controller with feedback based on global kinematics, such as the head center of gravity (CoG) rotational angle.[13,93] However, the integral gains have no physiological meaning and can be set to zero, as previous research demonstrated adequate controller performance for reflex behaviour with only a PD controller.[13] The parameters for these closed-loop controllers are usually calibrated to specific experimental loading cases using inverse methods, reducing their generalizability to adapt to different loading conditions. This limitation is largely due to a lack of electromyography (EMG) data for higher severity impacts (>8g) and deeper muscles, which has created a gap in understanding the role and complex interactions between different muscle activations during these events.[95] Therefore, leveraging knowledge of the physiology of the reflex mechanism is important for guiding the development of a closed-loop muscle activation controller to be used in a large range of impact severities and directions. The main mechanisms controlling muscles during impacts are the VCR, CCR, voluntary muscle activation and the startle reflex mechanism.

The VCR and CCR are primarily responsible for head and neck stabilization and, therefore, a crucial focal point for muscle activation during impact.[13,94,96,97] The VCR system receives input

from the semicircular canals and cochlea in the inner ear, with a delayed onset time relative to the external stimulus and is directly related to the angular and linear accelerations of the head. The CCR receives signals from modified muscle fibres diffusely distributed in the muscles and presents a fast onset time, with muscle stretch and stretch rate as the input. The VCR has a time delay of 13 ms and the CCR has a time delay of 18 ms.[94] The 13 ms delay was the time needed for the signal generated by the head rotation to affect muscle activation. The 18 ms delay was the time needed for the signal generated by the muscle stretch to affect the muscle activation.

A comprehensive review of frontal and rear impact studies revealed reflex onset times ranging from 55 ms to 99 ms after the impact, with an average onset time of approximately 74 ms[31,98–103], while the average onset time for the voluntary contraction of the neck muscles was between 100 ms and 117 ms for voluntary contraction.[104] As the peak head rotation in impacts occurs later than the reflexes, the influence of voluntary activation for the initial moments of the impact is expected to be low.

The startle reflex is a rapid, involuntary motor response triggered by sudden acoustic, tactile, or vestibular stimuli. This reflex engages a widespread and stereotypical activation of numerous muscle groups across the body.[105] After only a few repeated stimuli, the startle response diminishes significantly, with only minimal muscle activation remaining.[106] However, this habituation can be altered when an individual is alerted prior to stimulus exposure.[106] Additional sled impact studies have shown differing responses between aware and unaware participants, suggesting a modulation of the startle response due to cognitive pre-alerting.[61,107]

A closed-loop controller for muscle activation based on physiology, like the VCR and CCR mechanisms, could be flexible and better represent changes in the model boundary conditions.

This would help to overcome some of the limitations of case-specific open-loop optimizations that may not be applicable outside of specific impact conditions.

2.7 Quantifying Muscle Strain in HBMs

Recent efforts have focused on analyzing vertebral kinematics using HBM with muscle activation, especially in female models, due to the prevalence of WAD in this population.[13,24,33] However, no study has yet examined the muscle strain response in a detailed HBM. The majority of the models present a non-physiological path of the active muscle, usually straight lines connecting the insertion points.[108] Although this is sufficient to generate reasonable head and vertebral kinematics, it has challenges representing biofidelic muscle strains. Recent enhancements to the active muscle attachments to the vertebrae and passive muscle in the GHBMC models have significantly improved the representation of muscle action path, creating an opportunity to better observe the resulting muscle strains during simulated impacts.[5]

To accurately measure muscle strains during impact, the initial muscle length immediately before impact needs to be defined. The current detailed finite element HBM of the 50th percentile male from GHBMC had muscle geometries based on MRI data of a volunteer.[109] Even though the subject was in a relaxed physiological position, muscle pre-tension due to muscle activation is always present. Alternatively, PMHS do not have muscle activation, which limits this effect on the measurement of the initial muscle length. While some rigor mortis may be present, muscle measurements on PMHS subjects may better estimate the muscle resting length.[110–113]

Collectively, the combined data from the tests with PMHS, volunteers, and muscle measurements could be used to better define the boundary conditions of HBM simulations,

resulting in a more robust prediction of vertebral kinematics and corresponding soft tissue strains during impact. To date, this has not been examined in any known HBM.

One relevant contributor to WAD and muscle strain is posture. The cervical spine is usually assumed to be in a neutral posture when replicating pre-impact conditions of vehicle occupants.[114] The neutral posture assumes the spine is upright and the muscles are relaxed.[114] However, this definition of posture is often arbitrary, as the vertebral ranges of motion vary among flexion and extension, static and dynamic conditions, as well as consideration for hysteresis, depending on prior kinematic history.[115] Postures are resultant of a force balance that takes into consideration the soft tissues, bone geometry and muscle activity. These three items present differences among individuals and populations, creating uncertainty in vertebral positions and orientations in the neutral posture. Only recently, a detailed study observed the position of each vertebra of volunteers on sled seats used in impact studies.[116] Cervical vertebral kinematics have also been recorded using high-speed X-ray imaging in rear impacts in such sleds,[73] which has already demonstrated the influence of female posture on the vertebral kinematics for the VIVA model.[13]

2.8 Identification of Tissue-Level Injury in HBMs

The assessment of neck injury risk in ATDs and models is traditionally achieved using injury risk criteria. Over the years, different criteria were proposed: the Neck Injury Criterion (NIC), based on spinal cord damage and pressure gradients is calculated with accelerations and velocities of C1 and T1; the intervertebral Neck Injury Criterion (IV-NIC), is defined as the intervertebral motion divided by the physiological range of motion (ROM); the N_{ij} injury criterion, based on a combination of the axial force and the bending moment in frontal impacts; the Nkm, based on an combination of the shear force and the bending moment in rear impacts; the Lower-Neck Load

Index (LNL), based on the loads at the T1 related to facet joint injury; and the Neck Displacement Criterion (NDC), based on graphs of the angular velocity and displacement of the head relative to the T1.[117] Besides the listed more traditionally used criteria, there are many other proposed injury criteria for the neck in the literature, such as the modified N_{ij},[118] criteria based on individual forces and moments,[119] and criteria based on Displacements.[120]

From these criteria, NIC, N_{ij} and N_{km} were the most used in the literature. NIC was based on the hypothesis that pressure gradients caused by a sudden change in the fluid flow correlated with spinal ganglia cell injury in animal tests.[121] The measured pressures were mapped to the acceleration and velocity of C1 relative to T1. The damage threshold identified in the original study was NIC = 15, but also a lower pain threshold was defined as NIC = 10, and the lowest symptom threshold was NIC = 8.[117] Nevertheless, the NIC has shown some limitations. The peak NIC and the peak pressure gradient timing in PMHS were slightly different,[122] NIC was less sensitive to the differences in impact severity and segment motion compared to other injury criteria[120,123] and everyday activities can present a high NIC value.[124] The NIC equation is:

$$NIC = 0.2 * a + v^2 \qquad (1)$$

Where a is the relative horizontal acceleration between T1 and C1, v is the relative horizontal velocity between T1 and C1, and 0.2 is the approximate neck length.

The N_{ij} was proposed to assess severe neck injuries from frontal impacts through compressive load and moment measured at the occipital condyle.[125] The latest correlation between N_{ij} and the injury risk was determined based on porcine data, but historically, volunteer and PMHS data were used.[126] The injury threshold is N_{ij} = 1 based on the equation:

$$N_{ij} = \frac{F_z}{F_{int}} + \frac{M_y}{M_{int}} \qquad (2)$$

Where F_z is the axial force, M_y is the sagittal bending moment, F_{int} is the force intercept and M_{int} is the moment intercept. The force and moment intercepts are normalization constants. N_{ij} also presented some limitations. The loads were not representative of other injury scenarios, such as low-severity rear impacts[127] and eccentric compression.[128] A simulation of a real-life accident showing upper cervical injury did not cross the N_{ij} threshold,[129] and different ATDs and models require different intercepts.

N_{km} is a modification of N_{ij} to assess soft tissue injuries in rear impacts. The N_{km} is calculated by a combination of shear forces acting in the sagittal direction and bending moments measured at the occipital condyles.[127] The injury threshold is $N_{km} = 1$ based on the equation:

$$N_{km} = \frac{F_x}{F_{int}} + \frac{M_y}{M_{int}} \qquad (3)$$

Where F_x is the shear force. N_{km} also presented some limitations. Similar to N_{ij} the loads are not representative of other injury scenarios, and a simulation of a real-life accident showing upper cervical injury did not cross the N_{km} threshold.[129]

The displacement-based criteria, like the IV-NIC, are an alternative to the criteria based on forces and moments as N_{ij} and N_{km}. IV-NIC have the advantage of being able to predict the intervertebral level mode, severity, and time of soft tissue neck injuries,[130] but it is not applicable to ATDs due to the lack of vertebrae. As the IV-NIC is the ratio between the vertebral rotation and the ROM, the injury thresholds are IV-NIC = 1 or IV-NIC = -1, depending on the direction of the rotation.

When assessing injury, one advantage of HBMs is the capability to estimate tissue-level response. One way to build upon this HBM advantage would be a direct relation of tissue strain to injury thresholds or injury risk probability. An alternative approach achievable in detailed HBM

is directly comparing the values of tissue loads to the experimental data on tissue failure. For example, an injury criterion relating to force and activation of 1D Hill-type elements was proposed by Nölle et al. 2022[131]. However, Nölle et al. 2022 criterion is not directly applicable to the GHBMC model due to the muscle implementation being a combination of 1D and 3D muscles.

Therefore, using an HBM with the appropriate geometry and material properties, the local tissue response can be accessed for impact scenarios and help understand the origin of symptoms in WAD. However, the damage and pain initiation thresholds of the tissues of interest must first be determined from experimental studies or indirect methods. For the current study, the main soft tissues of interest related to whiplash are the muscles, the ligaments and the IVDs. The cartilage of the facet joints and the nerve roots are also regions of interest for WAD;[17,132] yet, current models for these structures require further development before the local analysis of strains can generate representative results.[45,133]

As experimental data about muscle strains of volunteers in rear impacts was not found, a data set containing vertebral kinematics could help inform the soft tissue response of the model. The close relation among bones and attached soft tissue suggests that, assuming material models and geometries with enough detail are implemented in the model, the biofidelic motion of the vertebrae would produce biofidelic muscle strains in a simulation. The study conducted by Sato et al. 2014[73] with 4 young adult males recorded vertebral kinematics during low-severity rear impacts and, therefore, could be used to verify a model at such a local level.

Previous experiments have been conducted to identify damage mechanisms in soft tissues. Living rabbit muscles were tested by clamping the tendons and axially tensioning them, measuring the failure strains for different activation and stretching rate levels. The maximum failure strains for the tested tibialis anterior muscles without activation can be approximated to 0.6 for any of the

tested rates,[47] while the active muscle started failing at a 0.38 strain, depending on the activation level.[46] The lowest failure strain identified was approximately 0.23 for the extensor digitorum longus muscle.[46] Similarly, different cervical ligaments from 16 cadavers were also tested in tension with different stretch rates, resulting in failure strains from 0.40 for the interspinous ligament at medium rates (20 1/s) to 1.15 for the anterior longitudinal ligament at quasi-static rates (0.5 1/s) (Table 2).[48] Several studies were conducted to observe the mechanical properties of the IVD. Usually, functional spinal units comprising two vertebrae, the ligaments and the IVD between them were subjected to different combinations and magnitudes of load. From the experiments, the annulus fibrosus average circumferential failure strain was determined as 0.3.[49]

Table 2: Strain failures for different strain rates for the neck ligaments presented by Mattucci et al. 2012

Presented by Ligament	Rate (1/s)	Failure strain
Anterior longitudinal ligament	0.05	1.15
	20	0.93
	150-250	0.9
Posterior longitudinal ligament	0.05	0.76
	20	0.73
	150-250	0.65
Capsular ligament	0.05	0.97
	20	1.12
	150-250	1.11
Ligamentum flavum	0.05	0.62
	20	0.58
	150-250	0.52
Interspinous ligament	0.05	0.65
	20	0.4
	150-250	0.45

Comparing the experimental data indicating soft tissue failure to simulated strains will help to inform the possibility of injury, the mechanism of injury and possible regions for improvement in the model.

3 Development and Validation of a Novel Closed-Loop Muscle Controller Based on the Reflex Mechanisms of the Neck to Approximate the Response of Live Humans.

3.1 Introduction

As discussed in the previous chapters, the cervical reflexes are critical for head and neck stabilization, particularly under impact conditions, influencing spinal stiffness and injury risk. Muscle activation during impacts cannot be replicated accurately by PMHS and ATDs. However, HBMs that incorporate both passive and active muscle elements, such as the GHBMC, can simulate these effects. Open-loop controllers were traditionally used to control muscle activation in HBMs, but usually require going through a new optimization process for every new impact scenario. Closed-loop controllers, guided by natural reflexes like the VCR and CCR, can offer a more adaptable solution, mitigating the need for rework from open-loop controllers.

The study presented in the current chapter aimed to develop a single closed-loop controller for neck muscle activation for the GHBMC 50th percentile male model based on known reflex mechanisms and assess how this approach compares to current open-loop controllers across a range of impact directions and severities. Controller parameters were optimized using volunteer data and independently assessed across twelve impact conditions. The kinematics from the closed-loop controller simulations presented a good correlation to the experimental data. The incorporation of the reflex mechanisms using a closed-loop controller can provide robust performance for a range of impact directions and severities, which is critical to improving HBM response under a larger spectrum of automotive impact simulations.

Chapter 3 is extracted (with small adaptations) from Correia, M. A., McLachlin, S. D. & Cronin, D. S. Vestibulocollic and Cervicocollic Muscle Reflexes in a Finite Element Neck Model During Multidirectional Impacts. *Ann Biomed Eng* **49**, 1645–1656 (2021).

3.2 Methods

The head and neck of a validated average male detailed HBM (M50-O v5.1, 50th percentile, GHBMC) were extracted for the purposes of assessing the activation controller. The extracted model included the neck musculature, represented by passive 3D and active 1D Hill-type elements, the cervical vertebrae (C1 to C7), the first thoracic vertebra (T1), cervical spine ligaments, IVDs, and the skin. The cervical muscles in the model were grouped into four sets according to the respective anatomical region: the left extensors, the right extensors, the left flexors, and the right flexors (Figure 14). The axis system used as the global frame of reference had the X-direction pointing forward, the Y-direction pointing to the left, and the Z-direction pointing downwards (Figure 9).

Nine different frontal impact severities were simulated, ranging from 2 g to 15 g, corresponding to the NBDL volunteer frontal impact sled test maximum accelerations,[69,134] for a total duration of 250 ms. The NBDL experimental head kinematics were reported for individual cases; in the current study, head kinematics were averaged for all test subjects for a specific sled acceleration for comparison to the model output. The average response and standard deviation (SD) for each impact severity were calculated using point-wise analysis for each impact severity.[82] The average linear forward X-acceleration and Y-rotational displacement measured at the first thoracic vertebra (T1) in the volunteer experiments were applied to T1 in the model.

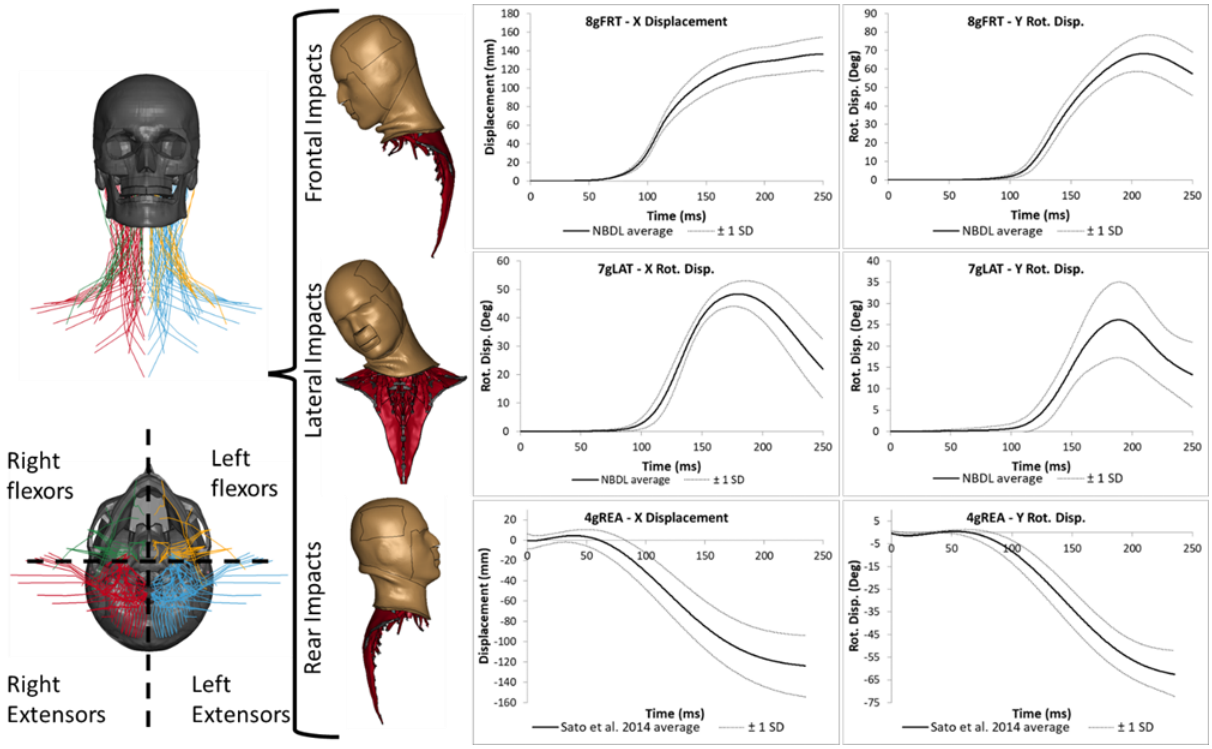


Figure 14: Summary of impact simulations

Four muscle groups (left/right flexors and left/right extensors) were used to simulate frontal, lateral, and rear impacts over a range of severities (2 g-15 g) and compared to the volunteer experimental data (plots).

Four different lateral impact severities were simulated, ranging from 4 g to 7 g, corresponding to the NBDL volunteer lateral impact sled test maximum accelerations,[69,134] for a total duration of 250 ms. The average right-to-left Y-velocity and X-rotational displacement measured at the first thoracic vertebra (T1) in the volunteer experiments were applied to T1 in the model.

Sato et al, 2014 presented two experiments with rear impact severities of 3 g and 4 g, corresponding to sled test accelerations from 12 male volunteers,[73] for a total duration of 235 ms. The average linear rearward X-acceleration, Z-acceleration, and Y-rotational displacement

measured at the first thoracic vertebra (T1) in the volunteer experiments were applied to T1 in the model.

3.2.1 Closed-Loop Muscle Activation Implementation

As previous literature demonstrated the good potential for PID and PD controllers to model muscle activation,[93,135] a scheme embedding two PD controllers (Figure 15) was investigated to represent the VCR and CCR reflexes for multiple impact cases for the first time. The VCR and CCR controllers were based on experiments with cats, monkeys and humans.[92,96,97,136]

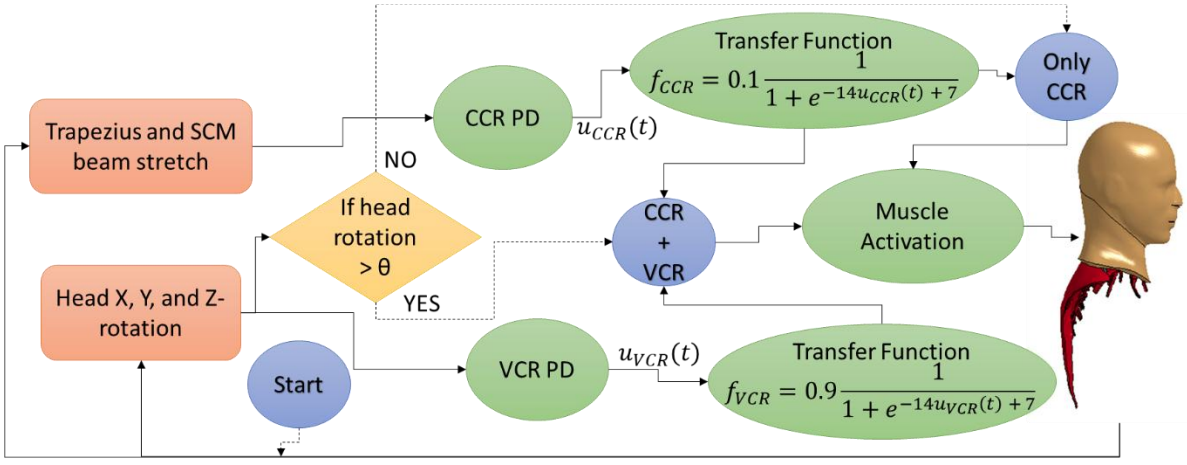


Figure 15: Schematics for the closed-loop controller
The flowchart demonstrates the CCR and VCR PD controllers and the summation of responses. The controller selects between CCR and CCR+VCR activation (yellow) for each time step using IF functions implemented in the controller.

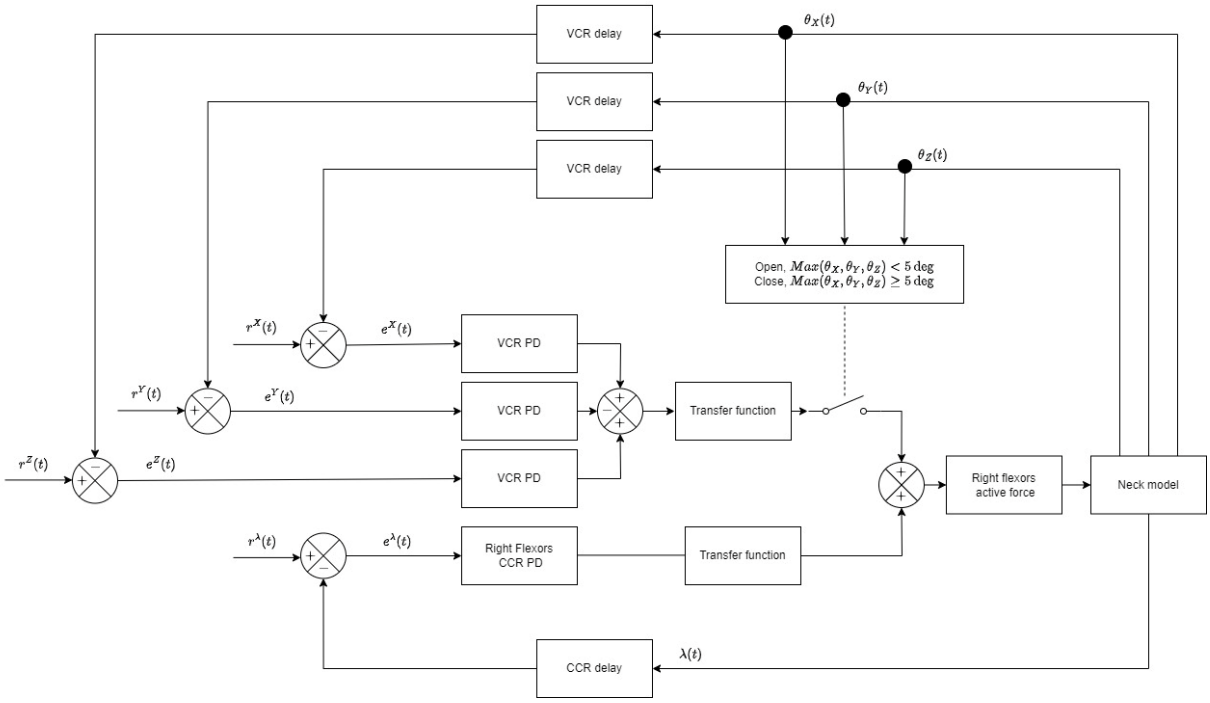


Figure 16: Block diagram of the closed-loop controller for the right flexors

The r values are reference quantities (equal to zero, in all cases during this study), the e values are the errors used as input to the PD controllers, the θ values are the head rotation in the three axes and λ is the muscle stretch. Similar configurations controlled the other three muscle groups. For each muscle group, the signals of the VCR PD outputs were adjusted accordingly to the muscles acting antagonistically or not in relation to the direction of head rotation.

The VCR system was represented by a PD controller that monitored head rotational displacements as input, while the CCR system was represented by a second PD controller that used muscle stretch as input. The input of the CCR was the sum of the stretches of all active Hill-type beam elements in series at the medial portion of the muscle with the highest volume (capable of producing the highest force) of each muscle group (Figure 17).

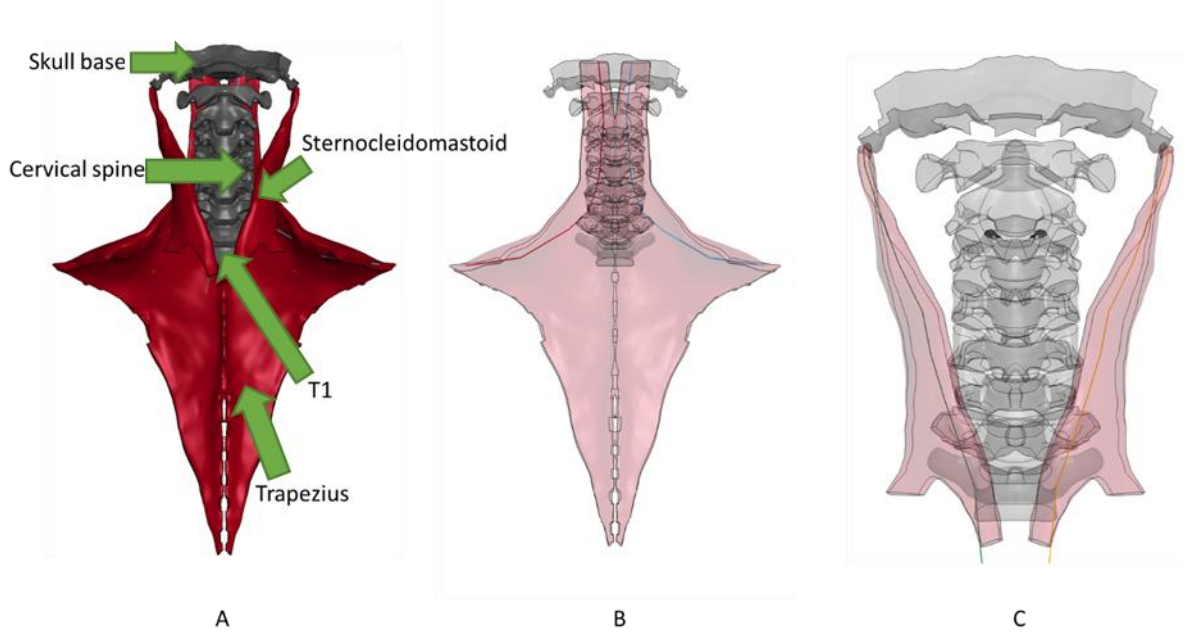


Figure 17: Muscle elements used as input for the controller

A) Frontal view of the sternocleidomastoid, trapezius, cervical spine, T1 and base of the skull. B) Active muscle fibres (coloured lines inside the trapezius) are used as input for the CCR portion of the control for the extensors. C) Active muscle fibres (coloured lines inside the sternocleidomastoid) are used as input for the CCR portion of the control for the flexors.

These elements were selected after observing which region had the highest deformation in frontal and rear impact simulations, representing the largest expected CCR neuronal signal. The modelled CCR response followed experiments conducted in decerebrated cats showing that the CCR is activated in two stages, a fast initial response and a slower later response that can be related to the head rotation magnitude (θ) (Figure 18).[96]

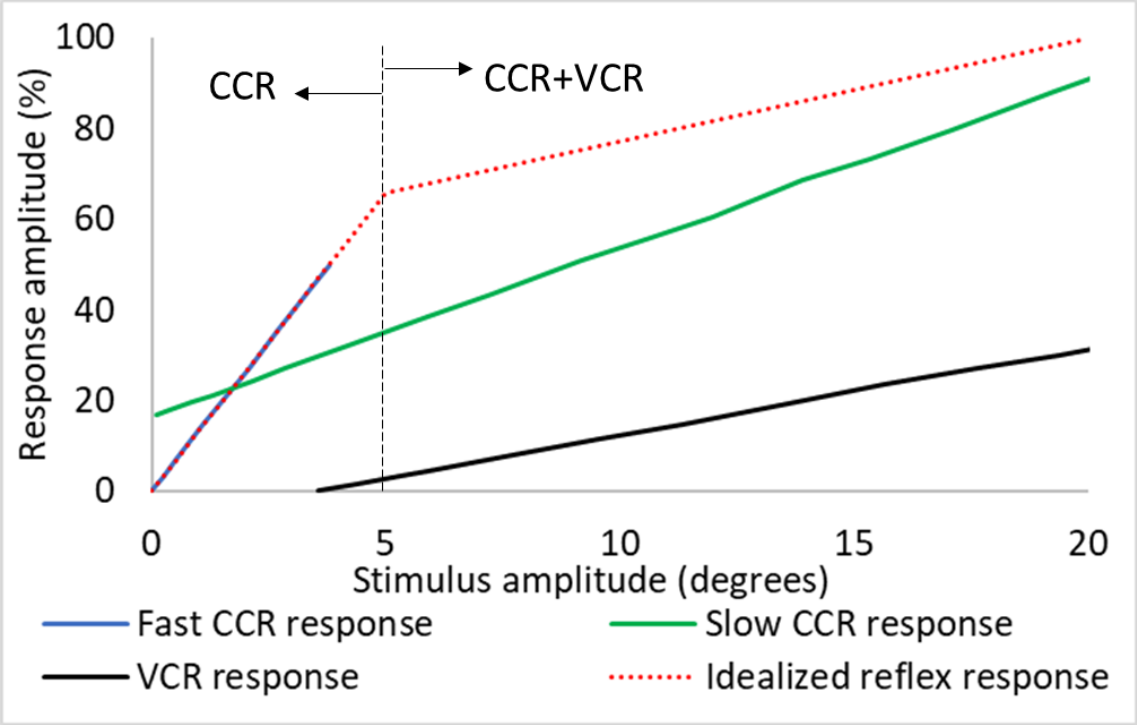


Figure 18: Reflex response amplitude versus stimulus amplitude

Curve fit (solid lines) to the experimental data for muscle activation, based on EMG measurements (response) from the literature,[96] due to the CCR and VCR versus the head rotation angle (stimulus). In addition, an idealized response (dotted line) for the closed-loop controller is shown. Before a head rotation angle of approximately 5 degrees is reached, mainly CCR is active, after which a combination of VCR and CCR is active.

Using MATLAB Simulink (Mathworks, Natick, MA, USA), the VCR and CCR PD parameters were simultaneously calibrated to the OMA activation curves for three frontal impact cases (2 g, 8 g, and 15 g). The experimental head rotation and simulated OMA muscle stretch from a previous study[37] were defined as the controller input signals. The three frontal impact scenarios were examined simultaneously, and the PD controller parameters were identified based on minimizing the average mean square error between the resultant PD controllers and OMA activation curves. It is important to note that the controller was not calibrated to a single impact scenario, and therefore, during the calibration process, it was not expected to precisely match any

one of the OMA curves. For the VCR, the proportional gain obtained through this methodology was 0.29, and the derivative gain was equal to 1.4. For the CCR, the proportional gain was 0.05, and the derivative gain was equal to 0.

As the idealized curve of the reflex mechanisms shows (Figure 18), the closed-loop controller needs to select if (1) only the CCR is active or (2) if both the CCR and VCR are active together. A study on decerebrated cats (i.e. no CCR response) identified that the VCR started responding after a head rotation of around 5°.[96] Based on this physiological separation of the VCR and CCR, the controller was designed such that if the head rotation measured in all three axes was lower than 5°, only the CCR was actuating. For angles greater than 5°, the CCR and VCR responses were both active. However, the maximum contribution of the CCR to muscle activation was limited to 10% (f_{CCR}, Figure 15), based on the lowest activation magnitude from the OMA.[37] The VCR could provide a maximum of 90% muscle activation, so that the total maximum activation was 100%.

Previously, it was shown that maintaining an activation ratio of 1:5 between the extensor and flexor muscles improved the kinematic response of the model.[37] Thus, in the current model, the CCR and VCR contribution for the flexors was multiplied by five to maintain this ratio, so that the overall contribution of the flexors to the activation strategy was similar to the extensors. Each one of the four muscle groups received a specific input from the controller based on the change in length of the particular fibres within the monitored muscle. The VCR gains were positive for the antagonistic muscle groups, relative to the head rotation, and negative for the agonists. The CCR gains were positive for the lengthening and shortening of the muscles relative to the resting length.

For each of the impact scenarios (Table 1), the proposed closed-loop activation (CLA) scheme was compared to three open-loop activation schemes previously presented in the literature (MMA, CMA, and OMA).[37]

Table 3: Simulated impact cases with activation schemes, peak sled accelerations, and experimental data sets representing frontal, lateral and rear impact conditions.

Case nomenclature	Muscle activation schemes	Peak sled acceleration (g)	Experimental Data
Frontal (FRT)	Closed-loop: CLA Open-loop: MMA, CMA, OMA	2, 3, 6, 8, 10, 12, 13, 14, 15	NBDL[68,69]
Lateral (LAT)	Closed-loop: CLA Open-loop: MMA, CMA, OMA	4, 5, 6, 7	NBDL[68,69]
Rear (REA)	Closed-loop: CLA Open-loop: MMA, CMA, OMA	3, 4	Sato et al., 2014[73]

The comparison considered the head CoG X-linear displacement, Z-linear displacements, Y-rotation and their respective accelerations for the frontal impacts. The rear impacts used the same parameters except for the Y acceleration due to the absence of this data from the study and large uncertainties when deriving it from the rotation. For the lateral impacts, X, Y and Z rotation and angular accelerations were used. The comparison between the head kinematics from the activation schemes and the experimental data was determined using correlation analysis (CORA, Partnership for Dummy Technology and Biomechanics, R. 3.6.1, Germany). The correlation rating was calculated as an average of the individual scores for each kinematic parameter measured from the simulation. These individual scores have considered a corridor rating (C) and a cross-correlation rating with equivalent weights. The corridors were defined as one and two SDs from the experimental data. The cross-correlation rating, on the other hand, was calculated as a weighted

average of the response phase (P), shape (V) and size (S). Their respective values, taken from previous literature weights, were Gp = 0.25, Gv = 0.50 and Gs = 0.25.[37,82,137]

$$\boldsymbol{Correlation\ rating} = \frac{\mathbf{1}}{\mathbf{2}}.\boldsymbol{C} + \frac{\mathbf{1}}{\mathbf{2}}.\left(\boldsymbol{G_v}.\boldsymbol{V} + \boldsymbol{G_s}.\boldsymbol{S} + \boldsymbol{G_p}.\boldsymbol{P}\right) \qquad (\mathbf{1})$$

3.3 Results

The head kinematics obtained for the proposed CLA activation model, for each frontal impact direction and acceleration, were extracted and compared to the human volunteer test results as well as the three open-loop activation schemes (MMA, CMA, OMA) (Figure 19).

The head kinematics resulting from the CLA presented an average correlation rating among the impact severities of 0.667 for frontal cases, 0.777 for lateral cases, and 0.690 for rear cases (

Figure 20), comparable to the respective correlation values of 0.691, 0.753, and 0.703 for the open-loop CMA results. Average correlation results for all impact cases were within 2% for the CLA (0.699) and CMA (0.709) muscle activation strategies.

The average correlation of the CMA was 9% lower than that of the OMA, where the latter strategy represented the highest possible correlation for the model since the open-loop activation parameters were calibrated for individual impact cases. The MMA presented the lowest average correlation for all impact scenarios, which may be expected since this method was not calibrated or optimized to the experimental data.

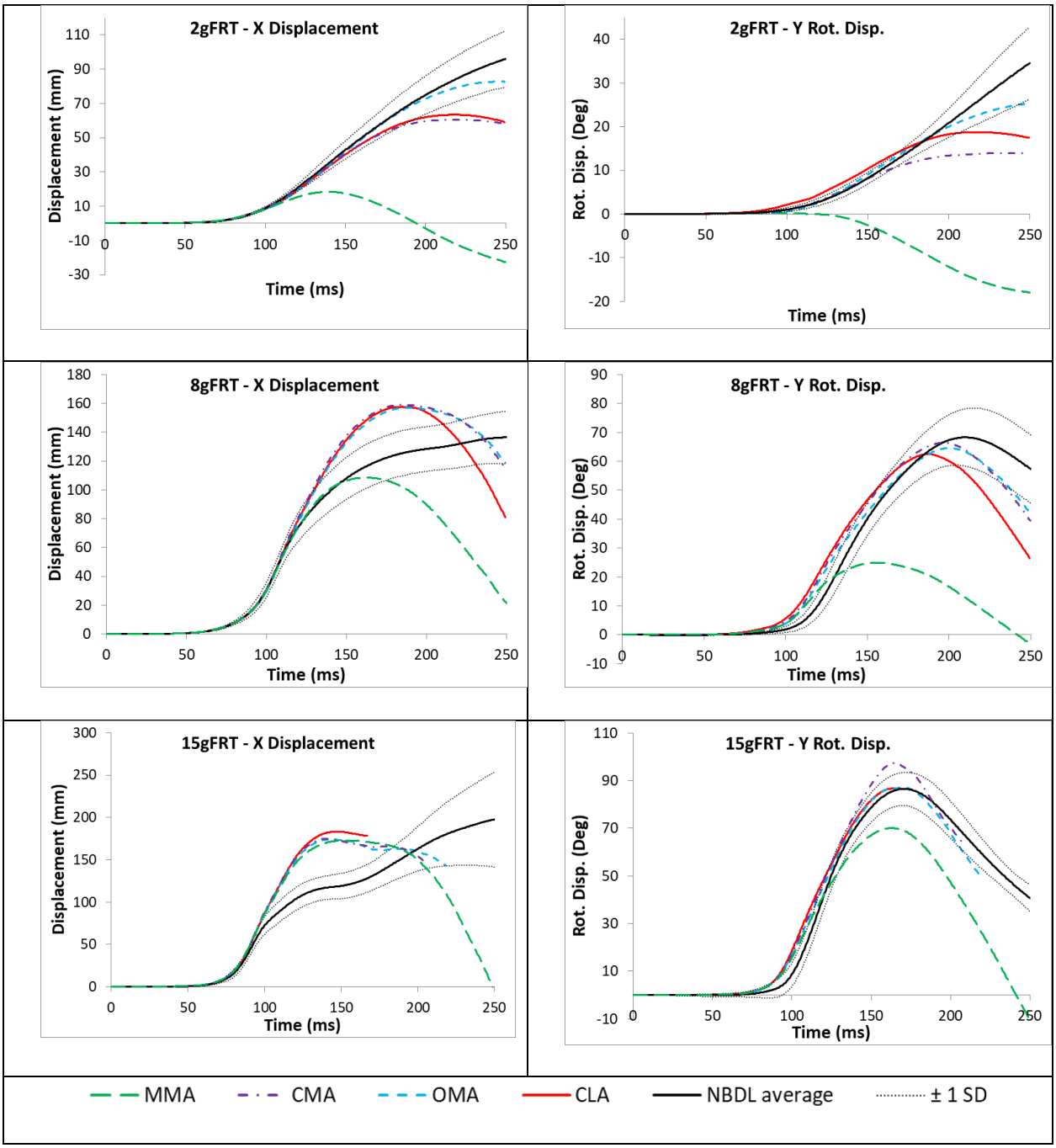
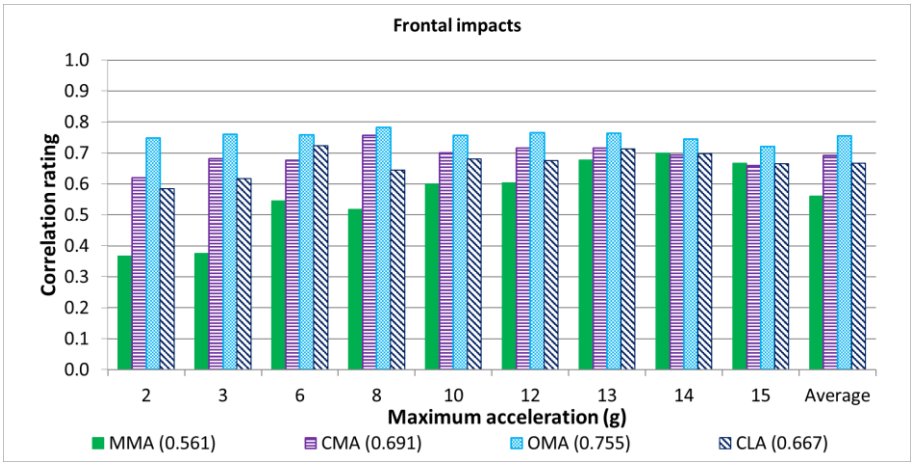
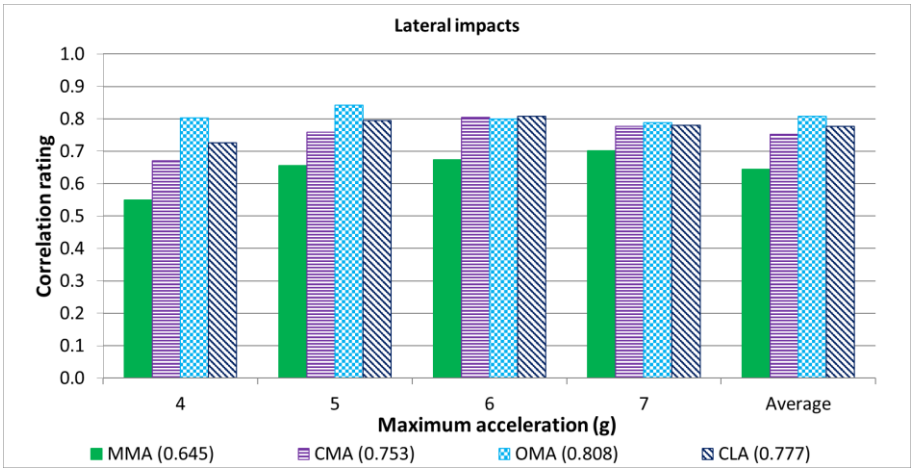


Figure 19: Head kinematics from frontal impacts

Comparison of the frontal impact head kinematics for the proposed CLA compared to the NBDL human volunteer test data average and SD. MMA, CMA, and OMA results are included for reference. The early interruption of the curves for the 15g impact is a result of bone fracture in the model.





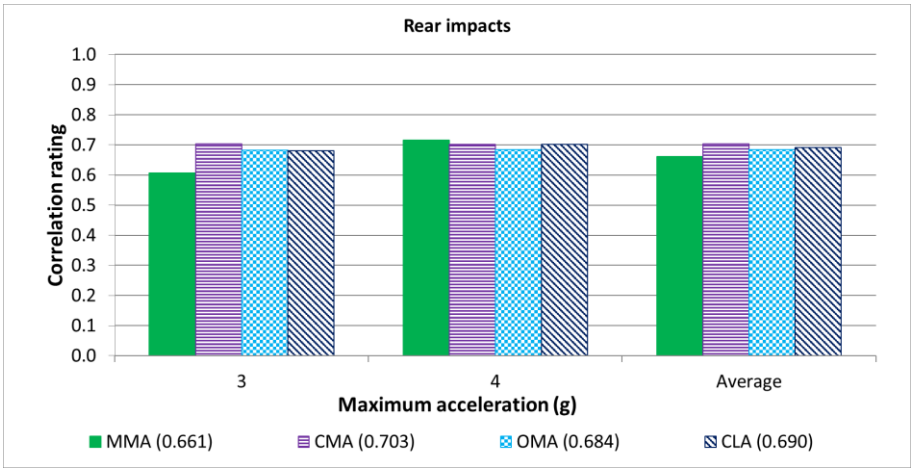


Figure 20: Comparison of the activation schemes

Correlation ratings for the muscle activation schemes (MMA, CMA, OMA, CLA) in frontal, lateral, and rear impacts. The average correlation rating for all cases is shown in brackets.

3.4 Discussion

Implementation of the head rotation (VCR) and muscle stretch (CCR) reflex responses in a closed-loop muscle controller demonstrated effective performance for simulating neck muscle activation across a broad range of impact scenarios, considering different impact directions and severities. In addition, this was the first study to examine a closed-loop controller for muscle activation over a wide range of impact severities and directions. The CLA scheme developed in this work produced similar head kinematics results to the open-loop CMA scheme.[37] As a single open-loop activation strategy, CMA was based on a known reflex mechanism, compared to the OMA, which used a specific activation strategy for each impact case, representing the maximum possible correlation for a given impact direction and severity.

The CLA scheme with two PD controllers resulted in an initial activation of the flexors, followed by the activation of the extensors, which was observed in frontal and rear impacts with volunteers.[61,66,98,138] However, the opposite was also observed in frontal impacts.[61,62] The order of activation of flexors and extensors was attributed to the CCR reflex implementation that activated the flexors even when they were shortening. The overall CLA correlation was comparable to the CMA but lower than that of the OMA. The calibration of the control parameters using the three frontal impact cases resulted in performance trade-offs; therefore, the CLA activation could not match the correlation rating of the OMA for these specific accelerations. The PD controller is a linear simplification of a complex non-linear reflex system. Although previous studies have identified that a PD controller can generate good approximations of individual impact cases[13], it is evident that these controller parameters would need to be optimized for different impact scenarios. To address this concern, the current study optimized the controller parameters across a wider range

of impact severities (2 g to 15 g) and subsequently examined the controller performance across 12 uncalibrated impact conditions.

The CLA also resulted in an activation onset time of up to 90 ms relative to the 74 ms of the CMA and MMA for the lower severity impacts. For context, the range of activation times of the trapezius and sternocleidomastoid reported in the literature varies from 55 to 99 ms in impact tests.[37] Implementing delays in the activation can approximate the neuronal delays in the reflex mechanisms, but the PD parameters also control the activation timing. Therefore, the neuronal delay in this study was considered to be integrated within the PD controller, and the overall activation time fell within the range of values presented in the literature. Nevertheless, it is important to note that the derivative gain of the CCR controller was zero, indicating a low sensitivity to the rate effects of the muscle stretch.

The CLA scheme presented similar kinematics to the CMA in rear impacts and better-correlated kinematics than the CMA in lateral impacts, which indicates that the model is stable and functional in a variety of impact directions. Furthermore, even with the use of simplified muscle grouping, the CLA obtained a reasonable response in complex cases such as lateral impacts.

For frontal impacts, the lowest correlation ratings were obtained in the cases with the lowest accelerations. This result was consistent for open-loop activation and CLA strategies and may be the result of the skin and adipose tissue having overly stiff properties. The model includes material properties from porcine tissue, which has been suggested to have a stiffer response to shear than the equivalent human tissues.[139] Such findings demonstrate that control parameters and muscle activation strategies may be somewhat model-specific, with no single set of idealized parameters for HBMs in general.

There were three main limitations identified in the present study. First, the stiffness of the soft tissues (skin and adipose tissue) could have increased the effective stiffness of the neck and affected the resulting global head kinematics, particularly for lower-severity impacts. Second, the input of the CCR PD controller (muscle stretch) was taken from a specific row of active Hill-type elements in the midsection of the largest muscle in each muscle group, which may delay or change the activation magnitude in movements that do not stretch this specific muscle region. While not investigated in this study, interactions with seatbelts or a seat headrest may alter the distribution of deformation within the neck and could affect the resulting muscle activation. Third, individual motor units within each muscle are activated independently by a motor neuron, while the model activates a whole muscle group with a unique input. However, the resultant head kinematics found in this study indicated adequate approximation for this global analysis as well as reasonable performance trends within the respective muscle groups. The method of using the stretch of the active Hill-type elements of the muscles and head rotation as the input of a CCR and VCR controllers, respectively, could be improved in future work through higher muscle group discretization and thorough optimization of the controller parameters. However, the presented results indicate that the application of a single controller calibrated only for a few impact cases generated reasonable head kinematics for impacts in three directions and over a wide range of impact severities. As expected, the optimization methods, which were customized to a specific model and impact condition to produce the intended output, generated a response more closely resembling the experimental data. If the impact conditions, such as the severity, change, the controller parameters need to be re-optimized, which leads to a different set of parameters for each case. Importantly, with the current interest in out-of-position impacts, autonomous braking, and different car seat orientations, the effective performance of the more flexible closed-loop

controller, which is based on known physiological mechanisms, is advantageous for these scenarios involving atypical boundary conditions without supporting experimental data for model optimization.

The controller of the muscle activation was based on the phenomenology of the neck reflex mechanism. It is expected that the controller could be applied to models with different anthropometrics, like a female model, without the necessity of major changes, as the mechanism of the reflex is not based on any specific geometry. However, reflex characteristics are variable among the population, for example, due to physical fitness and ageing, which could potentially significantly change the controller parameters. In addition, the reflex was based on the assumption of an unexpected impact and awareness before the impact would need a new controller equation to take the intentionality of the subject into consideration.

The proposed closed-loop controller obtained similar kinematics to current commercial implementations of the CMA open-loop activation in multiple directions and impact severities, while also representing known muscle reflex mechanisms. The new controller may also provide an improved response in multi-directional impact scenarios, which will be the focus of future studies. Importantly, the inclusion of the new closed-loop controller did not significantly increase the computational time of the model, demonstrating a computationally effective solution for multidirectional impacts.

3.5 Conclusion

The present chapter aimed to develop a single closed-loop controller for neck muscle activation in a contemporary male HBM based on known reflex mechanisms and assess how this approach compares to current open-loop controllers across a range of impact directions and

severities. Controller parameters were optimized using volunteer data and independently assessed across twelve impact conditions. The kinematics from the closed-loop controller simulations showed a good average CORA rating to the experimental data (0.699) for the impacts following the ISO/TR9790 standard. Compared to the previously optimized open-loop activation strategy, the average difference was less than 9%. The incorporation of the reflex mechanisms using a closed-loop controller can provide robust performance for a range of impact directions and severities, which is critical to improving HBM response under a larger spectrum of automotive impact simulations.

4 Implementation of Muscle Pre-Tension and Neck Posture to Replicate Local Kinematics of the Vertebrae and Muscles in Rear Impacts

4.1 Introduction

As discussed in Chapters 1 and 2, WAD are common injuries caused by low-acceleration rear impacts. These injuries are affected by neck muscle behaviour and neck posture, though definitive injury mechanisms remain elusive. Studies suggest the injury may occur at the moment the neck is developing an S-shaped curvature during rear impacts. However, clinical imaging often cannot detect such injuries, and tissue-level data from impact events are challenging to obtain. HBMs have the potential to evaluate realistic tissue-level stress and strain as long as the local vertebral kinematics are comparable to those in real impacts. Current muscle models assume the tissues are at zero stress and strain at the start of the calculation. However, cadaveric measurements indicated that muscles in situ are not at their slack length, presenting some pre-tension. Therefore, quantifying the effect of physiological muscle pre-tension and posture on intervertebral kinematics could offer insights into the injury mechanisms underlying WAD.

The study presented in the current chapter used a detailed neck model subjected to simulated low-acceleration rear impact conditions to investigate the effect of pre-impact neck posture and muscle pre-tension on intervertebral kinematics and tissue-level response. An improved muscle path implementation enabled the modelling of muscle pre-tension using experimental muscle pre-stretch data determined from previous cadaver studies. Cadaveric neck impact tests and human volunteer tests with the corresponding cervical spine posture were simulated using a detailed neck model with the reported boundary conditions and no muscle activation. Computed intervertebral

Chapter 4 is extracted (with small adaptations) from Correia, M. A., Corrales, M. A., McLachlin, S. D. & Cronin, D. S. Effect of muscle pre-tension and pre-impact neck posture on the kinematic response of the cervical spine in simulated low-speed rear impacts. *Numer Methods Biomed Eng* **39**, e3761 (2023).

kinematics of the model with pre-tension achieved, for the first time, the S-shape behaviour of the neck observed in low severity rear impacts of both cadaver and volunteer studies. The current chapter provided a method to incorporate muscle pretension in HBM and quantified the importance of pre-tension in calculating tissue-level distractions.

4.2 Methods

Similar to the previous chapter, the head and neck regions were extracted from the GHBMC 50th percentile male detailed full body occupant model version 5.1 (M50). The head and neck model was used to assess intervertebral kinematics in low-acceleration rear impact conditions with no muscle activation, with boundary conditions applied at the first thoracic vertebra, following the methods presented by Barker and Cronin, 2021[82].

A novel methodology for applying muscle pre-tension was implemented in the model in addition to an improved muscle path methodology, and adjustment of the neck posture to match the experimental data. Two types of impact simulations were conducted with the improved models: one replicating the experiments with volunteers and another replicating cadaveric experiments. Finally, the intervertebral kinematics and muscle strains obtained from the simulations were compared to available experimental data.

4.2.1 Muscle Pre-Tension

Muscle pre-stretch was defined using the available literature by comparing measured average muscle length data from embalmed cadavers to the optimal length of the muscle. The optimal length of the muscle was assumed to be a close approximation to the slack length.

Therefore, the experimental slack muscle length (L_S) was defined as the optimal muscle length (L_O) presented in a cadaveric study for 50th-percentile males:[112]

$$L_O \cong L_s \quad (1)$$

The experimental in situ length (L_E) was defined as the muscle length measured in the same embalmed cadavers while still attached to the body.[112] The experimental stretch (λ_E) along the length of the muscle was defined for each muscle by dividing the experimental in situ length by the experimental slack length:

$$\lambda_E = \frac{L_E}{L_S} \cong \frac{L_E}{L_O} \quad (2)$$

The muscles in the M50 model were grouped into flexors and extensors (Table 4), and the stretches were averaged for each group. The average experimental stretch ($\overline{\lambda_E}$) was considered the same as the average modelled stretch ($\overline{\lambda_M}$):

$$\overline{\lambda_E} \cong \overline{\lambda_M} \quad (3)$$

Table 4: Flexor and Extensor muscles in the M50 neck model

Flexors	Extensor
Longus capitis	Oblique capitis inferior
Longus colli	Oblique capitis superior
Rectus capitis anterior	Rectus captis major
Rectus capitis lateral	Rectus captis minor
Anterior scalene	Iliocostalis cervicis
Middle scalene	Longissimus capitis
Posterior scalene	Longissimus cervicis
Sternocleidomastoid	Multifidus
Omohyoid	Semisplenius capitis
Sternohyoid	Semisplenius cervicis
	Splenius capitis
	Splenius cervicis
	Levator scapulae
	Rhomboid minor
	Trapezius

The in situ muscle lengths in the model (L_M) were defined as the lengths of the muscles in the M50. To enable stress initialization during the simulation, the modelled slack length (L_{SM}) was defined as:

$$L_{SM} = L_M \frac{L_O}{L_E} = L_M \frac{1}{\lambda_M} \quad (4)$$

Therefore, the L_{SM} can be obtained by simply scaling the M50 muscles. The modelled L_{SM} was implemented by applying it to the flexor and extensor groups through scaling on the Z-axis ($\frac{1}{\lambda_M}$). This direction, in general, coincided with the line of action of the muscles. Pre-stretch deformation in the other directions was not considered in this study due to a lack of experimental data. The value of $\frac{1}{\lambda_M}$ calculated for the flexors using the experimental data[112] was 0.92 (-8%), while for the extensors it was 0.97 (-3%). Therefore, the flexors were scaled to be shorter by -8% while the lengths of the extensors were reduced by -3% through this methodology (Figure 21). The pre-tension stress in the model was obtained by deforming the muscle from the slack length to the modelled in situ length.

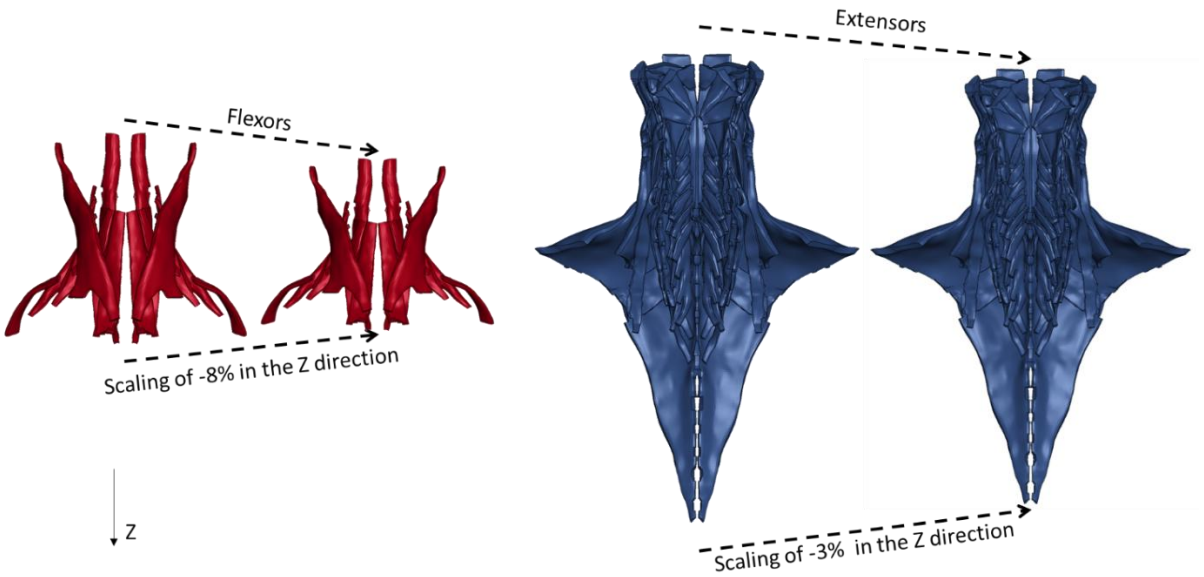


Figure 21: Muscle scaling process

Geometries of the flexors and extensors before and after the scaling process. The lengths of the flexor muscles were each scaled down by -8% in the Z direction, compared to a reduction of -3% for the extensors. The muscles before the scaling have lengths $L_{M,}$ and after the scaling down, they have new lengths L_{SM}.

4.2.2 Enhanced Muscle Path Implementation in the M50 Model

In the M50 neck model, the active musculature (1D Hill elements) was attached to the passive musculature (3D hexahedral elements) at discrete points (Figure 22a and Figure 22b), leading to strain concentrations at the coupling points. To maintain the muscle line of action in the M50 neck model, the active musculature elements were attached to the vertebra through supporting truss elements (Figure 22a), potentially affecting intervertebral kinematics. To address such limitations, a new approach ($M50_{CBS}$) was defined where the active and passive musculature were coupled together using a numerical constraint (the constrained beam-in-solid (CBS) method) as reported in a recent study.[5] To implement the CBS numerical constraint, the active muscle mesh in the $M50_{CBS}$ model was redefined to ensure that the active elements were embedded within the passive musculature with a mesh size that is similar to that of the passive muscle elements. The

redefinition of the active muscle mesh better represented the muscle line of action (Figure 22c) and led to a total of 12,238 1D Hill elements, compared to the 916 elements in the M50 neck model. The CBS method coupled the 1D elements inside the 3D passive elements through a user-defined number of points (four in this study) along the length of the active muscle elements (Figure 22b). The CBS method allowed for the removal of the non-physiological muscle support elements of the M50 neck model (Figure 22d). The cervical muscles in the model were not activated in any of the cases in the present study, to avoid the interference of this variable in the muscle strain measurements. Before, the cervical muscles in the model were grouped into four quadrants according to anatomical region: left flexors, right flexors, left extensors and right extensors. However, due to the sagittal symmetry in rear impacts, the current investigation only grouped them into two sets: extensors and flexors. The $M50_{CBS}$ without applying re-posturing or pre-tension was defined as the baseline model.

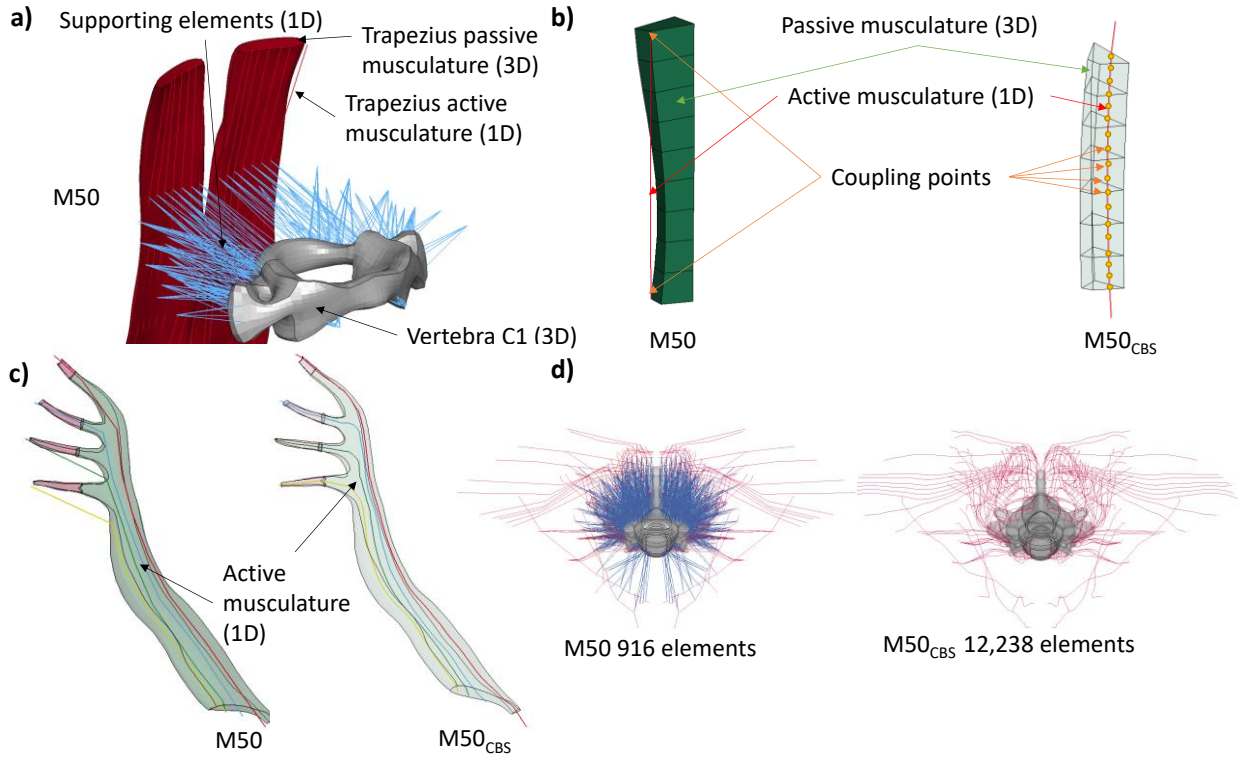


Figure 22: CBS implementation

a) M50 neck muscle with non-physiological support elements (blue) that are used to maintain the muscle pathways, b) discrete attachment points in the M50 model and the uniformly distributed attachment points in the $M50_{CBS}$, c) the improved line-of-action of the levator scapulae in the $M50_{CBS}$ compared to the M50 model and d) the M50 muscle coupling approach compared to the $M50_{CBS}$ muscle coupling approach.

4.2.3 Pre-impact Neck Model Reposturing

Previous studies have indicated that cervical spine posture can influence vertebral kinematics experienced during impacts.[24,33] The cervical spine posture of the $M50_{CBS}$ model was therefore adapted to replicate the boundary conditions for each impact condition. The C2 to C7 vertebrae (Figure 23) were re-postured without retaining stresses to reflect reported data from an average of 7 male MRI scans collected in a study using a similar seat to the one used during the rear impact sled tests with volunteers.[72] The repositioning of the model to the new postures was

conducted using the aforementioned vertebral positions as targets and PIPER software (piper-project.org),[140] using a methodology previously described in the literature.[16] The mesh quality of the re-postured model was maintained using a set of mesh enhancement tools[141] together with a methodology previously described.[16] After repositioning the C2-T1 vertebrae, the head was rotated so that the Frankfort plane was horizontal for the cadaveric data and 10° above the horizontal plane for the volunteer data, following the experimental methodology of each impact experiment.

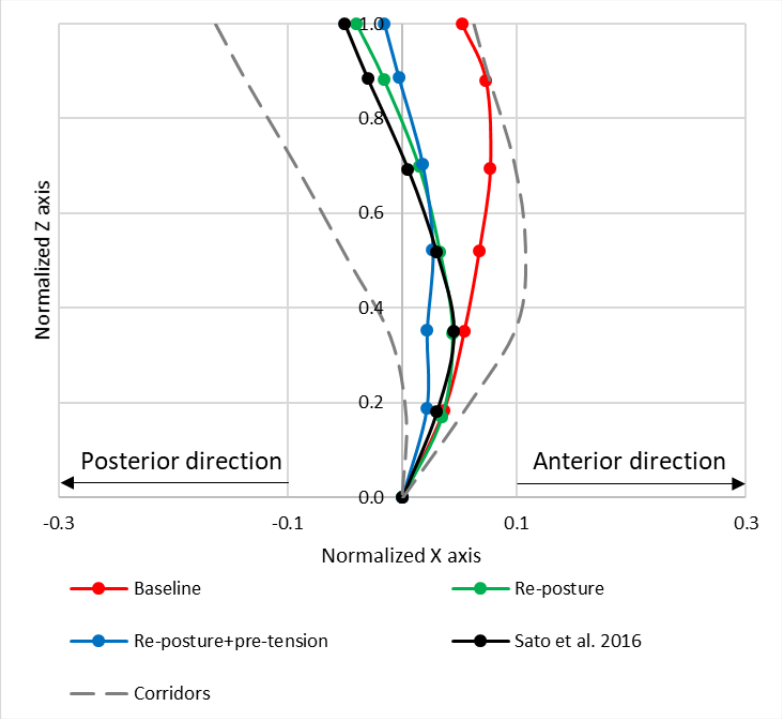


Figure 23: Simulated neck postures
Normalized position of C2 to T1 vertebral body geometric centers (solid markers) of the M50$_{CBS}$ baseline model, re-postured model, and re-postured model with pre-tension after a stabilization step (presented in the next section). T1 is at the origin, and the corridors were generated by normalizing and calculating the SD of the male data made available by Sato et al. 2016 for T1 to C2.

For the simulation of the volunteer rear impact tests, the default model value of 15° for the T1 angle was maintained since it was not clearly defined during the volunteer sled test study. The

T1 angle of 15° was within one SD of the range of T1 angles measured in volunteer seat postures with 20° inclinations, which was the same inclination used during the volunteer sled tests.[116]

For the cadaveric simulation, the T1 vertebra had an initial anterior inclination of 25° relative to the horizontal based on values measured during the cadaveric sled tests.[30] Additionally, for the cadaveric tests, the entire head and neck model was positioned to be consistent with the experiments.

4.2.4 Low-Acceleration Rear Impact Simulations

Low-acceleration rear impact simulations were carried out in three steps to accommodate the muscle pre-tension implementation (Figure 24). First, a stress initialization step using dynamic relaxation was run to statically define the initial stresses due to the deformations of the muscle from the modelled slack length to the in situ length. Second, an explicit simulation was run with T1 fixed in place to reach a quasi-equilibrium state, due to the applied pre-tension from the muscle pre-stretch. The stabilization period was run for 200 ms, when the head acceleration was approximately 1g, due to gravity loading. Third, the rear impact boundary conditions were applied to T1, with a peak acceleration of 4 g in both cases. In the cadaveric cases, rear impact boundary conditions were applied for 110 ms, which matched the duration of the experiments. For the case of the volunteers, the data was analyzed for the first 150 ms because upper cervical flexion was only observed during this time frame in the experiments. Only the T1 X kinematics were applied for the cadaveric simulations, as the Y and Z directions were constrained in the experiments, while the T1 X, Y, and Z kinematics were used for the case with volunteers.

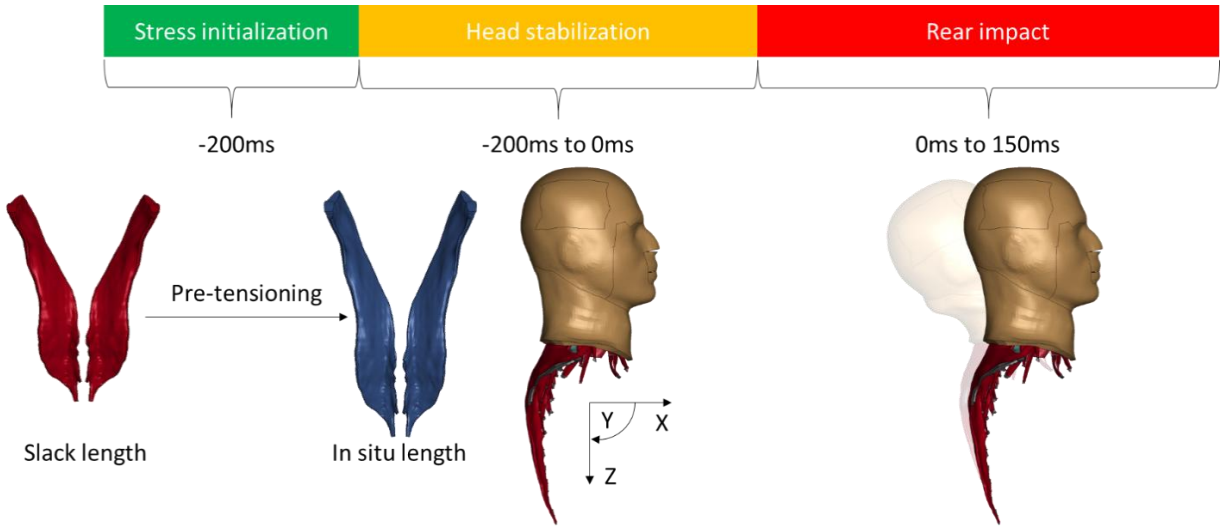


Figure 24: Rear impact simulation steps

The simulation steps were: stress initialization for the muscle pre-tension (dynamic relaxation), head stabilization to a quasi-equilibrium state (explicit simulation), and finally rear impact explicit simulation.

For the impact boundary conditions, the average X-displacement, Y-rotation and Z-displacement were applied to the T1 vertebra of the model to mimic the rear impact experiment with male volunteers.[73] The applied X-displacement was obtained by double integrating the X-acceleration presented in Sato et al. 2014[73]. The cadaveric experiments[30] were used as an initial check for the methodology, as the T1 boundary condition was simpler to replicate, and no muscle activation was present.

The resultant kinematics and 95th-percentile muscle strains were extracted and compared with the experimental data. The 95th percentile of the muscle strains was used as it mitigates the boundary effects in the tendon-muscle interface that potentially lead to unphysiological high strains.[142] The vertebral rotations were plotted at 25 ms intervals to observe the S-shape formation. All simulations were conducted using the M50$_{CBS}$ neck model solved using a commercial FE solver (LS-DYNA, R.9.3).

4.3 Results

The X-linear displacement and Y-rotation of the CoG of the head were extracted from the models of the volunteer impact simulations (Figure 25). The X-displacement and Y-rotational displacement of the head CoG in the models agreed with the experimental corridors. In addition, the effect of re-posturing and muscle pre-tension in the head CoG kinematics was modest, in agreement with recent studies[45] that have suggested that global metrics (e.g. head CoG kinematics) are generally not sensitive to model changes. However, the effect can be seen at the tissue level (e.g., vertebral kinematics and muscle strain).

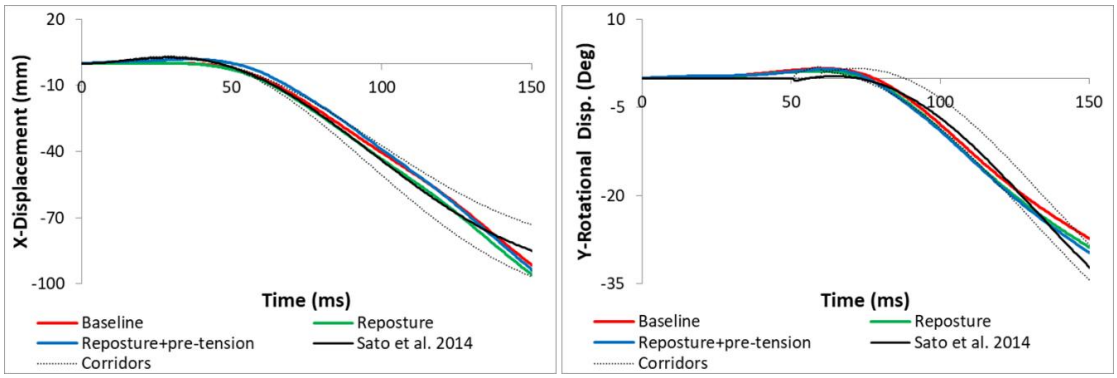


Figure 25: Simulated head kinematics for the rear impacts
Kinematics of the head CoG for the human volunteer 4g rear impact simulations. The X-displacement was calculated relative to T1. The corridors represent one SD from the average.

The intervertebral rotations were extracted from the model, from C2 to C7, for the cadaveric data (Figure 26). The values for C0(skull)/C1 were not plotted because, in the original study, experimental corridors for these segments were not reported. The cadaveric simulation with pre-tension presented an S-shape due to the higher C2/C3 joint flexion. The human volunteer simulation results (Figure 27) for C0 to C7 presented an S-shape up to 131 ms. For all the simulations, the C1/C2 joint presented a lower flexion compared to the experimental results, which was attributed to a high transverse ligament stiffness due to its simplified implementation.

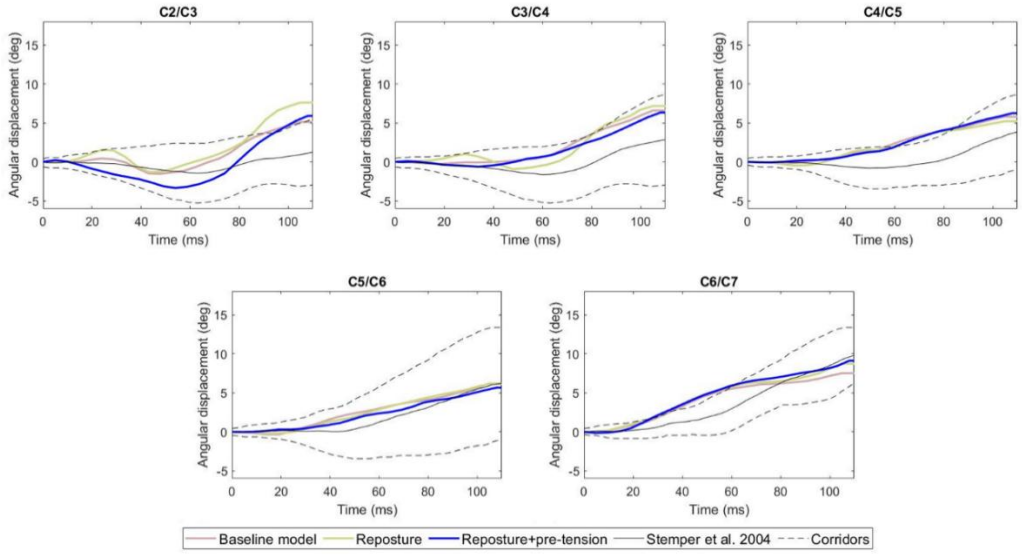


Figure 26: Intervertebral kinematics for the cadaveric specimen simulation

Intervertebral rotations from C2 to C7 for the simulated cadaveric rear impact, for three model conditions: baseline, re-postured model, and re-postured model with muscle pre-tension. The corridors represent one SD of the experimental data. The negative direction indicates flexion, and the positive direction indicates extension.

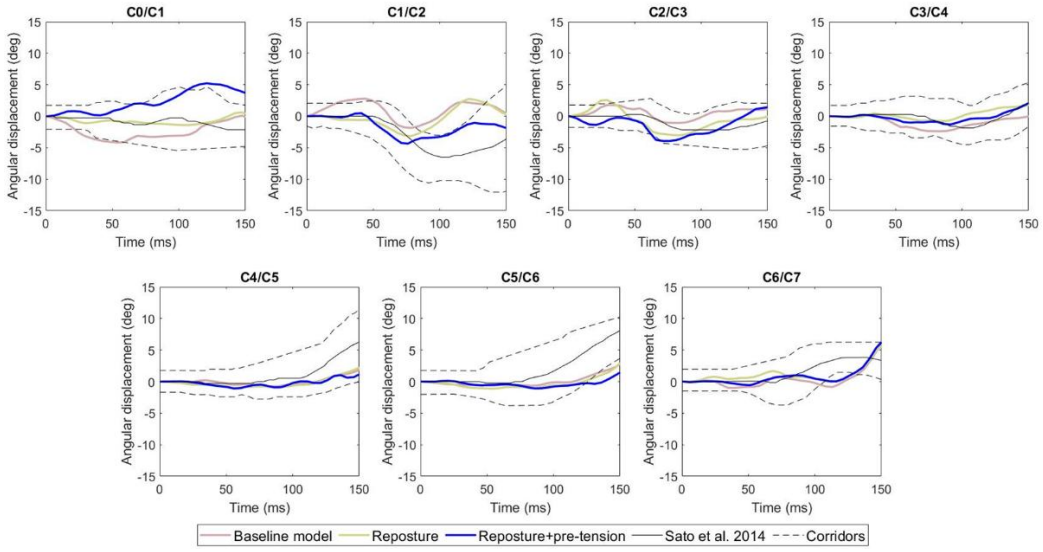


Figure 27: Intervertebral kinematics for the simulation of the volunteers

Intervertebral rotations from C0 (skull) to C7 for the human volunteer rear impact, for three model conditions: baseline, re-postured model, and re-postured model with muscle pre-tension. The corridors represent one SD of the experimental data. The negative direction indicates flexion, and the positive direction indicates extension.

It should be noted that upper cervical spine flexion and lower cervical spine extension were observed (Figure 29), demonstrating that the characteristic S-shape was only identified in the simulations for the re-postured case with muscle pre-tension (Figure 28). Overall, the joint kinematics also followed trends evident in the experimental response corridors.

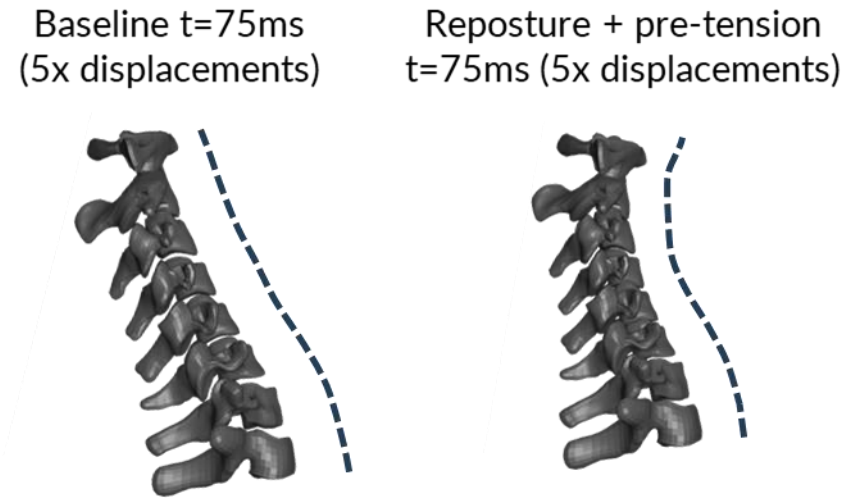


Figure 28: S-shape of the neck for the baseline and re-posture + pre-tension cases
The S-shape was subtle. Hence, the displacements were scaled by 5 times for better visualization in the figure. A similar S-shape to the experiments was obtained by the re-posture + pre-tension model because of a higher magnitude of upper cervical spine flexion.

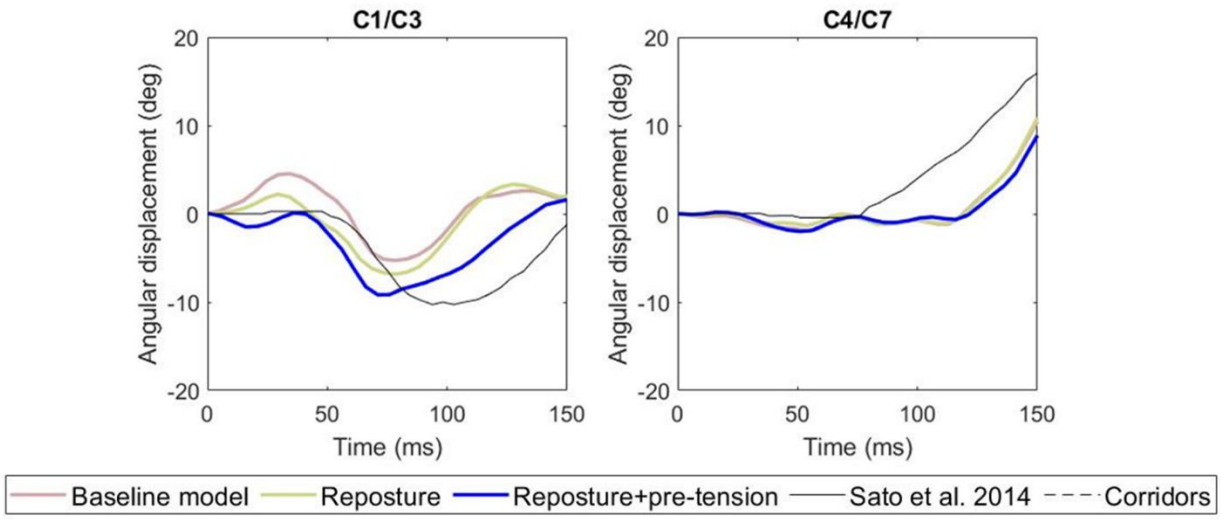


Figure 29: S-shape behaviour during the simulations

The expected S-shape behaviour was only achieved by the re-postured model with muscle pre-tension. The S-shape in the pre-tension model can be identified in the charts in the form of flexion of the upper cervical spine (C1/C4) from 0 to 131 ms. In contrast, the baseline and re-postured models presented extension prior to a brief flexion from 44 to 103 ms. The lower cervical spine (C4/C7) remained mostly neutral before the increase in extension at 122ms for all the models. Flexion is in the negative direction, and extension is in the positive direction.

The first principal strain distributions for the muscles were different among the models (Figure 30). For example, the 95th percentile maximum first principal strain was 0.20 for the model with pre-tension, 0.16 for the re-postured model without pre-tension and 0.15 for the baseline model (Figure 31).

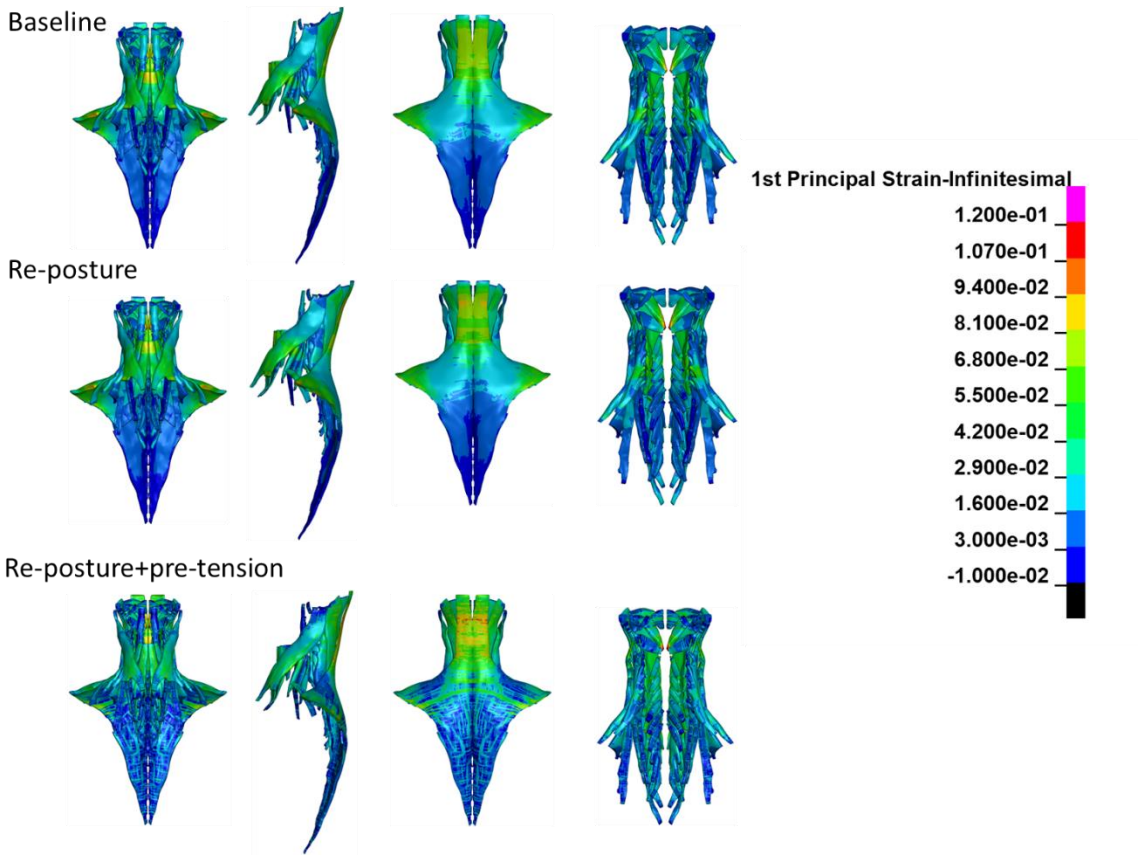


Figure 30: Muscle strain analysis for the simulations

Strain measurement for the baseline model, the re-postured model without pre-tension, and the re-postured model with pre-tension at 75 ms after impact onset, corresponding to peak flexion of the upper cervical spine. The last three images on the right present the deeper muscles.

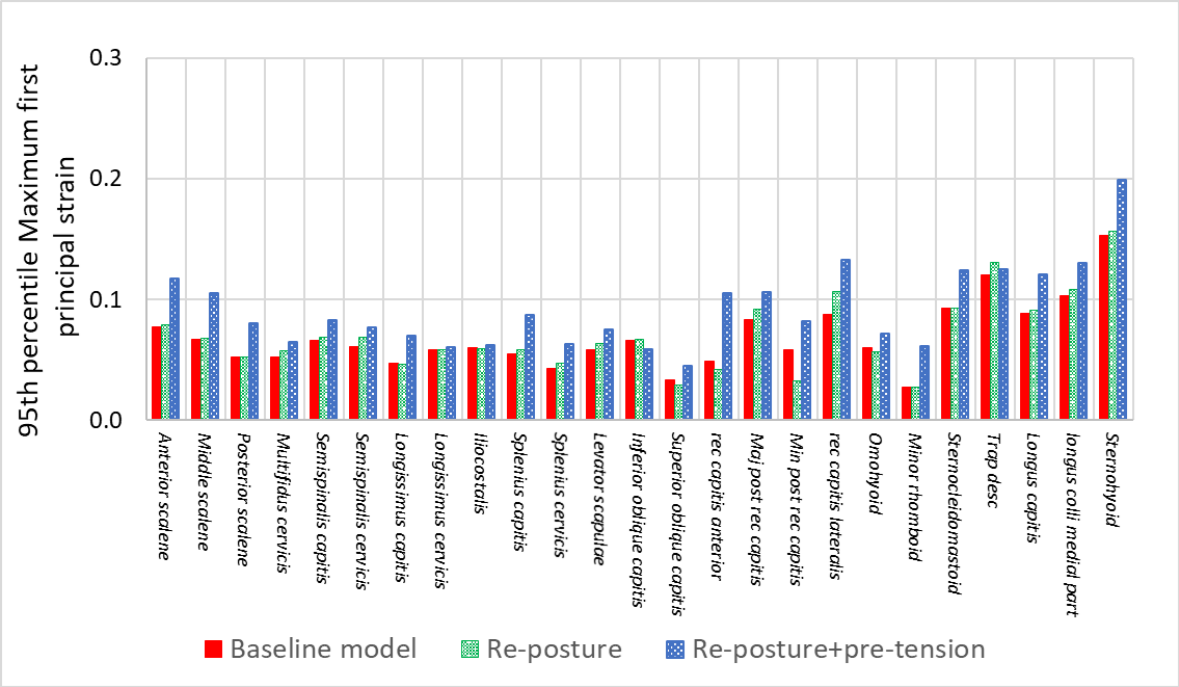


Figure 31: Maximum strain analysis for the simulations
95th percentile maximum first principal strain for each muscle in the volunteer 4 g rear impact simulations.

4.4 Discussion

The present work is the first to analyze, in detail, the effect of pre-impact neck posture and muscle pre-tension on cervical spine intervertebral kinematics and muscle strains during simulated low-acceleration rear impact. Each of the mentioned variables changed the vertebral kinematics compared to the case when the baseline neck model was used. Muscle pre-tensioning altered the posture during the stabilization step; however, the vertebral positions were close to the experimental average and within the experimentally measured posture variability (Figure 23).

The differences in head rotation of the models were modest, which agrees with a previous study showing that changes in local kinematics can occur without significant changes to the head kinematics.[45] Also, the intervertebral rotation differences were small, as expected for the non-

injurious low-severity impacts in experiments with volunteers. However, the S-shape observed in the experiments,[30,73] often suggested as the origin of the injury, was only obtained after the application of the methodology developed in the present paper (re-posture+pre-tension). It is also expected that, for higher accelerations, the S-shape effect would be increased and should be investigated in future studies. The baseline and re-postured models did not present the S-shape, which underscores the important contribution of the initial conditions of the muscle to vertebral configuration. As the model response was close to the corridors for the reported vertebral kinematics experimental data, it may be concluded that the pre-tensioned+re-postured model produces a more accurate intervertebral rotation response, representative of the rear impact response in humans.

The peak flexion of the upper cervical spine was defined as the maximum flexion of C1 in relation to C4. The peak flexion magnitude was the same between the experiments[73] and the model with pre-tension. Comparing the re-postured models with and without pre-tension, the strain distribution in the muscles was altered by muscle pre-tension. During the formation of the S-shape, the re-postured model without pre-tension presented high strains in the trapezius around the shoulders and the neck, while the re-postured+pre-tensioned model presented high muscle strains in the trapezius focused only on the neck region. The pre-tensioned model displayed higher strains in the deeper muscles at the base of the skull and the flexors compared to the other models. The 95th percentile maximum first principal strain increased from 0.16 to 0.20 with the addition of pre-tension to the re-postured model. The literature on experimental data indicates that the active stretch failure engineering strain of the neck muscle tissue ranges from 0.23 to 0.42, depending on the activation level [46]. Other studies have indicated that the muscle failure Green strain is between 0.50 to 0.62 when no activation is present [47,143]. In the present study, the majority of the strains

were less than the strain to failure, as reported in the literature. However, it is noted that with the pre-tensioned model, the 95th maximum strain in the sternohyoid was 0.20, which was close to the range of active stretch failure strain given in one literature study.[46] Although the current simulations did not include muscle activation to allow direct comparison to the active stretch data, the sternohyoid strain could indicate the possibility of muscle damage initiating during the S-shape step and increasing during the full neck extension step. The large muscle tissue strains determined using the pre-tensioned model may help explain why volunteers in the impact test complained about shoulder and neck pain after the test.[73] In other words, this result suggests that the muscle may start to tear or rupture, causing pain, but not enough to be considered major damage. This finding is corroborated by the observed injuries in the proximities of the sternohyoid in an experimental study with sudden neck movement in primates.[144] During the experiment, minor tears of the sternocleidomastoid to partial avulsion of the longus colli were identified. In addition, a sub-injurious rear impact study observing muscle activation with volunteers suggested that soft tissues proximal to the inner third of the superior sternum were a potential site for strain injury.[12]

There are limitations of the current study that should be acknowledged. First, subject morphological variability, head restraint and seatback angle were out of the scope of the present work, although studies have reported that these parameters affect vertebral kinematics. Second, some assumptions were necessary for the muscle geometry: the measurements available for muscle length were taken from cadavers after the onset of rigor mortis, possibly generating small differences from the actual in situ dimensions. The equivalence of the slack length to the optimal length, as well as the estimated optimal length from the literature, are approximations. The pre-tensioning of the muscles was uniformly applied to all extensor and flexor muscles instead of individual muscles, and the origins of muscles attached to the thoracic spine were constrained to

T1, which may reduce the compliance of this tissue. Third, the models did not consider muscle activation, which can influence vertebral kinematics, especially after 100 ms. It is also important to note that the methodology used in the present study is computationally intensive and is not easily transposed to uncertainty quantification or parametric studies, requiring different methodologies.[145–147] However, the current study presents a useful tool for improved biofidelic investigation of soft tissue response, which can improve understanding of injury pathways, previously inaccessible. In addition, the detailed and complex implementation of pre-stretch and re-posture in this study could inform simpler models that can be included in large parametric studies.

4.5 Conclusion

To date, HBM studies investigating head and neck response to low-acceleration rear impact have focused on global kinematics. The present study assessed the effect of pre-impact neck posture and muscle pre-tension using individual vertebral kinematics and muscle strain. The present computational study proposed a novel methodology to initialize the simulation with muscle pre-tension stresses in a model with biofidelic neck posture. In contrast to the pre-impact posture, the muscle-pre-tension influenced vertebral kinematics and the soft tissue strains calculated in the model. Accounting for muscle-pre-tension demonstrated the potential to advance computational studies that use HBMs, and, hence, to better quantify tissue-level injury mechanisms involved in whiplash-initiated injuries.

5 Quantify Tissue-Level Injury Risk Associated with the Vertebral Kinematic Response Following Rear Impact Using the Enhanced Neck Model

5.1 Introduction

As discussed in the previous chapters, WAD are a significant concern due to their high socioeconomic cost and unclear injury mechanisms. During rear impacts, the neck transitions from a neutral posture into an S-shape and then into a C-shape, with the S-shape usually being indicated as the injurious phase. Soft tissues like ligaments, intervertebral discs, facet joints, and muscles were raised as possible regions of WAD injury, but direct tissue injury data remain limited. Nevertheless, HBMs have the potential to assess the tissue-level strain response to complement traditional injury criteria and aid in the understanding of neck injury mechanisms. The head and neck model developed in Chapter 4, incorporating detailed muscle representation with methods like CBS and pre-tension, can offer more biofidelic predictions of muscle strain during impacts. Recent studies also highlighted the importance of muscle reflex mechanisms, such as the ones implemented in a closed-loop controller in Chapter 3, for accurate simulation of neck kinematics and loads. Therefore, HBMs require combining a detailed muscle representation (Chapter 4) with muscle reflex (Chapter 3) to be able to predict reasonable values of tissue-level strain and injury risk.

The study presented in the current chapter aimed to investigate the effect of muscle pre-tension and activation on muscle strain and injury risk resulting from low-severity rear impacts using a detailed Head-and-Neck Model (HNM). Three cases were simulated for three impact

Chapter 5 is extracted (with small adaptations) from Correia, M. A., McLachlin, S. D. & Cronin, D. S. Integration of Muscle Pre-tension and Activation to Evaluate Neck Muscle Strain Injury Risk during Simulated Rear Impacts Using a Finite Element Neck Model. *Stapp Car Crash Journal* **69**, 1–20 (2025).

severities: the baseline re-postured HNM, the HNM including muscle pre-tension, and the HNM with muscle pre-tension and muscle activation. The head kinematics, vertebral kinematics, muscle strains, and three neck injury criteria were calculated to assess injury risk. The maximum kinetics, kinematics, and muscle strains occurred later in the impact during the extension of the neck. The distribution and magnitude of muscle strain depended on muscle pre-tension and activation, and the largest predicted strains occurred at locations associated with muscle injury reported in the literature. The HNM with muscle pre-tension and muscle activation provided a tool to assess rear impact response and could inform injury mitigation strategies in the future.

5.2 Methods

The head and neck regions were extracted from the GHBMC M50-O v5.1 (M50) model, representing a 50th percentile male. The head and neck posture was changed[2] to match the volunteers sitting in a sled in rear impact experiments.[72] The muscles of the model were updated by implementing the CBS methodology, and the CBS was integrated with muscle pre-tension[2] and open-loop active muscle control.[1]

Rear impacts were simulated by applying measured T1 kinematics from 4 g rear impact experiments with volunteers from the literature.[73] The boundary conditions of higher severity impacts (7 g and 10 g) from PMHS testing[75] were also simulated.

To assess the effects of the different muscle implementations, the rear impact scenarios were simulated for three different versions of the model: the M50 extracted from the full body model; the M50 model with muscle pre-tension, but no muscle activation ($M50_P$); and the M50 model with pre-tension and closed-loop muscle activation ($M50_{PC}$). Finally, the head kinematics,

vertebral kinematics, muscle strains, and three neck injury criteria were calculated to quantify response and injury risk in the simulated scenarios.

5.2.1 Neck Muscle Pre-Tension Implemented in the M50$_P$ and M50$_{PC}$ Head and Neck Model

The neck muscle pre-tension was defined in this work as the muscle stretch corresponding to a neutral, relaxed posture before the simulated impact or muscle activation. The objective of the muscle pre-tension was to better replicate stresses present in the muscle tissue in vivo. The pre-tension stress in the model was obtained by deforming the muscle from the shorter muscle slack length (muscle length with no stresses) to the longer in situ length (muscle length in a neutral position prior to the impact simulation).

The simulations were carried out in 32 cores using a single precision commercial FE solver (LS-DYNA, R.9.3.0). The stress initialization for muscle pre-tension was conducted in two steps as reported in a recent study.[2] First, a dynamic relaxation simulation was conducted to obtain the deformations of the muscle from the slack length to the in situ length. Second, an explicit simulation was run for 200 ms with T1 fixed and gravity loading to allow the passive pre-stretched musculature to reach a quasi-equilibrium state. The two steps and the subsequent impact were conducted directly one after the other in the same simulation. The 200 ms stabilization period was run for the three models and led to initial strains (pre-stretch) in the muscles. The postures of the three models were not the same after the stabilization.

5.2.2 Closed-Loop Neck Muscle Activation Implemented in the M50$_{PC}$ Head and Neck Model

The closed-loop muscle activation was based on a controller scheme from a previous publication[1] based on the physiological reflex mechanisms of the neck (Figure 32).

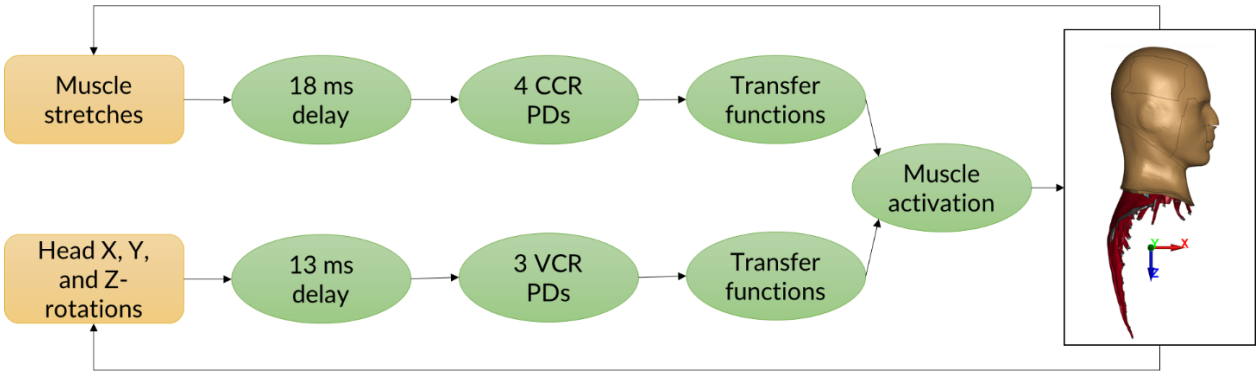


Figure 32: Closed-loop controller schematic of the muscle activation
The head rotation and muscle stretches are the inputs of the controller. The CCR and VCR delays for each of the four muscles were based on experimental data. The delays are applied to the inputs using PD controllers. The outputs of the PDs are combined and transformed into an activation level to be applied to the muscle through transfer functions.

For the current study, the controllers were updated with a time delay of 13 ms for the VCR and 18 ms for the CCR, based on experimental data.[94] The 13 ms delay was the time needed for the signal generated by the head rotation to affect muscle activation. The 18 ms delay was the time needed for the signal generated by the muscle stretch to affect the muscle activation. The input of the CCR was simplified as the changes in length between the origin and insertion point of the Hill-type beam elements at the medial portion of the trapezius and the sternocleidomastoid muscles (Figure 33). In addition, each one of the four muscle groups (right extensors, left extensors, left flexors, and right flexors) was controlled separately.[1]

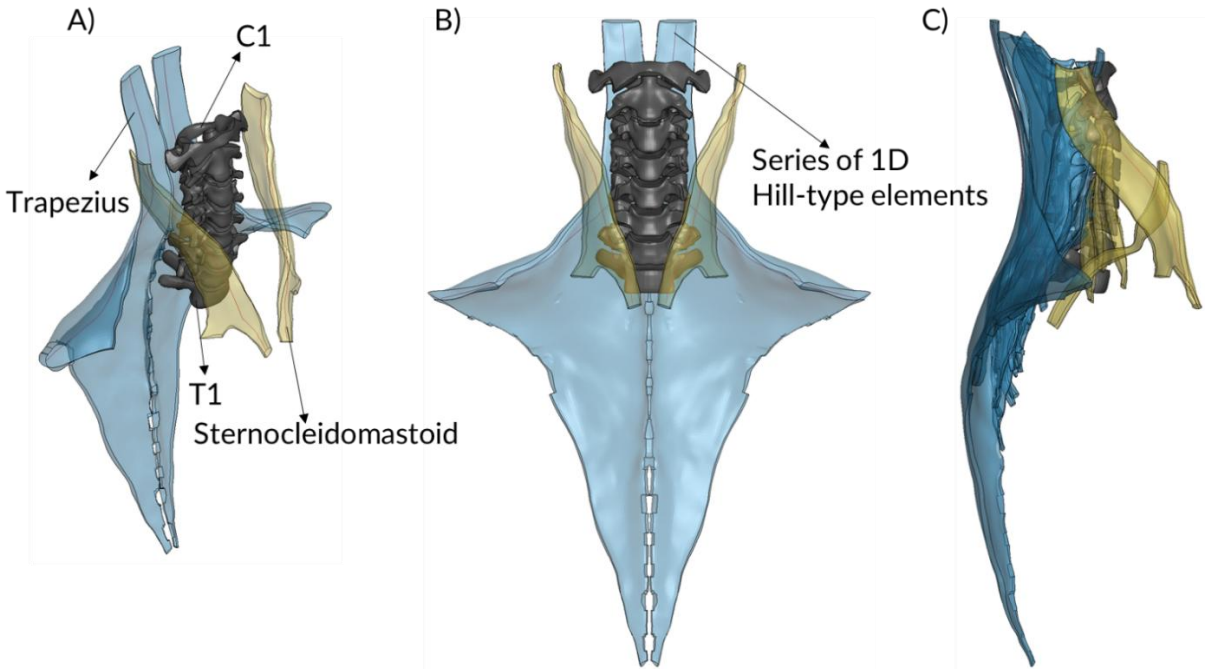


Figure 33: Muscles used as input for the CCR

A) Isometric view of the sternocleidomastoid, trapezius, and cervical spine. B) Frontal view of the series of 1D Hill-type elements (red lines) used as input for the closed-loop controller. C) Lateral view of the flexors (red) and extensors (blue).

The elements for the CCR input were selected from the muscles presenting the highest force and deformation after observing frontal and rear impact simulations without muscle activation. Due to the muscle pre-tension, the controller parameters had to be optimized for this new scenario. A Python code was implemented to optimize the proportional and derivative gains of the PD controllers. The optimization fitted the activation curves of the closed-loop controller to the co-contraction activation curves of an open-loop controller.[1] The optimization used the head rotation and muscle stretches from the open-loop controller simulation as the input signals. For the VCR, the proportional gain obtained through this methodology was 0.44, and the derivative gain was equal to 14.9. For the CCR, the proportional gain was 0.063, and the derivative gain was equal to 0 for the extensors, and 0.28 and 4.5, respectively, for the flexors. The VCR maintained an

activation ratio of 1:5 between the extensors and flexors to maintain the cocontraction ratio from a previous study.[1] The VCR gains were positive for the antagonistic muscle groups, relative to the head rotation, and negative for the agonist muscles. The CCR gains were positive for lengthening and zero for shortening of the muscles relative to the resting length. It is important to note that, during the simulation, Massively Parallel Processing (MPP) decomposition was used so that the 3D muscles and 1D Hill elements calculations occurred in the same core. The MPP decomposition was necessary to ensure numerical consistency between the two muscle parts.

5.2.3 Rear Impact Simulation

Low-acceleration rear impact simulations were run using three different models: M50, $M50_P$, and $M50_{PC}$ to calculate the muscle deformations during the impact. The average X-displacement, Y-rotation, and Z-displacement of the T1 vertebra of the experiment with 4 male volunteers from Sato et al. 2014[73] were applied to the T1 vertebra of the models. The X-rotation, Z-rotation, and Y-translation of T1 were free to move. The muscle, skin, and flesh ends were constrained to T1 to represent the boundary condition of the torso. These boundary conditions represented a rear impact with a peak acceleration of approximately 4 g and were selected as the recorded vertebral kinematics were available for comparison with the model results. The applied X-displacement was obtained by double integrating the X-acceleration presented in the literature. Also, two additional 7 g and 10 g impacts were simulated with the $M50_{PC}$ for a subsequent analysis of the effect of the severity on the possibility of injury. The $M50_{PC}$ was selected for the severity analysis because it presented the highest muscle strains and, therefore, the most injurious scenario. For these high-severity impacts, the X-acceleration, Y-rotation, and Z-acceleration from Deng et al. 2000[75] study with PMHS were applied to the T1 of the $M50_{PC}$.

The resultant head and vertebral kinematics of the simulations were extracted and compared to the experiments to verify the simulations. The 95th percentiles of the maximum principal strains (MPS) from the muscles were extracted and compared with muscle failure data. The strain time histories and strain distribution were inspected for the 3D passive elements in all simulations. The highest spurious values were associated with the muscle-tendon interface, and the 95th percentile criterion consistently reported the relevant muscle strains occurring in the muscle while excluding the high strains at the tendon-muscle interface. Furthermore, the NIC, the N_{km} injury criterion, and the IV-NIC were calculated for the simulations to compare the capabilities of these criteria to identify possible muscle injury. Although N_{km} is usually measured at the occiput (close to C0/C1), this criterion was used in all vertebral joints for comparison to the IV-NIC. The forces and moments at the cervical spine required to calculate the injury criteria were obtained following a similar approach to the cross-section method used by Johnson et al. 2020.[126] No filtering was applied to the force and moment histories, and the data was sampled at 200 Hz. In addition, the physiological ranges of motion of each vertebral level were based on the averages found by a study with cadaveric specimens.[148] The intercept values necessary to calculate the injury criteria were obtained from the literature.[127]

Table 5: Intercept values for the calculation of the injury criteria.

Criterion	Intercept values	Injury threshold
NIC	-	NIC = 10^{117} (Pain threshold)
N_{km}	F_{int} = 845 N[127] M_{int} = 47.5 N m/ 81.1 N m[127] (extension/ flexion)	$N_{km} = 1$[127]

5.3 Results

5.3.1 Low-Severity 4 g Impact Simulations with the M50, M50$_P$ and M50$_{PC}$ Head and Neck Models

All the obtained results were zeroed to the 0 ms time at the onset of the impact. The kinematics of the center of gravity (CoG) of the head were extracted from the rear impact simulations. The CoG X-displacement of the M50 and M50$_P$ were within the corridors of one standard deviation of the experiments (Figure 34).[73] However, the M50$_{PC}$ X-displacement was slightly higher than the corridors. The CoG Y-rotational displacement presented a similar trend to X-displacement initially. The M50 and M50$_P$ models were inside the experimental corridors up to the rebound phase at 170 ms, while the M50$_{PC}$ was inside during rebound up to 220 ms. The contrasting M50$_{PC}$ response to the other models was a result of the high forces generated by the small activation of the extensors during the stabilization phase of the model. Although this effect could be reduced by modifying the muscle activation parameters, for consistency with the previously published model, the activation parameters were kept constant throughout the study. The extensors are larger muscles, even a low activation was enough to increase the head rearward excursion in the M50$_{PC}$ model (Figure 35). In addition, the developed M50$_P$ and M50$_{PC}$ models took 3 days to run on 32 CPUs, mainly due to the additional time required for the dynamic relaxation.

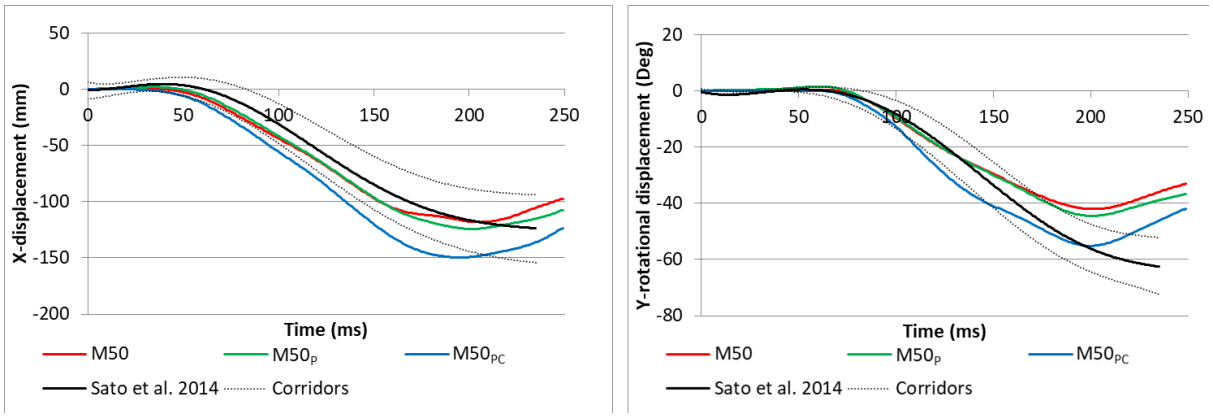


Figure 34: Kinematics of the head CoG for the 4g rear impact simulations

The X-displacement was calculated relative to T1. The corridors represent one standard deviation from the experimental average from Sato et al 2014[73]. The difference in the $M50_{PC}$ displacement is due to the higher forces generated in the extensors by combining CLA and pre-tension.

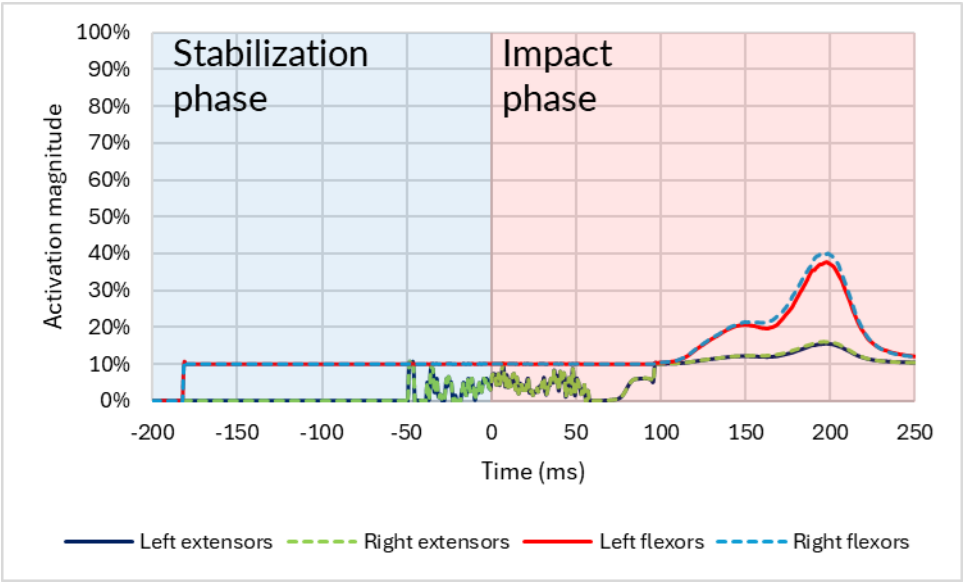


Figure 35: Muscle activation level for the $M50_{PC}$ in the 4g impact simulation

The muscles presented a baseline activation of around 10% before the impact. The timing of the muscle reflex activation was around 96 ms, within the expected EMG values between 55 and 99 ms.[37] In addition, the activation magnitude of the extensors was lower than the flexors, as expected. The flexors quickly deformed enough to achieve full CCR activation (10%) while the extensor oscillated around t = 0. The oscillation was due to the neck achieving the final posture while the extensors presented some small variation on their stretch. The oscillation stopped after the impact reduced the deformation of the extensors.

The intervertebral rotations were extracted from the simulations, from C0 (skull) to C7 (Figure 37). The upper cervical flexion was more pronounced for the $M50_{PC}$ during the S-shape phase (Figure 36), and the neck extension was more pronounced during the C-shape phase. The extension of the vertebra of the $M50_{PC}$ was outside the corridors due to the activation of the extensors. Overall, the model joint kinematics followed trends evident in the experimental response.

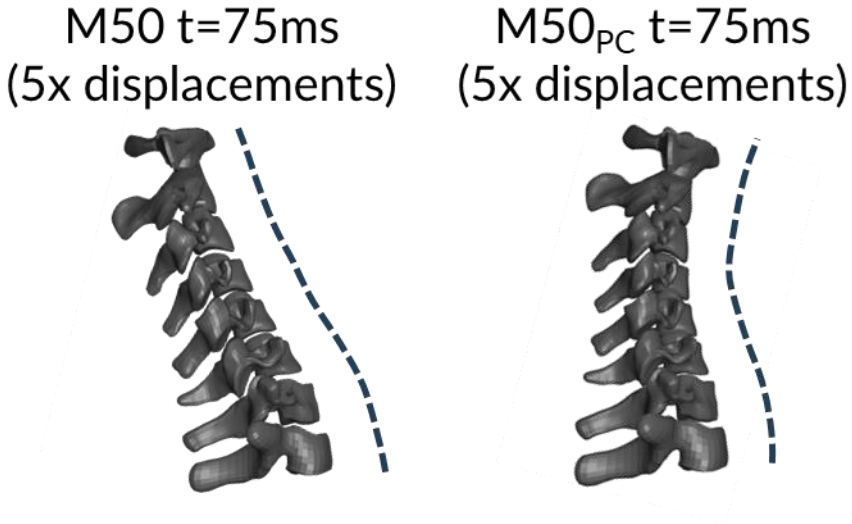


Figure 36: S-shape of the neck for the M50 and $M50_{PC}$ cases
The S-shape was subtle. Hence, the displacements were scaled by 5 times for better visualization in the figure. The S-shape of the $M50_{PC}$ was more evident than the S-shape of the M50 due to the increased flexion of the upper cervical spine.

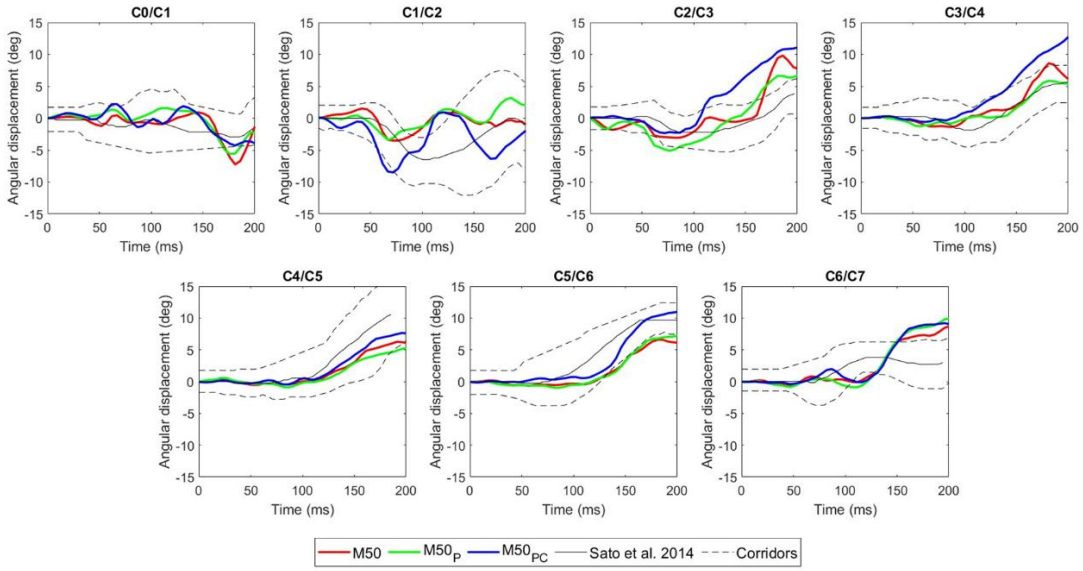


Figure 37: Intervertebral rotations from C0 (skull) to C7 for the three models

The corridors represent one standard deviation of the experimental data. The negative direction indicates flexion, and the positive direction indicates extension. The increase in head flexion is clearly seen at the C1/C2 level for the M50PC.

All three models presented similar trends concerning the injury criteria. The NIC (Figure 38) of all the models were below the pain threshold. The N_{km} (Figure 39) of the models were, in general, low during the S-shape phase (50 to 100 ms) but increased at the C-shape phase (above 100 ms). The IV-NIC (Figure 40) of the models also presented values higher than 1 during hyperextension of the C-shape phase. However, the $M50_P$ crossed the value of IV-NIC = -1 at the C2-C3 joint during flexion. Overall, the model with pre-tension and without muscle activation obtained the lowest values for all injury criteria. In addition, the LNL was calculated for the models and indicated the same trends as the other injury criteria.

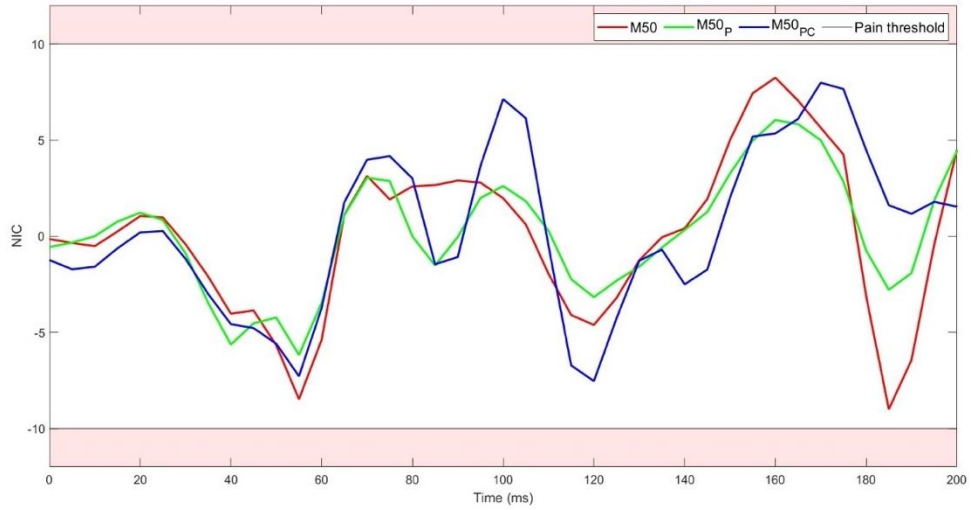


Figure 38: NIC values for the simulations

NIC values for the rear impact simulation for all three models were below the experimental pain threshold (NIC = 10).

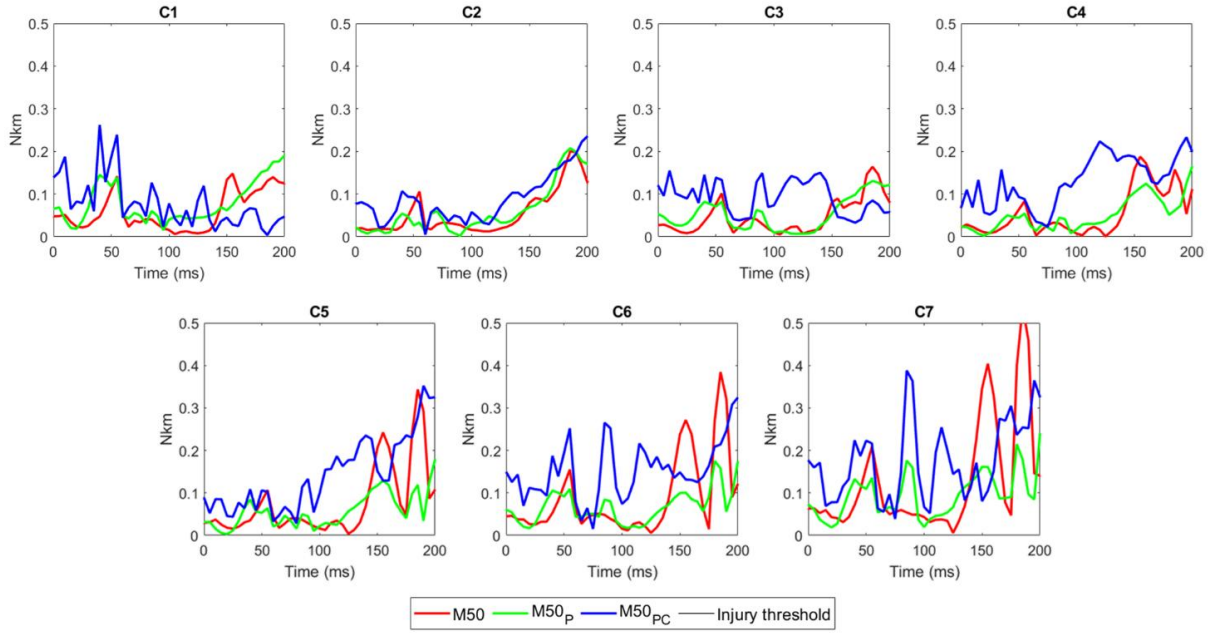


Figure 39: N_{km} values for the rear impact simulation for all three models

When calculating the N_{km}, the value of the M_{int} in flexion was used for the vertebral flexion and the M_{int} in extension was used for the vertebral extension. Generally, the highest Nkm values were identified during the C-shape phase after 100 ms.

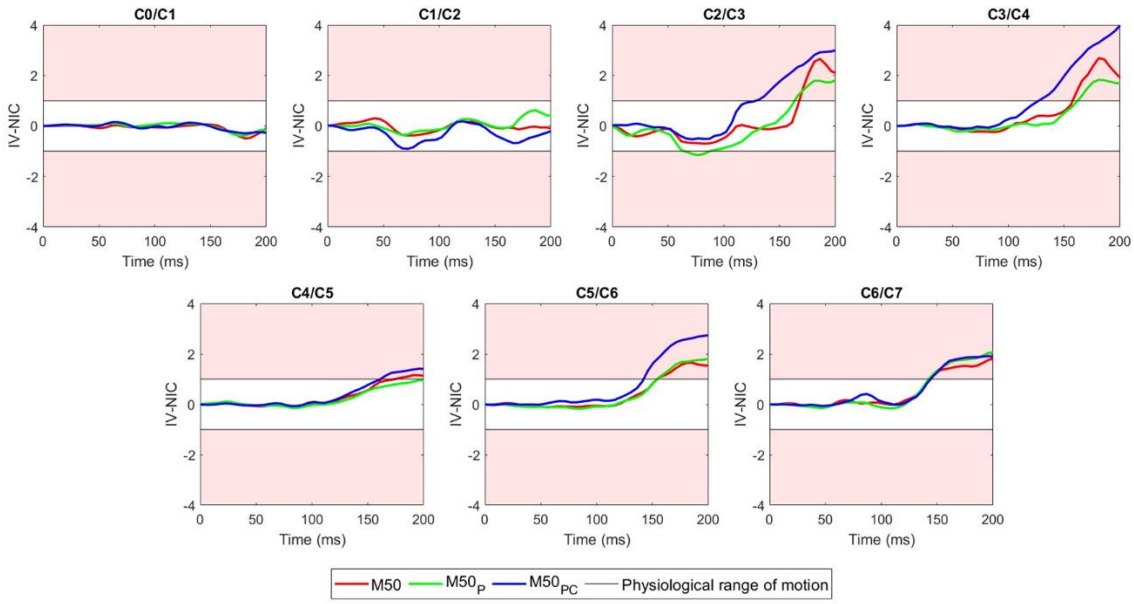


Figure 40: IV-NIC values for the rear impact simulation for all three models

When calculating the IV-NIC, the value of the physiological range of motion in flexion was used for the vertebral flexion (negative values) and the physiological range of motion in extension was used for the vertebral extension (positive values). For almost all cases, the rotations were higher than the ROM during the C-shape phase after 100ms.

The distributions of strains in the muscles were different among the models (Figure 41). For example, the sternocleidomastoid MPS was higher than the splenius capitis for the $M50_P$ model, while the opposite was true for the M50 and $M50_{PC}$. Also, the $M50_{PC}$ decreased the sternocleidomastoid MPS while it increased the longus capitis MPS compared to the $M50_P$. Additionally, the average MPS increased with the addition of pre-tension and increased again with the addition of muscle activation. The average 95^{th} percentile MPS were 0.12, 0.13, and 0.15 for the M50, $M50_P$, and $M50_{PC}$, respectively. The three muscles presenting the highest strains were all extensors: the rectus capitis lateralis (strains from 0.29 to 0.32), the trapezius (strains from 0.20 to 0.27) and the semispinalis cervicis (strains from 0.18 to 0.23).

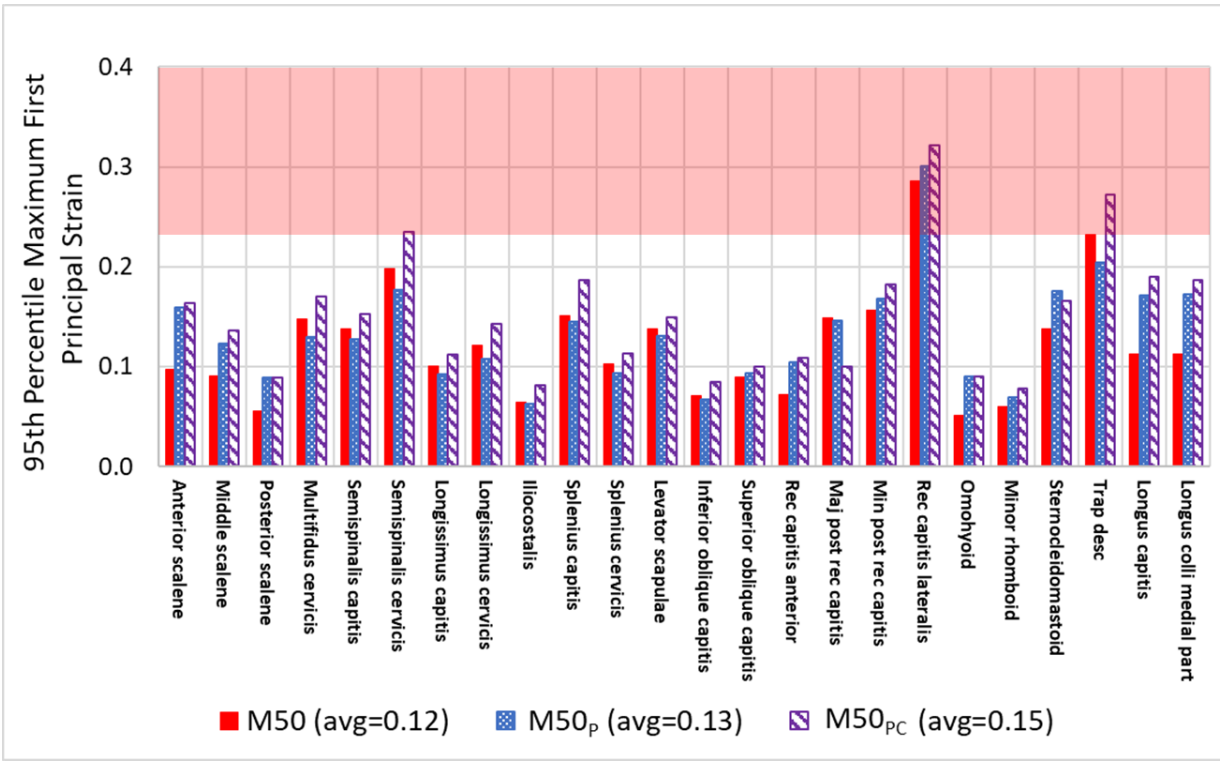


Figure 41: Maximum muscle strain for the three models

95th percentile maximum first principal strain for each muscle in the 4 g rear impact simulation for all three models. The average strains (avg) are shown inside parentheses. The red region shows values above the minimal injurious strain of 0.23.

5.3.2 High-severity 7 g and 10 g Impact Simulations with the M50PC Head and Neck Model

For the subsequent comparisons of increasing severity impacts, the intervertebral rotations were also extracted from the simulations, from C0 (skull) to C7 (Figure 43). As expected, the 10 g impact generated the highest intervertebral angular displacements in flexion and extension (Figure 42). However, the 7 g impact presented slightly lower intervertebral angular rotations compared to the 4 g impact. The 10 g simulation provided useful data up to a simulation time of 175 ms and then terminated due to numerical instabilities in the tendon elements at the level of C1. Based on kinematic observation of the tendon elements, the model works without issues up to 175 ms after the impact. The large rotations of the vertebrae were a result of the impact severity.

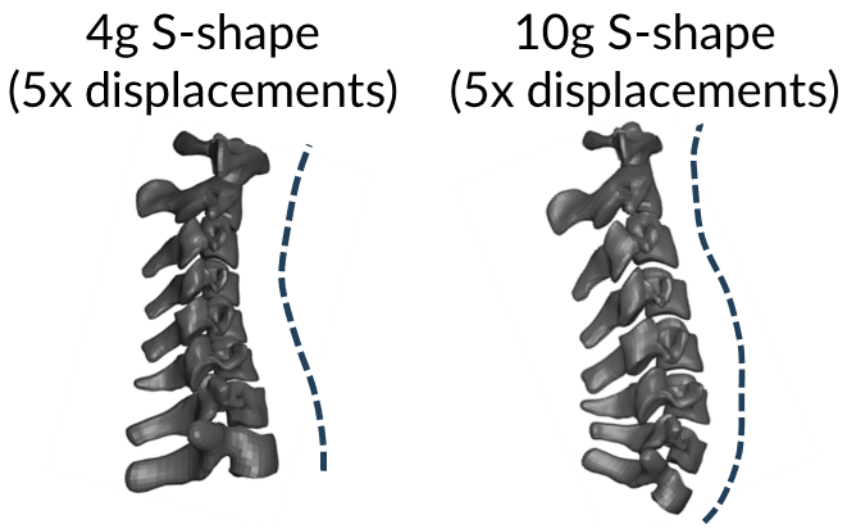


Figure 42 : S-shape of the $M50_{PC}$ for the 4g and the 10g impacts

The S-shape was subtle. Hence, the displacements were scaled by 5 times for better visualization in the figure. As expected, the flexion of the upper cervical spine and the extension of the lower cervical spine were higher for the 10g impact than for the lower severities, generating a more aggressive S-shape.

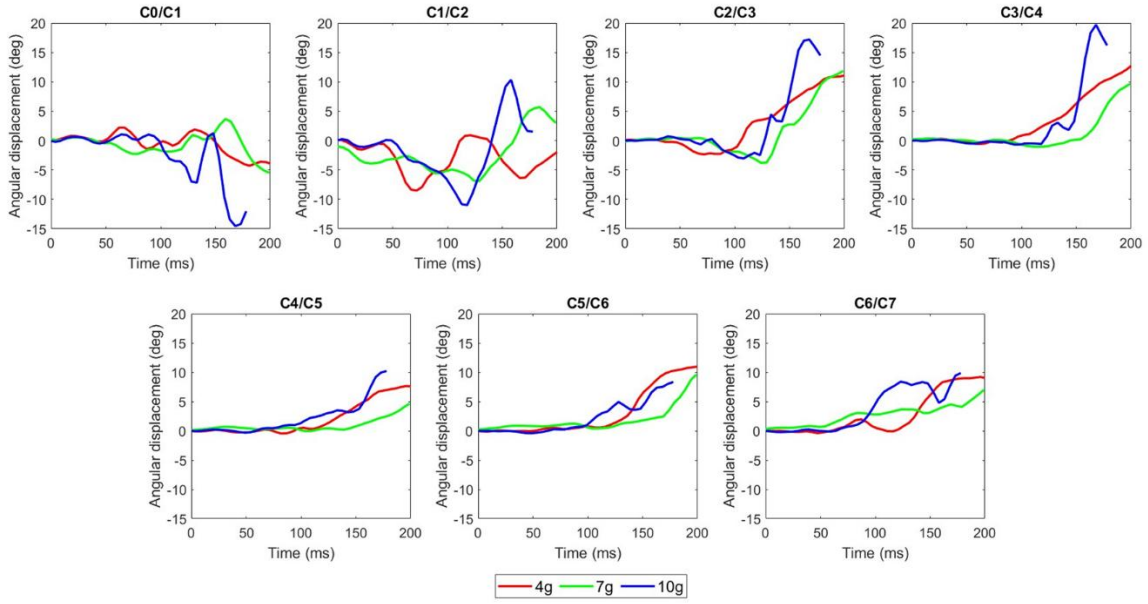


Figure 43: Intervertebral rotations for the simulations with different impact severities

$M50_{PC}$ intervertebral rotations from C0 (skull) to C7 for 4 g, 7 g, and 10 g impact severities. The negative direction indicates flexion, and the positive direction indicates extension. The

angular displacement increased for the 10g case, but was relatively similar for the 4g and 7g impacts.

The calculated injury criteria values increased with impact severity, except for the IV-NIC of the 7 g case compared to the 4 g case. The N_{km} (Figure 44) was low during the S-shape phase for all severities but increased at the C-shape phase. The IV-NIC (Figure 45) also presented values higher than 1 during hyperextension of the C-shape phase for all the severities. However, the 10g case crossed the value of IV-NIC = -1 at the C1-C2 joint during flexion.

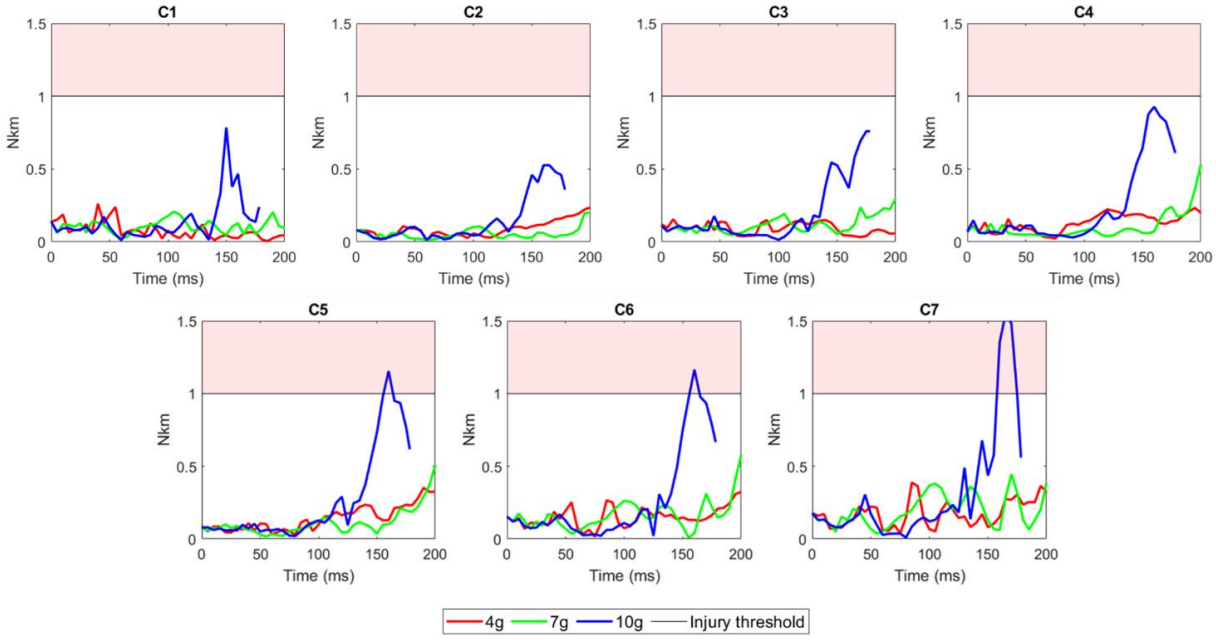


Figure 44: $M50_{PC}$ N_{km} values for the 4 g, 7 g, and 10 g rear impact simulations
When calculating the N_{km}, the value of the M_{int} in flexion was used for the vertebral flexion and the M_{int} in extension was used for the vertebral extension. The N_{km} displacement increased for the 10g case, but was relatively similar for the 4g and 7g impacts.

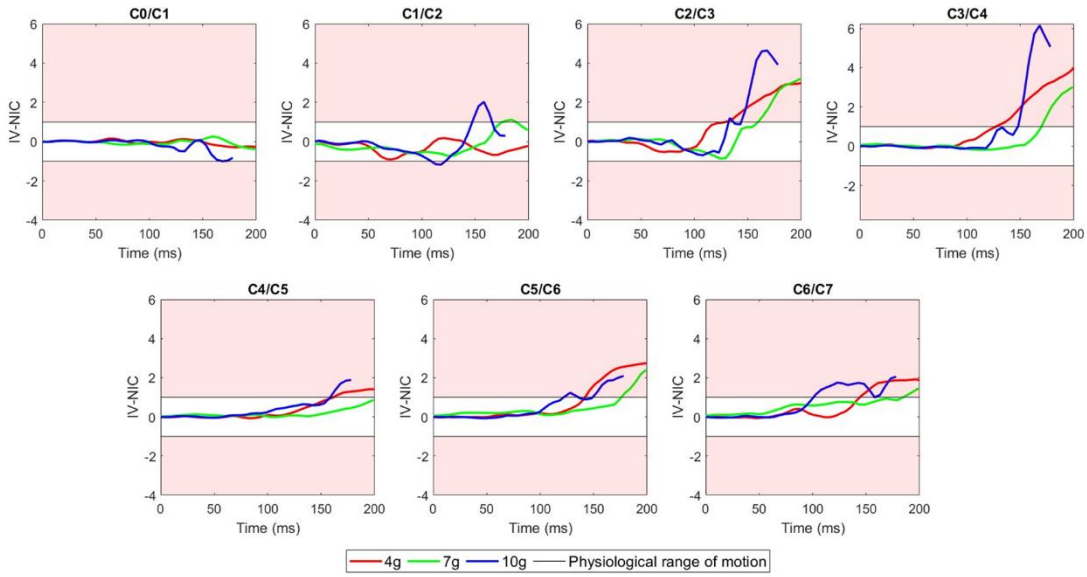


Figure 45: M50PC IV-NIC values for the 4 g, 7 g, and 10 g rear impact simulations
When calculating the IV-NIC, the value of the physiological range of motion[148] *in flexion was used for the vertebral flexion (negative values) and the physiological range of motion in extension was used for the vertebral extension (positive values). The IV-NIC increased for the 10g case, but was relatively similar for the 4g and 7g impacts.*

The highest average muscle strain (0.22) was found in the 10 g impact, while the 4 g and 7 g cases had the same average strain (0.15) (Figure 46). For all the severities, the three extensors presenting the highest strains were: the rectus capitis lateralis (strains from 0.25 to 0.44), the trapezius (strains from 0.27 to 0.41), and the semispinalis cervicis (strains from 0.21 to 0.33). However, for the 10 g impact, a flexor, the rectus capitis lateralis, also presented a high strain (0.43) in contrast to the lower severities (0.11 to 0.15) in which only the extensors presented the highest strains.

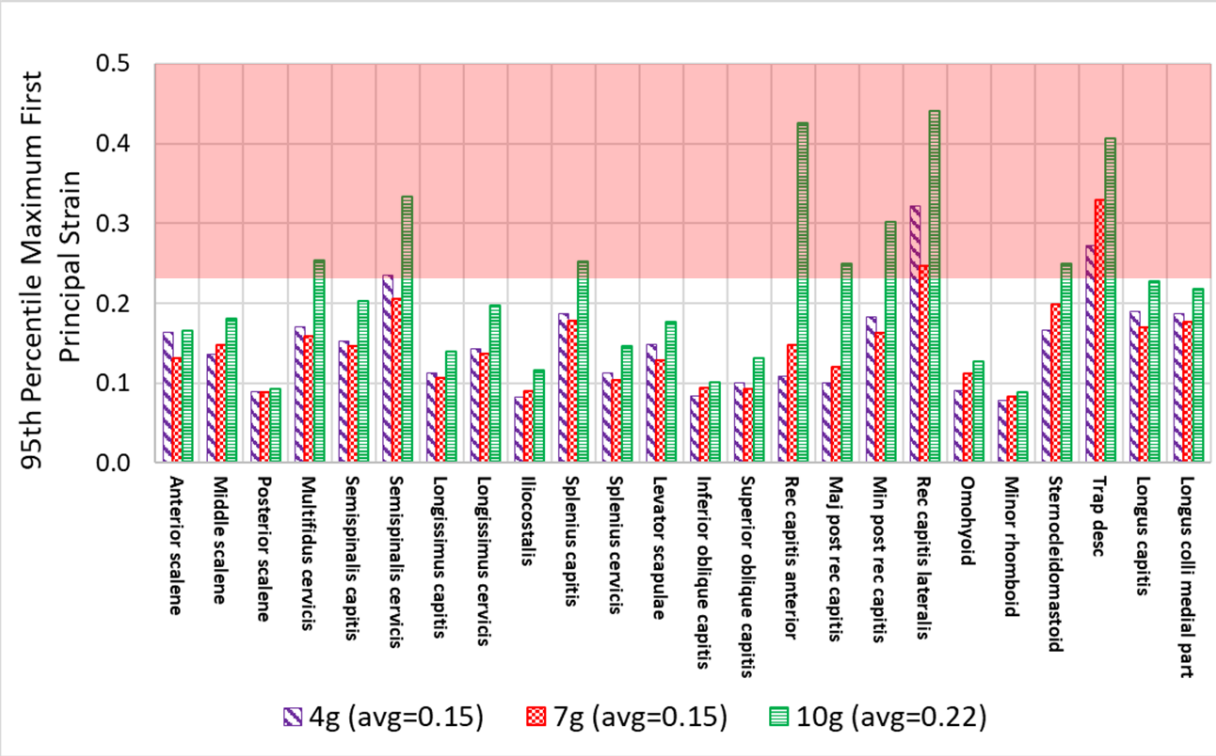


Figure 46: Maximum strain for the simulations with different severities

95th percentile maximum first principal strain for each muscle in the M50$_{PC}$ for the 4 g, 7 g, and 10 g rear impact simulations. The average strains (avg) are shown inside parentheses. The red region shows values above the minimal injurious strain of 0.23.

5.4 Discussion

The integration of the muscle pre-tension and a closed-loop muscle activation controller was successfully implemented in the GHBMC head and neck model, resulting in head and vertebral kinematics from the model that were within or close to the response corridors of the human volunteers for a 4 g impact. The M50$_{PC}$ obtained slightly higher head displacements and rotations, which is expected due to the additional force produced by the muscles, especially the larger extensors.

Compared to the M50, the $M50_P$ increased the upper cervical spine flexion from 7.5 to 8.9 degrees, and the $M50_{PC}$ increased it to 11.1 degrees. Both $M50_P$ and $M50_{PC}$ approximated peak C1-C4 flexion to the experimental average of 10.3 degrees, as expected for a better representation of the muscle forces. Nevertheless, the additional loads of the muscle activation of the $M50_{PC}$ were required to achieve C1-C2 peak flexion similar to the experiments. However, the $M50_{PC}$ resulted in a higher extension at the C2-C3 level during the C-shape phase, indicating a trade-off between these two phases in the current model. The simulated vertebral joints presented negligible shear compared to the experiments from Sato et al. 2014.[73] The low shear possibly indicates differences in the intervertebral disk implementation and bony geometry that may have led to the trade-offs observed in the model.

The distributions of the muscle strains were different among models (Figure 41) even though the differences in head kinematics were small. This contrast shows that obtaining precise values for usually neglected aspects of the muscles, such as pre-tension, is essential to quantify soft tissue injurious strains in low severity impacts. The highest values of MPS in all models were in the trapezius, rectus capitis lateralis and semispinalis cervicis. These three muscles are extensors. For the M50, the trapezius and rectus capitis lateralis MPS surpassed the lowest strain at which injury was identified in the literature (0.23).[46] For the $M50_P$, only the rectus capitis lateralis surpassed the lowest strain in which injury was identified in the literature. For the $M50_{PC}$, the trapezius, rectus capitis lateralis, and semispinalis cervicis MPS surpassed the lowest strain in which injury was identified in the literature. The muscle strains indicated a potential risk of injury in the posterior region of the lower cervical spine and at the posterior region near the base of the skull. The injury regions identified agreed with MRI studies[59,149,150] of whiplash patients that identified a higher increase of fatty tissue (a signal of injury) at the semispinalis cervicis, multifidus, trapezius, and

rectus capitis posterior major and minor (both in close proximity to the rectus capitis lateralis) after the impact. The possibility of injury also agreed with the reported pain felt by the volunteers during the sled tests[73] used for the boundary conditions of the simulations.

Importantly, even with the higher flexion of the $M50_{PC}$ the IV-NIC, and N_{km} indicated a higher risk of injury during the C-shape phase. The trend indicated by these injury criteria was in agreement with the timing of higher strains in the muscles. However, the pain threshold was not crossed by any of the models for the NIC, indicating that this metric may be insensitive to such low severity impacts. The IV-NIC crossed the injury threshold from C2 to C7 for all models, while the N_{km} did not cross the injury threshold for all cases. Nevertheless, the N_{km} values are sensitive to the selection of the intercepts,[126] which may be causing this discrepancy. For the IV-NIC, the C2-C3 values for the $M50_{P}$ were slightly beyond the injury threshold, which may indicate that for higher severities of similar impacts, the S-shape may become increasingly injurious. This data also agrees with experimental data that indicated injury at C2-C3 and C5-C6 levels, showing the importance of muscle pre-tension to the injury analysis at low severity impacts. Nevertheless, the hyperextension phase still presented higher values of the injury criteria, which is in agreement with the analysis of tissue strains during neck extension conducted in the rectus capitis posterior minor.[19] Overall, the pre-tension reduced the injury criteria values even though it increased average muscle strains, indicating that the investigated injury criteria may not be adequate for understanding the soft tissue response. The ligaments, vertebrae and discs did not present injurious loads in any of the simulations, which was also in contrast to what was identified by the injury criteria. In addition, a new injury criterion relating force and activation of 1D Hill-type elements to muscle injury was proposed by Nölle et al. 2022[131], and could be adapted to the GHBMC model in the future to further investigate the muscle injury possibility.

The overall analysis of the increase in impact severity indicated that the vertebral angular displacements and calculated injury criteria were highest for the 10 g case, as expected. The 4 g and 7 g presented comparable values for the intervertebral kinematics and the $N_{km.}$ One possible explanation is that the vertebral kinematics being maintained between these two severities may be due to muscle activation. This would agree with previous studies[151] that indicated that muscle activation could help protect the neck against injury. Another possible explanation is the use in the simulations of boundary conditions from two different studies for the different severities; therefore, the 7 g response of the model may not follow a progressive increase compared to the 4 g pulse. However, the 7 g and 10 g cases were from the same study and therefore presented the expected increase in vertebral kinematics with severity. The distribution of muscle strain also increased for the 10 g impact, with the extensors displaying the highest strain. In contrast, the $M50_{PC}$ had one flexor, rectus capitis anterior, presenting one of the highest strains. This flexor is a small muscle at the base of the skull, which explains the large deformations only when the muscle is actively contracted. The 10 g impact IV-NIC also surpassed the physiological range of motion during the S-shape in opposition to the 4 g or 7 g cases. The high severity needed to onset the possibility of injury during the S-shape phase agrees with the literature that uses this mechanism to justify males being less prone to whiplash injury than females due to anthropometric differences.[24,152] The 10 g simulation terminated prematurely due to numerical instability in a tendon element connected to a muscle beam element. The small beam elements for the active muscle presented extremely high relative stretches near the tendons in the 10 g impact severity, generating instabilities during the Hill-type element muscle force calculation. The simulation could be run to completion if longer elements were implemented in the future.

The current study includes some limitations. The scarcity of in vivo force and strain data for muscle tissue and vertebral kinematics during rear impacts makes further validation of the simulated results challenging. Recent ultrasound studies[153,154] were able to measure volumetric changes in large muscles during voluntary contraction, and may be adapted to help validate the simulated deformations during impacts. For comparison with the IV-NIC, the N_{km} was used to observe the loads in all vertebral joints, although it was developed for measuring loads at the occiput level. It was assumed that the N_{km} intercepts of all vertebral levels were the same as those of the occiput. However, obtaining N_{km} intercepts for each vertebral joint would be ideal. The simplified grouping of the muscles into flexors and extensors may not capture all the complexities of pre-tension and activation of individual muscles. The sternohyoid and sternothyroid-thyrohyoid muscles were not considered in the strain analysis as they reported high localized strains in the T1 region, especially for the $M50_{PC}$. The localized high strains were deemed artifacts due to the muscles, adipose tissue, and skin being fixed to T1 for the extracted head and neck model. In addition, the $M50_{PC}$ model generated a higher head extension than the experiments, indicating the need to further adapt the closed-loop controller for a model with pre-tension. One parameter that could be modified would be the cocontraction ratio between flexors and extensors, which was not updated for the model with pre-tension.

5.5 Conclusion

The current chapter analyzed the effect of muscle pre-tension and muscle activation on head and vertebral kinematics in addition to the possibility of injury, using the M50 head and neck model. The $M50_{PC}$ model exhibited a pronounced upper cervical S-shape that better matched experimental peak flexion but showed more exaggerated C-shape and head kinematics than volunteer tests. Muscle strain increased with pre-tension and activation, varying among different

models. The $M50_{PC}$ model indicated regions of injury consistent with experimental pain reports, with muscle activation specifically highlighting potential deep muscle injuries. Strains increased with impact severity, and the C-shape phase was identified as the primary injurious phase. The $M50_{PC}$ was the only model to indicate injury at the C2-C3 level during the S-shape, aligning with prior literature. While this study focused on muscle response, other tissues and regions, such as facet joints, remain relevant for WAD. Further experimental validation is needed, but the present results point to the possibility of using the updated HBM to help identify injury regions and enhance the understanding of soft-tissue injury mechanisms.

6 Thesis Conclusions, Limitations and Future Work

6.1 Thesis Conclusions

The current thesis successfully improved the GHBMC neck model to enable the prediction of tissue-level response. The model improvements were achieved through objectives from three studies: (1) development of a novel closed-loop muscle controller based on the reflex mechanisms of the neck to approximate the response of living subjects, (2) implementation of muscle pre-tension and neck posture to replicate local kinematics of the vertebrae and muscles in rear impacts, and (3) quantification of the tissue-level response associated with WAD injury risk.

The proposed closed-loop controller from the first study obtained similar kinematics to previous implementations of the CMA open-loop activation for multiple impact directions and impact severities, while also representing known muscle reflex mechanisms. The controller parameters were optimized using volunteer data and evaluated independently across 14 impact conditions. The closed-loop controller simulations displayed a good correlation with experimental data, achieving an average CORA rating of 0.699 for impacts following the ISO/TR9790 standard. Compared to a previously optimized open-loop activation strategy, the average difference was under 9%. Importantly, the inclusion of the new closed-loop controller did not significantly increase the computational time of the model, demonstrating a computationally efficient solution with improved biofidelity.

The second study assessed the effect of pre-impact neck posture and muscle pre-tension using vertebral kinematics reported in the literature and the predicted muscle strain. A novel methodology to include muscle pre-tension stresses in a model with biofidelic neck posture was developed. The muscle-pre-tension influenced vertebral kinematics and the soft tissue strains

calculated in the model. Specifically, only the model with pre-tension presented a magnitude of upper cervical spine flexion in agreement with human volunteer experiments. The improvements to the muscle implementation advanced the tissue-level measurement capabilities of the HBM that can be used to design safer vehicles and mitigate injuries in impact events.

The third study combined the new closed-loop muscle activation with the novel muscle pre-tension implementation in the detailed average stature male neck model and was used to assess response and injury risk. Achieving the upper cervical spine S-shape in the $M50_{PC}$ better represented the experimental peak flexion but had a more pronounced C-shape and head kinematics than the tests with volunteers. The muscle strain increased progressively with the inclusion of pre-tension and muscle activation. The $M50_{PC}$ strains indicated high strains in muscles associated with reported regions of pain from experiments. Furthermore, only the model with muscle activation showed possible muscle injury in the deep muscles (semispinalis cervicis) as reported in the literature. In addition, the strains increased with impact severity as expected. The predicted maximum muscle strains and injury metrics in all but one model configuration identified that the C-shape (hyperextension) was the main injurious phase for the impact severities investigated. Only the $M50_{PC}$ surpassed the IV-NIC injury threshold at the C2/C3 level during the S-shape, as was previously suggested in the literature. It is important to note that the current study focused on the muscle response, although other tissues, such as the facet joints, have been suggested as potential pain sources in WAD. The current study was the first to analyze the relationship between muscle strain during rear impacts and neck injury criteria. Although further experiments are still needed to validate the simulated results, the proposed models can help inform regions of interest for injury analysis and are a step toward improving understanding of soft-tissue injury mechanisms.

6.2 Limitations

Overall, the developed models worked as expected and were stable. Nevertheless, the presented study has two main sets of limitations: model simplifications and experimental data challenges. In the first set of limitations, the muscle model was simplified, with uniform pre-tensioning and activation applied to each muscle group, which may not capture all the detailed behaviour of the single muscles. In addition, the muscle ends were constrained to T1, leading to localized high strains in specific muscles. The closed-loop controller integrated feedback from specific muscles, and although the controller produced good results, future implementations should consider feedback from a larger number of muscles. Another important simplification of the closed-loop controller is the fact that the current work was limited to the VCR and CCR, while other reflexes, such as the stereotypical startle reflex or voluntary contraction, could also affect the model response. Finally, the closed-loop controller only considered displacement and strains as input, because for the model, the resultant head kinematics were in good agreement with the experiments. The addition of the relatively noisy acceleration and strain-rate inputs would possibly increase instability, requiring filtering that is not easily inferred from the experimental data. For the second set of limitations, the scarcity of in vivo data for muscle strain during impacts made validation of the simulated results challenging. However, for the first time, the computational neck model was able to reproduce the complex vertebral kinematics, including the S-shape magnitude, reported for human volunteers. In the future, techniques like ultrasound may be adapted to provide important data, such as muscle deformation, for model validation. Finally, in the current study, the updated muscle implementation improved the strain distribution and vertebral kinematic response relative to human volunteers, but more extensive data on muscle length and pre-strain may refine muscle modelling approaches.

6.3 Future Work

Future studies should investigate the developed closed-loop controller performance in out-of-position impacts and oblique impacts, which are of interest to WAD and the development of autonomous vehicles. Additionally, potential age and gender effects in the neck reflex should be investigated to better represent other population cohorts. Pending the development of more appropriate techniques like elastomyography, future experiments should investigate measurements of the muscle pre-tension in vivo and whether the pre-tension mechanism is a passive property, as hypothesized here, or a result of muscle tonus.

Contemporary HBMs designed for lower computation time should be compared with the detailed and more computationally demanding neck models to inform about the appropriate application cases for each model. Further, the implementation of the neck model developments from this thesis in a full-body model should help to mitigate the boundary condition effects observed. However, for the validation of the closed-loop controller and pre-tension in the full-body scenario, the model should closely replicate the added complexity of the seat properties and the posture of the volunteers in the entire spine. Importantly, the implementation of the IVD in the M50 should be improved to better represent the shearing of the vertebral joints displayed in the experiments. Finally, the model improvements proposed in this thesis could be used to develop more biofidelic neck injury criteria relating experimental tissue test data to simulated tissue behaviour.

Letter of Copyright Permission

A) Copyright permission for Figure 1

ELSEVIER LICENSE
TERMS AND CONDITIONS

Feb 23, 2025

This Agreement between Matheus Augusto Correia ("You") and Elsevier ("Elsevier") consists of your license details and the terms and conditions provided by Elsevier and Copyright Clearance Center.

License Number	5974961402953
License date	Feb 23, 2025
Licensed Content Publisher	Elsevier
Licensed Content Publication	Clinical Biomechanics
Licensed Content Title	The anatomy and pathophysiology of whiplash
Licensed Content Author	Nikolai Bogduk
Licensed Content Date	May 1, 1986
Licensed Content Volume	1
Licensed Content Issue	2
Licensed Content Pages	10
Start Page	92
End Page	101
Type of Use	reuse in a thesis/dissertation

Portion	figures/tables/illustrations
Number of figures/tables/illustrations	1
Format	both print and electronic
Are you the author of this Elsevier article?	No
Will you be translating?	No
Title of new work	Investigation of Neck Posture and Muscle Activity on Cervical Spine Impact Kinematics Using a Finite Element Human Body Model
Institution name	University of Waterloo
Expected presentation date	Apr 2025
Portions	Figure 1
The Requesting Person / Organization to Appear on the License	Matheus Augusto Correia
Requestor Location	Mr. Matheus Correia University of Waterloo 200 University Ave W Waterloo, ON N2L3G1 Canada
Order reference number	Rear impact kinematics
Publisher Tax ID	GB 494 6272 12
Total	0.00 CAD
Terms and Conditions	

B) Copyright permission for Figure 3

SPRINGER NATURE LICENSE
TERMS AND CONDITIONS

Feb 20, 2025

This Agreement between Matheus Augusto Correia ("You") and Springer Nature ("Springer Nature") consists of your license details and the terms and conditions provided by Springer Nature and Copyright Clearance Center.

License Number	5973410171768
License date	Feb 20, 2025
Licensed Content Publisher	Springer Nature
Licensed Content Publication	Nature Reviews Drug Discovery
Licensed Content Title	Targeting the sarcomere to correct muscle function
Licensed Content Author	Peter M. Hwang et al
Licensed Content Date	Apr 17, 2015
Type of Use	Thesis/Dissertation
Requestor type	academic/university or research institute
Format	print and electronic
Portion	figures/tables/illustrations
Number of figures/tables/illustrations	1

Would you like a high resolution image with your order?	no
Will you be translating?	no
Circulation/distribution	1 - 29
Author of this Springer Nature content	no
Title of new work	Investigation of Neck Posture and Muscle Activity on Cervical Spine Impact Kinematics Using a Finite Element Human Body Model
Institution name	University of Waterloo
Expected presentation date	Apr 2025
Portions	Figure 1
The Requesting Person / Organization to Appear on the License	Matheus Augusto Correia
Requestor Location	Mr. Matheus Correia University of Waterloo 200 University Ave W Waterloo, ON N2L3G1 Canada
Order reference number	Sarcomere
Billing Type	Invoice
Billing Address	Matheus Correia University of Waterloo 200 University Ave W Waterloo, ON N2L3G1 Canada

References

1. Correia, M. A., McLachlin, S. D. & Cronin, D. S. Vestibulocollic and Cervicocollic Muscle Reflexes in a Finite Element Neck Model During Multidirectional Impacts. *Ann Biomed Eng* **49**, 1645–1656 (2021).

2. Correia, M. A., Corrales, M. A., McLachlin, S. D. & Cronin, D. S. Effect of muscle pre-tension and pre-impact neck posture on the kinematic response of the cervical spine in simulated low-speed rear impacts. *Numer Methods Biomed Eng* **39**, e3761 (2023).

3. Correia, M. A., McLachlin, S. D. & Cronin, D. S. Integration of Muscle Pre-tension and Activation to Evaluate Neck Muscle Strain Injury Risk during Simulated Rear Impacts Using a Finite Element Neck Model. *Stapp Car Crash Journal* **69**, 1–20 (2025).

4. Correia, M. A., Hadagali, P., McLachlin, S. D. & Cronin, D. S. Passive Neck Muscle Implementation in Finite Element Models Influences Upper Cervical Spine Kinematics in Low-Speed Rear Impacts. in (2023).

5. Corrales, M., Correia, M. & Cronin, D. Active and Passive Musculature Coupling Strategy to Improve Muscle Strain Prediction. in *IRCOBI* (2021). doi:10.13140/RG.2.2.16323.73768.

6. Swain, R. & Larue, G. S. Looking back in the rearview: Insights into Queensland's rear-end crashes. *Traffic Injury Prevention* **25**, 138–146 (2024).

7. Hayashi, K. *et al.* Predictors of high-cost patients with acute whiplash-associated disorder in Japan. *PLoS ONE* **18**, e0287676 (2023).

8. Fice, J. B. & Cronin, D. S. Investigation of whiplash injuries in the upper cervical spine using a detailed neck model. *Journal of Biomechanics* **45**, 1098–1102 (2012).

9. Kitagawa, Y., Yamada, K., Motojima, H. & Yasuki, T. Consideration on gender difference of whiplash associated disorder in low speed rear impact. *2015 IRCOBI Conference Proceedings - International Research Council on the Biomechanics of Injury* 233–245 (2015).

10. Bumberger, R., Acar, M. & Bouazza-Marouf, K. Importance of intervertebral displacement for whiplash investigations. *International Journal of Crashworthiness* **25**, 376–390 (2020).

11. Fice, J. B. *et al.* Neck Muscle and Head/Neck Kinematic Responses While Bracing Against the Steering Wheel During Front and Rear Impacts. *Annals of Biomedical Engineering* **49**, 1069–1082 (2021).

12. Olive, O. D., Marianne, M., Henry, P. M. & Hung-Kay, C. D. Muscle activity during low-speed rear impact. *Chinese Journal of Traumatology - English Edition* **22**, 80–84 (2019).

13. Putra, I. P. A. *et al.* Optimization of Female Head–Neck Model with Active Reflexive Cervical Muscles in Low Severity Rear Impact Collisions. *Annals of Biomedical Engineering* **49**, 115–128 (2021).

14. Putra, I. P. A. & Thomson, R. Analysis of control strategies for VIVA OpenHBM with active reflexive neck muscles. *Biomech Model Mechanobiol* **21**, 1731–1742 (2022).

15. Yoganandan, N., Harinathan, B. & Vedantam, A. Cervical Column and Cord and Column Responses in Whiplash With Stenosis: A Finite Element Modeling Study. *Journal of Engineering and Science in Medical Diagnostics and Therapy* **7**, 021003 (2024).

16. Corrales, M. A. & Cronin, D. S. Sex, Age and Stature Affects Neck Biomechanical Responses in Frontal and Rear Impacts Assessed Using Finite Element Head and Neck Models. *Frontiers in Bioengineering and Biotechnology* **9**, 1–14 (2021).

17. Stemper, B. D. & Corner, B. D. Whiplash-associated disorders: Occupant kinematics and neck morphology. *Journal of Orthopaedic and Sports Physical Therapy* **46**, 834–844 (2016).

18. Vasavada, A. N., Brault, J. R. & Siegmund, G. P. Musculotendon and Fascicle Strains in Anterior and Posterior Neck Muscles During Whiplash Injury: *Spine* **32**, 756–765 (2007).

19. Hallgren, R. C. & Rowan, J. J. Assessment of potential strain injury to rectus capitis posterior minor muscles during whiplash type distortions of the cervical spine. *Journal of Osteopathic Medicine* **121**, 747–753 (2021).

20. Bogduk, N. The anatomy and pathophysiology of whiplash. *Clinical Biomechanics* **1**, 92–101 (1986).

21. Grauer, J. N., Panjabi, M. M., Cholewicki, J., Nibu, K. & Dvorak, J. Whiplash produces an S-shaped curvature of the neck with hyperextension at lower levels. *Spine* **22**, 2489–2494 (1997).

22. Sato, F., Taichi, N., Ono, K., Svensson, M. & Kaneoka, K. Characteristics of Dynamic Cervical Vertebral Kinematics for Female and Male Volunteers in Low-speed Rear Impact, based on Quasi-static Neck Kinematics. in *IRCOBI* 261–277 (2015).

23. Ono, K. *et al.* Prediction of neck injury risk based on the analysis of localized cervical vertebral motion of human volunteers during low-speed rear impacts. in *International Research Council on the Biomechanics of Impact - 2006 International IRCOBI Conference on the Biomechanics of Impact, Proceedings* 103–113 (2006).

24. John, J. D., Kumar, G. S. & Yoganandan, N. Rear-impact neck whiplash: Role of head inertial properties and spine morphological variations on segmental rotations. *Journal of Biomechanical Engineering* **141**, 1–10 (2019).

25. Alektoroff, K. & Papanagiotou, P. Whiplash injury of the cervical spine. *Radiologe* **61**, 710–713 (2021).

26. Sterling, M. A proposed new classification system for whiplash associated disorders - Implications for assessment and management. *Manual Therapy* **9**, 60–70 (2004).

27. Walton, D. M. & Elliott, J. M. An integrated model of chronic whiplash-associated disorder. *Journal of Orthopaedic and Sports Physical Therapy* **47**, 462–471 (2017).

28. Olszko, A. V *et al.* Initial analysis of archived non-human primate frontal and rear impact data from the biodynamics data resource. *Traffic Injury Prevention* **19**, S44–S49 (2018).

29. Beeman, S. M., Kemper, A. R. & Duma, S. M. Neck forces and moments of human volunteers and post mortem human surrogates in low-speed frontal sled tests. *Traffic Injury Prevention* **17**, 141–149 (2016).

30. Stemper, B. D., Yoganandan, N. & Pintar, F. A. Response corridors of the human head-neck complex in rear impact. in *Annual Proceedings - Association for the Advancement of Automotive Medicine* vol. 48 149–163 (2004).

31. Ono, K., Kaneoka, K., Wittek, A. & Kajzer, J. Cervical Injury Mechanism Based on the Analysis of Human Cervical Vertebral Motion and Head-Neck-Torso Kinematics During Low Speed Rear Impacts. *SAE Technical Paper Series* **1**, 339–356 (1997).

32. Yoganandan, N., Pintar, F. A. & Cusick, J. F. Biomechanical analyses of whiplash injuries using an experimental model. *Accident Analysis and Prevention* **34**, 663–671 (2002).

33. Sato, F. *et al.* Effects of whole spine alignment patterns on neck responses in rear end impact. *Traffic Injury Prevention* **18**, 199–206 (2017).

34. Magnusson, M. L. *et al.* Cervical electromyographic activity during low-speed impact. 118–125 (1998).

35. Arbogast, K. B. *et al.* Comparison of kinematic responses of the head and spine for children and adults in low-speed frontal sled tests. *Stapp car crash journal* **53**, 329–72 (2009).

36. Albert, D. L., Beeman, S. M. & Kemper, A. R. Evaluation of Hybrid III and THOR-M neck kinetics and injury risk under various restraint conditions during full-scale frontal sled tests. *Traffic Injury Prevention* **19**, S40–S47 (2018).

37. Correia, M. A., McLachlin, S. D. & Cronin, D. S. Optimization of muscle activation schemes in a finite element neck model simulating volunteer frontal impact scenarios. *Journal of Biomechanics* **104**, (2020).

38. Östh, J., Davidsson, J., Pipkorn, B. & Jakobsson, L. Muscle Activation Strategies in Human Body Models for the Development of Integrated Safety. *ESV - 24th International Technical Conference on the Enhanced Safety of Vehicles (ESV)* 1–15 (2015).

39. Hwang, P. M. & Sykes, B. D. Targeting the sarcomere to correct muscle function. *Nat Rev Drug Discov* **14**, 313–328 (2015).

40. Newham, D. J., Jones, D. A., Ghosh, G. & Aurora, P. Muscle fatigue and pain after eccentric contractions at long and short length. *Clinical Science* **74**, 553–557 (1988).

41. Nosaka, K. & Sakamoto, K. Effect of elbow joint angle on the magnitude of muscle damage to the elbow flexors. *Medicine and Science in Sports and Exercise* **33**, 22–29 (2001).

42. Lieber, R. L. & Friden, J. Muscle damage is not a function of muscle force but active muscle strain. *Journal of Applied Physiology* **74**, 520–526 (1993).

43. Beeman, S. M., Kemper, A. R., Madigan, M. L. & Duma, S. M. Effects of bracing on human kinematics in low-speed frontal sled tests. *Annals of Biomedical Engineering* **39**, 2998–3010 (2011).

44. Yang, K. H. *Stepping Through Finite Element Analysis*. *Basic Finite Element Method as Applied to Injury Biomechanics* (Elsevier Inc., 2018). doi:10.1016/B978-0-12-809831-8.00007-6.

45. Corrales, M. A. & Cronin, D. S. Importance of the cervical capsular joint cartilage geometry on head and facet joint kinematics assessed in a Finite element neck model. *Journal of Biomechanics* **123**, 110528 (2021).

46. Hasselman, C. T., Best, T. M., Seaber, A. V. & Garrett, W. E. A Threshold and Continuum of Injury During Active Stretch of Rabbit Skeletal Muscle. *The American Journal of Sports Medicine* **23**, 65–73 (1995).

47. Best, T. M., McElhaney, J. H., Garrett, W. E. & Myers, B. S. Axial Strain Measurements in Skeletal Muscle at Various Strain Rates. *Journal of Biomechanical Engineering* **117**, 262–265 (1995).

48. Mattucci, S. F. E., Moulton, J. A., Chandrashekar, N. & Cronin, D. S. Strain rate dependent properties of younger human cervical spine ligaments. *Journal of the Mechanical Behavior of Biomedical Materials* **10**, 216–226 (2012).

49. Newell, N. *et al.* Biomechanics of the human intervertebral disc: A review of testing techniques and results. *Journal of the Mechanical Behavior of Biomedical Materials* **69**, 420–434 (2017).

50. Brault, J. R., Siegmund, G. P. & Wheeler, J. B. Cervical muscle response during whiplash: Evidence of a lengthening muscle contraction. *Clinical Biomechanics* **15**, 426–435 (2000).

51. Hincapié, C. A., Cassidy, J. D., Côté, P., Carroll, L. J. & Guzmán, J. Whiplash Injury is More Than Neck Pain: A Population-Based Study of Pain Localization After Traffic Injury. *Journal of Occupational & Environmental Medicine* **52**, 434–440 (2010).

52. Mang, D. W. H., Siegmund, G. P. & Blouin, J.-S. A comparison of anti-whiplash seats during low/moderate speed rear-end collisions. *Traffic Injury Prevention* **21**, 195–200 (2020).

53. Freeman, M. D. & Leith, W. M. Estimating the number of traffic crash-related cervical spine injuries in the United States; An analysis and comparison of national crash and hospital data. *Accident Analysis & Prevention* **142**, 105571 (2020).

54. Elliott, J. M. *et al.* Biopsychosocial sequelae and recovery trajectories from whiplash injury following a motor vehicle collision. *The Spine Journal* S1529943023001080 (2023) doi:10.1016/j.spinee.2023.03.005.

55. Rodriquez, A. A., Barr, K. P. & Burns, S. P. Whiplash: Pathophysiology, diagnosis, treatment, and prognosis. *Muscle and Nerve* **29**, 768–781 (2004).

56. Siegmund, G. P., Winkelstein, B. A., Ivancic, P. C., Svensson, M. Y. & Vasavada, A. The Anatomy and Biomechanics of Acute and Chronic Whiplash Injury. *Traffic Injury Prevention* **10**, 101–112 (2009).

57. Taylor, J. & Twomey, L. Whiplash Injury and Neck Sprain: A Review of Their Prevalence, Mechanisms, Risk Factors, and Pathology. *Crit Rev Phys Rehabil Med* **17**, 285–300 (2005).

58. Barnsley, L., Lord, S. & Bogduk, N. Whiplash injury. *Pain* **58**, 283–307 (1994).

59. Lund, N. *et al.* Fatty infiltrate and neck muscle volume in individuals with chronic whiplash associated disorders compared to healthy controls – a cross sectional case–control study. *BMC Musculoskelet Disord* **24**, 181 (2023).

60. Ólafsdóttir, J. M., Östh, J. K. H., Davidsson, J. & Brolin, K. B. Passenger Kinematics and Muscle Responses in Autonomous Braking Events with Standard and Reversible Pre-tensioned Restraints. *International Research Council on Biomechanics of Injury Conference* **46**, 602–617 (2013).

61. Fanta, O. *et al.* Pre-activation and muscle activity during frontal impact in relation to whiplash associated disorders. *Neuroendocrinology Letters* **34**, 708–716 (2013).

62. Kumar, S., Narayan, Y. & Amell, T. Analysis of low velocity frontal impacts. *Clinical Biomechanics* **18**, 694–703 (2003).

63. Carlsson, A., Siegmund, G. P., Linder, A. & Svensson, M. Y. Motion of the head and neck of female and male volunteers in rear impact car-to-car Tests at 4 and 8 km/h. in *IRCOBI* (2010).

64. Siegmund, G. P., Blouin, J.-S., Brault, J. R., Hedenstierna, S. & Inglis, J. T. Electromyography of Superficial and Deep Neck Muscles During Isometric, Voluntary, and Reflex Contractions. *Journal of Biomechanical Engineering* **129**, 66 (2007).

65. Hedenstierna, S., Halldin, P. & Siegmund, G. P. Neck Muscle Load Distribution in Lateral , Frontal , and Rear-End Impacts A Three-Dimensional Finite Element Analysis. *Spine* **34**, 2626–2633 (2009).

66. Dehner, C. *et al.* Muscle Activity Influence on the Kinematics of the Cervical Spine in Frontal Tests. *Traffic Injury Prevention* **14**, 607–613 (2013).

67. Mathews, E. A. *et al.* Electromyography responses of pediatric and young adult volunteers in low-speed frontal impacts. *Journal of Electromyography and Kinesiology* **23**, 1206–1214 (2013).

68. NHTSA. National Highway Traffic Safety Administration. *NBDL human volunteer sled tests without car body 1522 to 1651* https://www-nrd.nhtsa.dot.gov/database/VSR/bio/QueryTest.aspx (2012).

69. Thunnissen, J., Wismans, J., Ewing, C. L. & Thomas, D. J. Human Volunteer Head-Neck Response in Frontal Flexion: A New Analysis. in *SAE Technical Paper Series* vol. 299 439–460 (San Diego, 1995).

70. Wismans, J., van Oorschot, H. & Woltring, H. Omni-Directional Human Head- Neck Response. *SAE Transactions* **95**, 819–837 (1986).

71. Cormier, J., Gwin, L., Reinhart, L., Wood, R. & Bain, C. A Comprehensive Review of Low-Speed Rear Impact Volunteer Studies and a Comparison to Real-World Outcomes. *Spine* **43**, 1250–1258 (2018).

72. Sato, F. *et al.* Investigation of whole spine alignment patterns in automotive seated posture using upright open MRI systems. *2016 IRCOBI Conference Proceedings - International Research Council on the Biomechanics of Injury* 113–130 (2016).

73. Sato, F. *et al.* Dynamic cervical vertebral motion of female and male volunteers and analysis of its interaction with head/neck/torso behavior during low-speed rear impact. in *2014 IRCOBI Conference Proceedings - International Research Council on the Biomechanics of Injury* 227–249 (2014).

74. Kang, Y. S., Moorhouse, K., Herriott, R. & Bolte IV, J. H. Comparison of Cervical Vertebrae Rotations for PMHS and BioRID II in Rear Impacts. *Traffic Injury Prevention* **14**, 37–41 (2013).

75. Deng, B., Begeman, P. C., Yang, K. H., Tashman, S. & King, A. I. Kinematics of Human Cadaver Cervical Spine during Low Speed Rear-End Impacts. in *SAE Technical Papers* vols 2000-Novem (2000).

76. Brolin, K., Halldin, P. & Leijonhufvud, I. The effect of muscle activation on neck response. *Traffic Injury Prevention* **6**, 67–76 (2005).

77. Ejima, S., Ono, K., Kaneoka, K. & Fukushima, M. Development and Validation of the Human Neck Muscle Model Under Impact Loading. *Ircobi* 245–255 (2005).

78. Iwamoto, M., Nakahira, Y., Kimpara, H., Sugiyama, T. & Min, K. Development of a human body finite element model with multiple muscles and their controller for estimating

occupant motions and impact responses in frontal crash situations. *Stapp car crash journal* **56**, 231–268 (2012).

79. Vasavada, A. N., Li, S. & Delp, S. L. Influence of muscle morphometry and moment arms on the moment-generating capacity of human neck muscles. *Spine* **23**, 412–422 (1998).

80. de Bruijn, E., van der Helm, F. C. T. & Happee, R. Analysis of isometric cervical strength with a nonlinear musculoskeletal model with 48 degrees of freedom. *Multibody System Dynamics* **36**, 339–362 (2016).

81. Barker, J. B., Cronin, D. S. & Nightingale, R. W. Lower Cervical Spine Motion Segment Computational Model Validation: Kinematic and Kinetic Response for Quasi-Static and Dynamic Loading. *Journal of Biomechanical Engineering* **139**, 061009 (2017).

82. Barker, J. B. & Cronin, D. S. Multilevel Validation of a Male Neck Finite Element Model With Active Musculature. *Journal of Biomechanical Engineering* **143**, 011004 (2021).

83. Yang, K. H. *et al. Basic Finite Element Method as Applied to Injury Biomechanics*. (Elsevier, 2018). doi:10.1016/C2015-0-06702-8.

84. John, J. D., Saravana Kumar, G. & Yoganandan, N. Cervical spine morphology and ligament property variations: A finite element study of their influence on sagittal bending characteristics. *Journal of Biomechanics* **85**, 18–26 (2019).

85. Putra, I. P. A. *et al.* Comparison of control strategies for the cervical muscles of an average female head-neck finite element model. *Traffic Injury Prevention* **20**, S116–S122 (2019).

86. Meyer, G. A., McCulloch, A. D. & Lieber, R. L. A nonlinear model of passive muscle viscosity. *Journal of Biomechanical Engineering* **133**, 1–9 (2011).

87. Hedenstierna, S., Halldin, P. & Brolin, K. Evaluation of a combination of continuum and truss finite elements in a model of passive and active muscle tissue. *Computer Methods in Biomechanics and Biomedical Engineering* **11**, 627–639 (2008).

88. Kleinbach, C. *et al.* Implementation and validation of the extended Hill-type muscle model with robust routing capabilities in LS-DYNA for active human body models. *BioMedical Engineering Online* **16**, 1–28 (2017).

89. Panzer, M. B., Fice, J. B. & Cronin, D. S. Cervical spine response in frontal crash. *Medical Engineering and Physics* **33**, 1147–1159 (2011).

90. Östh, J., Brolin, K. & Happee, R. Active muscle response using feedback control of a finite element human arm model. *Computer Methods in Biomechanics and Biomedical Engineering* **15**, 347–361 (2012).

91. Kato, D., Nakahira, Y. & Iwamoto, M. A Study of Muscle Control with Two Feedback Controls for Posture and Reaction Force for more Accurate Prediction of Occupant Kinematics in Low-Speed Frontal Impacts. in *International Technical Conference on the Enhanced Safety of Vehicles (ESV)* 1–11 (2017).

92. Peng, G. C. Y., Hain, T. C. & Peterson, B. W. A dynamical model for reflex activated head movements in the horizontal plane. *Biological Cybernetics* **75**, 309–319 (1996).

93. Kato, D., Kimpara, H., Nakahira, Y. & Iwamoto, M. Effects of Controlled Muscle Activations on Human Head–Neck Responses during Low-Speed Rear Impacts. *IRCOBI Proceedings* 33–34 (2016).

94. Happee, R., de Bruijn, E., Forbes, P. A. & van der Helm, F. C. T. Dynamic head-neck stabilization and modulation with perturbation bandwidth investigated using a multisegment neuromuscular model. *Journal of Biomechanics* **58**, 203–211 (2017).

95. Le, P. *et al.* An Exploratory Electromyography-Based Coactivation Index for the Cervical Spine. *Human Factors* **60**, 68–79 (2018).

96. Peterson, B. W., Goldberg, J., Bilotto, G. & Fuller, J. H. Cervicocollic reflex: Its dynamic properties and interaction with vestibular reflexes. *Journal of Neurophysiology* **54**, 90–109 (1985).

97. Reynolds, J. S. & Gdowski, G. T. Head movements produced during whole body rotations and their sensitivity to changes in head inertia in squirrel monkeys. *Journal of Neurophysiology* **99**, 2369–2382 (2008).

98. Blouin, J. S., Descarreaux, M., Bélanger-Gravel, A., Simoneau, M. & Teasdale, N. Attenuation of human neck muscle activity following repeated imposed trunk-forward linear acceleration. *Experimental Brain Research* **150**, 458–464 (2003).

99. Foust, D. R., Chaffin, D. B., Snyder, R. G. & Baum, J. K. Cervical Range of Motion and Dynamic Response and Strength of Cervical Muscles. in 730975 (1973). doi:10.4271/730975.

100. Hernández, I. A., Fyfe, K. R., Heo, G. & Major, P. W. The role of sternocleidomastoid muscle in simulated low velocity rear-end impacts. *Eur Spine J* **15**, 876–885 (2006).

101. Magnusson, M. L. *et al.* Cervical electromyographic activity during low-speed rear impact. *European Spine Journal* **8**, 118–125 (1999).

102. Siegmund, G. P., Sanderson, D. J. & Inglis, J. T. The effect of perturbation acceleration and advance warning on the neck postural responses of seated subjects. *Exp Brain Res* **144**, 314–321 (2002).

103. Snyder, R. G., Chaffin, D. B. & Foust, D. R. *Bioengineering Study of Basic Physical Measurements Related to Susceptibility to Cervical Hyperextension-Hyperflexion Injury*. (1975).

104. Mazzini, L. & Schieppati, M. Activation of the neck muscles from the ipsi- or contralateral hemisphere during voluntary head movements in humans. A reaction-time study.

Electroencephalography and Clinical Neurophysiology/Evoked Potentials Section **85**, 183–189 (1992).

105. Yeomans, J. Tactile, acoustic and vestibular systems sum to elicit the startle reflex. *Neuroscience & Biobehavioral Reviews* **26**, 1–11 (2002).

106. Siegmund, G. P., Inglis, J. T. & Sanderson, D. J. Startle response of human neck muscles sculpted by readiness to perform ballistic head movements. *The Journal of Physiology* **535**, 289–300 (2001).

107. Siegmund, G. P., Sanderson, D. J., Myers, B. S. & Inglis, J. T. Awareness Affects the Response of Human Subjects Exposed to a Single Whiplash-Like Perturbation: *Spine* **28**, 671–679 (2003).

108. Alizadeh, M. *et al.* Biomechanical musculoskeletal models of the cervical spine: A systematic literature review. *Clinical Biomechanics* **71**, 115–124 (2020).

109. Gayzik, F. S. *et al.* Development of a full body CAD dataset for computational modeling: A multi-modality approach. *Annals of Biomedical Engineering* **39**, 2568–2583 (2011).

110. Knaub, K. *et al.* Measurement of human neck muscle volume geometry and physiologic cross sectional area in 5th, 50th, and 95th percentile subjects using cadaveric dissection and MRI. *25th International Worshop on Humon Subjects for Biomechanical Research* 69–78 (1997).

111. Anderson, J. S., Hsu, A. W. & Vasavada, A. N. Morphology, architecture, and biomechanics of human cervical multifidus. *Spine* **30**, 86–91 (2005).

112. Borst, J., Forbes, P. A., Happee, R. & Veeger, D. Muscle parameters for musculoskeletal modelling of the human neck. *Clinical Biomechanics* **26**, 343–351 (2011).

113. Knaub, K. & Myers, B. S. *Project F.2(c) Cervical Spine Muscle*. (1998).

114. Newell, R. S., Blouin, J. S., Street, J., Cripton, P. A. & Siegmund, G. P. The neutral posture of the cervical spine is not unique. in *IRCOBI* (2014). doi:10.1016/j.jbiomech.2018.08.012.

115. Newell, R. S., Blouin, J. S., Street, J., Cripton, P. A. & Siegmund, G. P. The neutral posture of the cervical spine is not unique in human subjects. *Journal of Biomechanics* **80**, 53–62 (2018).

116. Sato, F. *et al.* The Effect of Seat Back Inclination on Spinal Alignment in Automotive Seating Postures. *Frontiers in Bioengineering and Biotechnology* **9**, 1–17 (2021).

117. Li, F. *et al.* A review of neck injury and protection in vehicle accidents. *Transportation Safety and Environment* **1**, 89–105 (2019).

118. Duma, S. M., Crandall, J. R., Rudd, R. W. & Kent, R. W. Small female head and neck interaction with a deploying side airbag. *Accident Analysis & Prevention* **35**, 811–816 (2003).

119. McIntosh, A. S., Kallieris, D. & Frechede, B. Neck injury tolerance under inertial loads in side impacts. *Accident Analysis & Prevention* **39**, 326–333 (2007).

120. Tencer, A. F., Mirza, S. & Huber, P. A Comparison of Injury Criteria Used in Evaluating Seats for Whiplash Protection. *Traffic Injury Prevention* **5**, 56–66 (2004).

121. Boström, O. *et al.* A New Neck Injury Criterion Candidate Based on Injury Findings in the Cervical Spinal Ganglia after Experimental Neck Extension Trauma. in *Conference proceedings-international research council on the biomechanics of injury IRCOBI* (Dublin (Ireland), 1996).

122. Eichberger, A. *et al.* Pressure measurements in the spinal canal of post-mortem human subjects during rear-end impact and correlation of results to the neck injury criterion. *Accident Analysis & Prevention* **32**, 251–260 (2000).

123. Siegmund, G. P., Heinrichs, B. E., Chimich, D. D., DeMarco, A. L. & Brault, J. R. The effect of collision pulse properties on seven proposed whiplash injury criteria. *Accident Analysis & Prevention* **37**, 275–285 (2005).

124. Funk, J. R. *et al.* Head and Neck Loading in Everyday and Vigorous Activities. *Ann Biomed Eng* **39**, 766–776 (2011).

125. Nusholtz, G. S., Di Domenico, L., Shi, Y. & Eagle, P. Studies of neck injury criteria based on existing biomechanical test data. *Accident Analysis & Prevention* **35**, 777–786 (2003).

126. Johnson, D., Koya, B. & Gayzik, F. S. Comparison of Neck Injury Criteria Values Across Human Body Models of Varying Complexity. *Front. Bioeng. Biotechnol.* **8**, 985 (2020).

127. Schmitt, K.-U., Muser, M., Niederer, P. & Walz, F. A New Neck Injury Criterion Candidate For Rear-End Collisions Taking Into Account Shear Forces And Bending Moments. in (2001).

128. Whyte, T. *et al.* A neck compression injury criterion incorporating lateral eccentricity. *Sci Rep* **10**, 7114 (2020).

129. Smotrova, E., Morris, L. & McNally, D. Comparison of standard automotive industry injury predictors and actual injury sustained during significant whiplash events. *Eur Spine J* **30**, 3043–3058 (2021).

130. Ivancic, P. C. & Sha, D. Comparison of the whiplash injury criteria. *Accident Analysis & Prevention* **42**, 56–63 (2010).

131. Nölle, L. V., Mishra, A., Martynenko, O. V. & Schmitt, S. Evaluation of muscle strain injury severity in active human body models. *Journal of the Mechanical Behavior of Biomedical Materials* **135**, 105463 (2022).

132. Bogduk, N. & Yoganandan, N. Biomechanics of the cervical spine Part 3: Minor injuries. *Clinical Biomechanics* **16**, 267–275 (2001).

133. Rycman, A., McLachlin, S. & Cronin, D. S. A Hyper-Viscoelastic Continuum-Level Finite Element Model of the Spinal Cord Assessed for Transverse Indentation and Impact Loading. *Frontiers in Bioengineering and Biotechnology* **9**, 1–13 (2021).

134. Ewing, C. L. & Thomas, D. J. Human Head and Neck Response To Impact Acceleration. *DTIC Document* (1972).

135. Ivancic, A. & Pradhan, V. The influence of isometrically derived neck muscle spatial tuning patterns on head response in dynamic conditions. (2017).

136. Keshner, E. A. Head-trunk coordination during linear anterior-posterior translations. *Journal of Neurophysiology* **89**, 1891–1901 (2003).

137. Somasundaram, K. *et al.* Evaluating thoracolumbar spine response during simulated underbody blast impact using a total human body finite element model. *Journal of the Mechanical Behavior of Biomedical Materials* **100**, (2019).

138. Kumar, S., Ferrari, R. & Narayan, Y. The effect of trunk flexion in healthy volunteers in rear whiplash-type impacts. *Spine* **30**, 1742–1749 (2005).

139. Gepner, B. D. *et al.* Performance of the obese GHBMC models in the sled and belt pull test conditions IRCOBI co. *Conference proceedings International Research Council on the Biomechanics of Injury, IRCOBI* **2018-Septe**, 355–368 (2018).

140. Beillas, P. *et al.* Specifications of a Software Framework to Position and Personalise Human Body Models P. in *IRCOBI* 594–595 (2015).

141. Janak, T., Lafon, Y., Petit, P. & Beillas, P. Transformation Smoothing to use after Positioning of Finite Element Human Body Models. *Conference proceedings International Research Council on the Biomechanics of Injury, IRCOBI* **2018-Septe**, 224–236 (2018).

142. Miller, L. E. *et al.* Evaluation of Brain Response during Head Impact in Youth Athletes Using an Anatomically Accurate Finite Element Model. *Journal of Neurotrauma* **36**, 1561–1570 (2019).

143. Morrow, D. A., Haut Donahue, T. L., Odegard, G. M. & Kaufman, K. R. Transversely isotropic tensile material properties of skeletal muscle tissue. *Journal of the Mechanical Behavior of Biomedical Materials* **3**, 124–129 (2010).

144. Macnab, I. Acceleration Injuries of the Cervical Spine. *J Bone Joint Surg Am* **46**, 1797–1799 (1964).

145. Viano, D. C. Analysis of the lack of restraint with and without belt pretensioning in 40.2 km/h rear impacts. *Traffic Injury Prevention* **0**, 1–7 (2022).

146. Frej, D. & Jaśkiewicz, M. Comparison of Volunteers' Head Displacement with Computer Simulation—Crash Test with Low Speed of 20 km/h. *Sensors* **22**, 9720 (2022).

147. Burnett, R. A., Parenteau, C. S. & White, S. D. The effect of seatback deformation on out-of-position front-seat occupants in severe rear impacts. *Traffic Injury Prevention* **24**, 184–188 (2022).

148. Ivancic, P. C. *et al.* Intervertebral Neck Injury Criterion for Simulated Frontal Impacts. *Traffic Injury Prevention* **6**, 175–184 (2005).

149. Snodgrass, S. J. *et al.* Greater muscle volume and muscle fat infiltrate in the deep cervical spine extensor muscles (multifidus with semispinalis cervicis) in individuals with chronic idiopathic neck pain compared to age and sex-matched asymptomatic controls: a cross-sectional study. *BMC Musculoskelet Disord* **23**, 973 (2022).

150. Elliott, J. *et al.* Fatty Infiltration in the Cervical Extensor Muscles in Persistent Whiplash-Associated Disorders: A Magnetic Resonance Imaging Analysis. *Spine* **31**, E847–E855 (2006).

151. Liang, Z. *et al.* Quantitative cervical spine injury responses in whiplash loading with a numerical method of natural neural reflex consideration. *Computer Methods and Programs in Biomedicine* **219**, 106761 (2022).

152. Stemper, B. D., Yoganandan, N. & Pintar, F. A. Gender dependent cervical spine segmental kinematics during whiplash. *Journal of Biomechanics* **36**, 1281–1289 (2003).

153. Zheng, Y., Shin, H., Kamper, D. G. & Hu, X. Automatic Detection of Contracting Muscle Regions via the Deformation Field of Transverse Ultrasound Images: A Feasibility Study. *Ann Biomed Eng* **49**, 354–366 (2021).

154. Budzikowski, J. D. & Murray, W. M. Multi-sweep 3-dimensional ultrasound is accurate for in vivo muscle volume quantification, expanding use to larger muscles. *Journal of Biomechanics* **151**, 111501 (2023).

Appendices

A) Lateral impact kinematics for the closed-loop controller

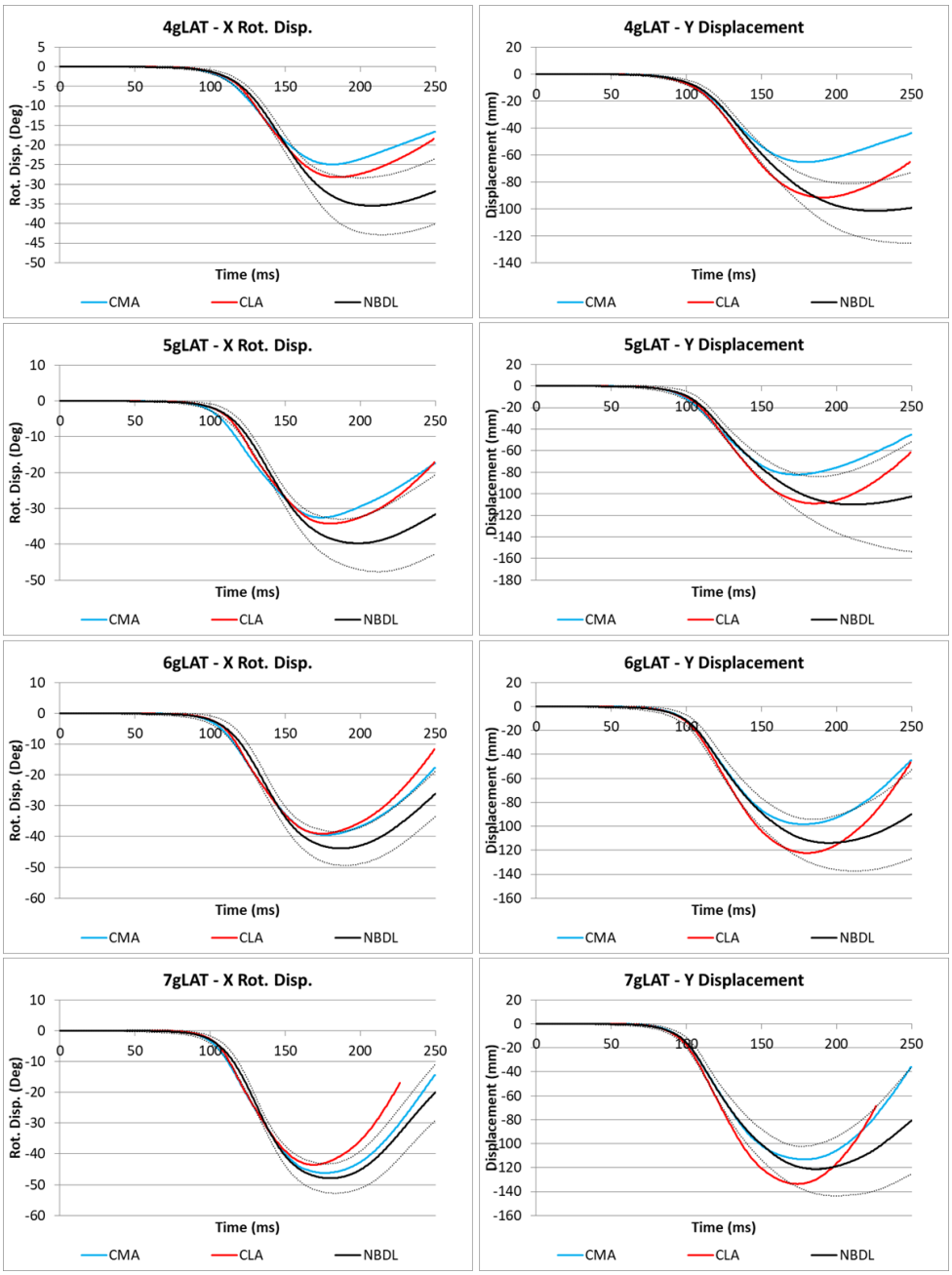


Figure A: Head kinematics from lateral impacts

Comparison of the lateral impact head kinematics for the proposed CLA compared to the NBDL human volunteer test data average and SD. CMA results are included for reference.

B) Rear impact kinematics for the closed-loop controller

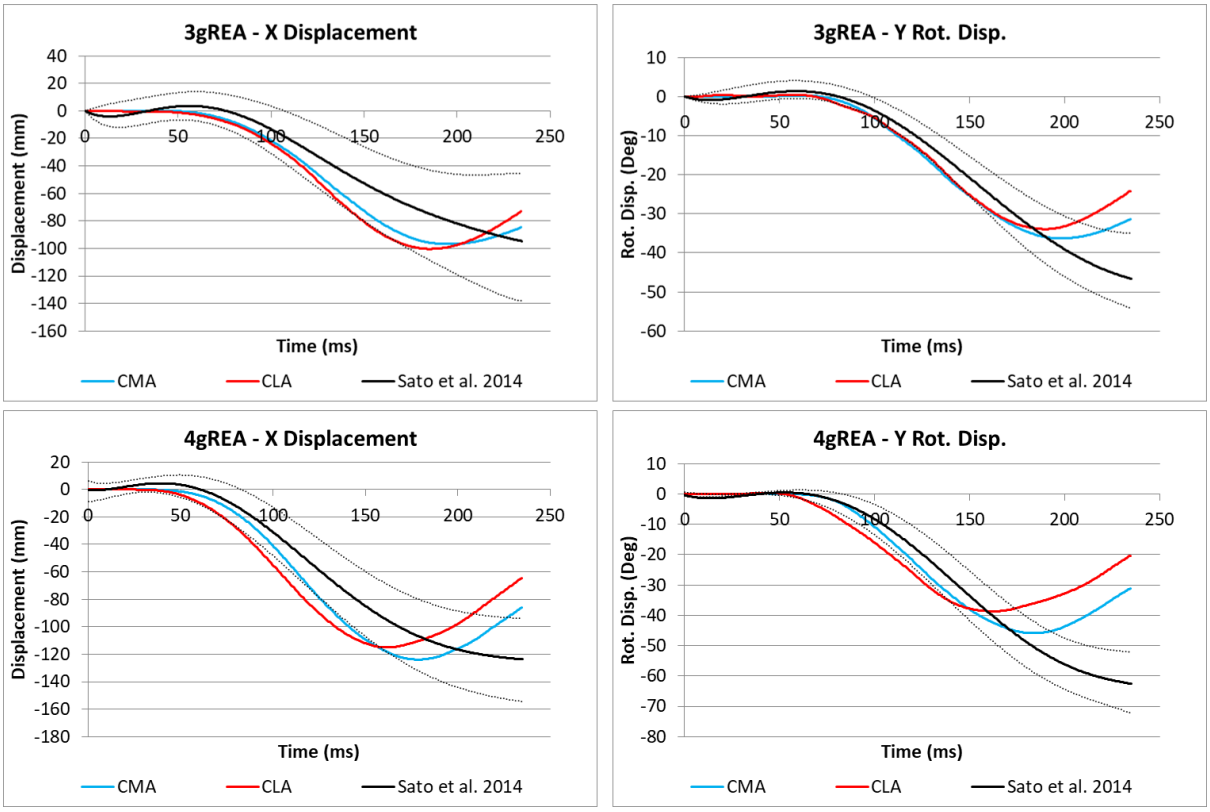


Figure B: Head kinematics from rear impacts

Comparison of the rear impact head kinematics for the proposed CLA compared to the NBDL human volunteer test data average and SD. CMA results are included for reference.